TABLE OF CONTENTS

TABLE OF CONTENTS (continued)

NASA Contractor Report 3429



# Analytical Testing

W. G. Flannelly, J. A. Fabunmi,
and E. J. Nagy

CONTRACT NAS1-15414
MAY 1981

NASA

NASA Contractor Report 3429

# Analytical Testing

W. G. Flannelly, J. A. Fabunmi,
and E. J. Nagy
*Kaman Aerospace Corporation*
*Bloomfield, Connecticut*

Prepared for
Langley Research Center
under Contract NAS1-15414

National Aeronautics
and Space Administration

**Scientific and Technical
Information Branch**

1981

TABLE OF CONTENTS

TABLE OF CONTENTS (continued)

## LIST OF ILLUSTRATIONS

LIST OF ILLUSTRATIONS (continued)

## LIST OF TABLES

## SUMMARY

Analytical methods for combining flight acceleration and strain data with shake test mobility data to predict the effects of structural changes on flight vibrations and strains are presented. This integration of structural dynamic analysis with flight performance is referred to as analytical testing. The objective of this methodology is to analytically estimate the results of flight testing contemplated structural changes with minimum flying and change trials. The category of changes to the aircraft includes mass, stiffness, absorbers, isolators, and active suppressors. Examples of applying the analytical testing methodology using flight test and shake test data measured on an AH-1G helicopter are included. The techniques and procedures for vibration testing and modal analysis are also described.

## INTRODUCTION

Helicopter structural dynamics and rotor-induced vibratory loads impact the design, analysis, and evaluation of vibrations. The vibration environment can be generalized by relationships between critical points of airframe response and points of vibratory forcing. Vibration, conceived of in terms of how much these critical points shake, continues to be a major problem in helicopter dynamics. Structural fatigue, a result primarily of vibration, is of much greater consequence to the structural integrity of the helicopter and the reliability of its systems.[1,2] The large number of airframe locations at which vibrations affect structural integrity, performance, and overall mission effectiveness complicates the issue. The vibration problem is also complicated by the many dynamic conditions that must be evaluated during helicopter development. The number of configuration changes in the operation of typical Army helicopters is enormous. If each of these changes is flight tested for baseline rotorcraft conditions represented by gross weight, center of gravity, fuel loading, cargo loading, and flight conditions, then thousands of structural dynamic conditions must be evaluated. Favorable vibrations at one airframe location due to structural changes may, in fact, degrade vibration at other points. Thus, the vibration solution process becomes one of engineering compromise.

Structural dynamics analysis has not proven to be one of the most useful engineering tools in helicopter development.[1] As conventionally practiced, most helicopter vibration tests provide limited information for resolving vibration issues. Helicopter flight vibration tests provide a direct measure of the actual vibration environment while airframe ground vibration tests are most often conducted to correlate analytical predictions of airframe resonances and mode shapes. If there is reasonable agreement between analysis and test, then confidence in the validity of the analysis is enhanced. However, if reasonable agreement is not obtained, then an impasse results. Vibration problems are extremely difficult to quantify and have been solved by trial-and-error ground and flight vibration testing.

The integration of structural dynamics analysis with flight performance, herein referred to as analytical testing, appears to offer a practical methodology to the vibration solution process in helicopter development. This report describes analytical methods for combining flight acceleration and strain data with shake test mobility data to estimate the effects of contemplated changes on aircraft vibrations and stresses for various flight conditions and maneuvers. The category of changes to the aircraft includes external stores, weapons, cargo, changes in structure or materials of structure, absorbers, isolators, or active vibration suppressors. The objective of analytical testing methodology is to analytically estimate the results of flight testing such changes with minimum flying and change trials and to provide accurate and consistent dynamics information for reduced cost and testing time.

The present investigation applied the analytical testing methodology in conjunction with full-scale helicopter ground and flight test vibration data. An AH-1G test vehicle was utilized in this project to provide ground vibration data of realistic quality. Flight test data of the AH-1G was obtained from another Army program on an as-available basis. The analytical testing examples in this report use AH-1G data to illustrate possible generic applications of the methodology. The authors do not suggest or imply applicability of these examples to the AH-1G or any other specific helicopter. The applications described herein were directed to the practical acquisition of helicopter vibration data for analytical testing and the possible utilization of the method.

The reader is cautioned not to interpret the results of these illustrations as representing experimental validation of analytical testing in any possible application.

## LIST OF SYMBOLS

| | |
|---|---|
| A | modal acceleration, g/N (g/lb) |
| c | change factor (a constant), such as the proportionality of skin thickness of the change |
| d | generalized damping, N-s/m (lb-s/in.) |
| D | diameter of modal circle, m/N (in./lb) |
| [D] | damping matrix, N-s/m (lb-s/in.) |
| E | rigid body acceleration coefficient, g/N (g/lb) |
| f | force, N(lb), or frequency, Hz |
| F | mode frequency function, defined in text |
| g | structural damping coefficient or units of acceleration |
| G | gravitational acceleration, 9.8066 $m/s^2$ (32.174 $ft/s^2$) |
| i | imaginary operator, $\sqrt{-1}$ |
| k | generalized stiffness, N/m (lb/in.) |
| [K] | stiffness matrix, N/m (lb/in.) |
| m | absorber mass or generalized mass, kg ($lb\text{-}s^2/in.$) |
| M | moment, N-m (lb-ft) |
| [M] | mass matrix, kg ($lb\text{-}s^2/in.$) |
| P | rotor revolution, thus 2P denotes twice rotor revolution |
| q | vibratory displacement, m (in.) |
| $\ddot{q}$ | vibratory acceleration, g |
| {r} | vector of complex responses, defined in text |
| R | mobility residual, g/N (g/lb) |
| s | arc length of modal circle or, in Matrix Difference Method, $s \approx -\frac{\Delta\omega_x}{\Omega_x}$ |
| t | time, s |
| [T] | transformation matrix = $\left[\frac{\partial \Delta q}{\partial q}\right]$ |
| v | sweep speed required for swept sine shake testing, Hz/s |
| $V_H$ | maximum speed attainable in level flight at maximum continuous power |

| | |
|---|---|
| $x$ | displacement, m (in.) |
| $\ddot{x}$ | linear acceleration, $m/s^2$ ($in./s^2$) |
| $\{y(\omega)\}$ | displacement vector of a steadily vibrating undamped multiple degree of freedom system |
| $\{\ddot{y}(\omega)\}$ | Fourier transform of the accelerations |
| $Y$ | displacement mobility, m/N (in./lb) |
| $Y^C$ | mobility of structural change, m/N (in./lb) |
| $Y^{(\epsilon)}$ | strain mobility, $N^{-1}$ ($lb^{-1}$) |
| $\ddot{Y}$ | acceleration mobility, g/N (g/lb) |
| $Z$ | impedance, N/m (lb/in.) in Appendices A and B |
| $Z^C$ | impedance change |
| $[Z]$ | impedance matrix, N/m (lb/in.) |
| $\alpha$ | angle of bar in simple bar truss or logarithmic sweep speed for swept sine shake testing, dec/min |
| $\beta$ | frequency ratio |
| $\delta$ | distance between colinear displacements, m (in.) |
| $\Delta$ | indicates change in variable following the symbol |
| $\Delta_f$ | mode resolution, Hz |
| $\epsilon$ | strain, nondimensional |
| $\zeta$ | viscous damping factor |
| $\theta$ | rotation response, deg |
| $\lambda(\omega)$ | frequency dependent complex eigenvalue, $Hz^2$ |
| $\mu$ | frequency function |
| $\tau$ | characteristic time for secular response, s |
| $\phi$ | phase angle |
| $\phi$ | normalized mode |
| $\Psi$ | orthonormal mode, $kg^{-1/2}$ ($in.^{1/2}/lb^{1/2}$-s) |
| $\Psi^{(\epsilon)}$ | orthonormal strain mode |
| $\omega$ | forcing frequency, rad/s |
| $\Omega_n$ | natural frequency of the nth mode, rad/s |
| $\Omega_T$ | absorber tuning frequency, rad/s |
| $(\ )^I$ | imaginary component of complex variable |
| $(\ )^R$ | real component of complex variable |

| | |
|---|---|
| $( )^*$ | complex conjugate |
| $( )/\phi$ | denotes amplitude and phase of complex variable |
| $[ ]$ | rectangular or square matrix |
| $\{ \}$ | column matrix |
| $\lfloor \rceil$ | row matrix |
| $[ ]^T$ | matrix transpose |
| $[ ]^{-1}$ | matrix inverse |
| $[ ]^+$ | matrix pseudoinverse |
| $\lceil \rfloor$ | diagonal matrix |
| $\lceil I \rfloor$ | identity matrix |
| $\partial/\partial x$ | partial derivative |

## THE PRACTICAL ASPECTS OF ANALYTICAL TESTING

Analytical testing can be applied in three stages of helicopter development; namely, during preliminary design, after construction but before flight, and during development flight testing. In other words, the vibration data can originate from analysis or test or in combination.

During the first stage of helicopter development, the helicopter exists on paper and flight vibrations are simulated using available theoretical information. Hub excitation estimates are obtained from rotor analyses and estimates of downwash impingement and wake interferences can be obtained from aerodynamic considerations. These estimated excitations for various maneuvers can be applied to mobilities obtained from airframe finite element or similar dynamic analyses to yield estimates of in-flight stresses and vibrations. The prediction of helicopter vibrations ultimately requires consideration of the response of the coupled rotor/airframe. In general, the degree of rotor/airframe coupling is strongly dependent on the characteristics of both structural and aerodynamic interface coupling.

Substructures and changes can be combined with the basic structure in the analytical testing processes which can be implemented on interactive minicomputers.[3] Therefore, the finite element program for each structural module needs to be executed only one time to yield resonance and mode shape data. Modal damping can be accounted for during analytical testing. This process minimizes finite element program sizes and running times while allowing a large number of nodes in the combined structure. In addition, it allows the representation of nonproportional damping and, consequently, complex modes. The complex modes, resonances, and modal damping of the combined structure can be obtained by treating the combined mobilities as test data. Uncertainties of theoretical resonances and modal damping can be evaluated by direct perturbation of these parameters in the modal synthesis. The modal synthesis may also include high frequency residual mobilities for local mode driving-point effects. Uncertainties in rotor loads estimates[4] and in estimates of downwash impingement and wake interference can be systematically assessed with variation in excitation magnitudes and phasings during this stage of helicopter development.

In the second stage of helicopter development, after construction but before flight, a shake test aircraft should be available. This non-flying shake test aircraft would be used for analytical testing of changes, ground flying for fatigue evaluation,[5] and analysis of accidents. In this stage, shake testing data can be used to refine the existing finite element models.[6,7,8] Mobilities from finite element models of substructure can be combined with mobilities from tests of other subsystems to obtain total system mobilities, resonances, modal damping, and complex modes. In general, the fuselage system mobilities and the mobilities of complex components, such as engines, may be obtained through shake testing while mobilities of contemplated changes, flexible portions of the airframe, and low mass structural appendages would be obtained through finite element modeling. This separation between finite element modeling and shake testing for analytical testing purposes offers optimum utilization of finite element analysis and modal analysis shake testing. The major accomplishment in this stage is the application of refined mobilities for identifying favorable structural changes to adjust airframe resonances and nodes. Theoretical estimates of the vibratory loads are combined with these mobilities to estimate changes in vibrations and stresses.

During the third stage of helicopter development, analytical testing uses only ground and flight vibration data to estimate changes in flight responses caused by structural and configuration changes. As the flight envelope of the prototype aircraft is expanded, flight vibration data can be applied directly since the theoretical estimates of external excitations are no longer needed. Anticipated changes such as stores, weapons, cargo, and structure can be examined for flight effects on vibrations and stresses before actual flight. Knowledge of the number, types, or locations of the external excitations is not required. The only flight data necessary are accelerations and strains measured during the initial flight tests.

## ANALYTICAL TESTING THEORY

The matrix equations of motion for a damped linear structure can be generalized in the frequency domain as

$$\left([K] - \omega^2 [M] + i [D(\omega)]\right) \{q\} = \{f\} \tag{1}$$

where [K], [M], and [D(ω)] are Nth ordered stiffness, mass, and damping matrices, respectively. The matrix terms on the lefthand side of equation (1) define the displacement impedance matrix, [Z], or

$$[Z] \{q\} = \{f\} \tag{2}$$

The dynamic responses can thus be characterized by the simple matrix equation given by

$$\{q\} = [Y] \{f\} \tag{3}$$

where

$$[Y] = [Z]^{-1} \tag{4}$$

and the variables in equation (3) are complex valued and frequency dependent. The matrix [Y] is the transfer function which relates the input excitations, {f}, to the output responses, {q}. If the response vector is displacement, velocity, or acceleration, then the transfer function is defined as the displacement, velocity, or acceleration mobility, respectively. Compliance, mobility, and inertance are sometimes used in the literature to define the corresponding displacement, velocity, and acceleration mobilities.

### Types of Mobilities

Mobilities are defined as partial derivatives of response with respect to excitation in the frequency domain. In general, there are two separate types of mobilities used in analytical testing which can be distinguished by considering the nature of the response and the excitation.

If the response is vibration (displacement, velocity, acceleration) and the excitation is force or moment, then the mobility matrix consists of the following components

$$[Y] = \begin{bmatrix} \partial q_j/\partial f_k & \partial q_j/\partial M_k \\ \partial \theta_j/\partial f_k & \partial \theta_j/\partial M_k \end{bmatrix} \tag{5}$$

where $q$ and $\theta$ are the respective translation and rotation responses; $f$ and $M$ are the force and moment excitations, respectively. The reciprocity principle for vibration mobilities is satisfied such that

$$\begin{aligned} \partial q_j/\partial f_k &= \partial q_k/\partial f_j \\ \partial \theta_j/\partial f_k &= \partial q_k/\partial M_j \\ \partial \theta_j/\partial M_k &= \partial \theta_k/\partial M_j \end{aligned} \tag{6}$$

If the response is strain and the excitation is force, then the strain mobility matrix becomes

$$\left[Y^{(\varepsilon)}\right] = \left[\partial \varepsilon_j/\partial f_k\right] \tag{7}$$

Let $q_{j+1}$ represent a displacement colinear with $q_j$ and separated a distance $\delta_j$ from $q_j$. Then, the strain at $j$ is defined such that

$$\varepsilon_j \equiv \lim_{\delta_j \to 0} (q_{j+1} - q_j)/\delta_j \tag{8}$$

and the strain mobility becomes

$$\partial \varepsilon_j/\partial f_k \equiv \lim_{\delta_j \to 0} (Y_{j+1,k} - Y_{jk})/\delta_j \tag{9}$$

This type of strain mobility is useful for evaluating stiffness changes. The application of $\partial \varepsilon/\partial f$ to analytical testing is discussed in the next chapter. Note that the reciprocity principle is not satisfied for strain mobility; i.e.,

$$\partial \varepsilon_j / \partial f_k \neq \partial \varepsilon_k / \partial f_j \tag{10}$$

## Analytical Testing Equations

The solution to helicopter vibration problems consists, in part, of predicting and confirming the flight vibration or strain effects of dynamic changes in the airframe, on the rotor, or at the rotor/airframe interface. Let $\{q\}$ and $\{\varepsilon\}$ represent the baseline vibration and strain, respectively. Then, $\{q'\}$ and $\{\varepsilon'\}$ represent the change in baseline vibration and strain due to a dynamic change. In theory, $\{q'\}$ and $\{\varepsilon'\}$ can result from either a change in the mobility matrix or a change in the vibratory loading. The basic analytical testing method considers changes in the mobility matrix which can be synthesized by discrete as well as multiple and distributed dynamic impedance adjustments. The category of impedance changes that can be accommodated includes mass, stiffness, absorbers, isolators, and active suppressors. As shown in Appendix A, the matrix equation for determining the change in baseline vibration for a general multidimensional impedance change is

$$\{q'\} = \{q\} - \left[Y_{qI}\right] \left[Y_{II}^{C} + Y_{II}\right]^{-1} \left\{q_I\right\} \tag{11}$$

where $Y_{II}^{C}$ is defined from the impedance change. The mobilities $Y_{qI}$ and $Y_{II}$ represent transfer functions for the baseline structure at the change interface and do not include the effects of the impedance change. In other words, for a properly modeled impedance change, the effects on flight vibrations are evaluated without incorporating the change in the baseline structure. Therefore, only one NASTRAN or similar dynamic analysis is required to implement equation (11). If changes in strain, as opposed to vibration, are considered, then equation (11) becomes

$$\{\varepsilon'\} = \{\varepsilon\} - \left[Y_{qI}^{(\varepsilon)}\right] \left[Y_{II}^{C} + Y_{II}\right]^{-1} \left\{q_I\right\} \tag{12}$$

In summary, the changed flight responses (vibration or strain) are characterized by the dynamics of the impedance change, the baseline flight responses, and the baseline mobility responses. The operational equations can be used with either theoretically derived vibration and strain data or ground and flight

vibration and strain measurements. In the next chapter, equations (11) and (12) are considered for examining mass, stiffness, and absorber changes to illustrate the analytical testing methodology.

## Limitations of the Method

Basic to the analytical testing method are the assumptions that the structure is linear and that changes to the structure do not change the external loadings. These conditions are only approximated in an actual helicopter flight. The airframe is not a linear system, as shake tests of the AH-1G showed, but it appears that it can be represented as linear for most practical engineering purposes.

The second assumption is a workable approximation under some conditions of change and not under others. It is important to note that the mobilities used in analytical testing must be physically realizable and consistent for any driving-point. Mobilities obtained using a lumped mass representation of the rotor at the hub violate this requirement but the practical effect of the violation is not known. Ideally, the mobilities of the airframe would contain the dynamic effects of a rotating rotor in a vacuum and this might be approximated by coupling theoretical rotor mobilities with shake test airframe mobilities in the analytical testing equation, except that the partial derivatives of in-plane hub motions with respect to in-plane hub forces have periodic coefficients. It is not analytically difficult to handle this problem, and therefore remove this particular limitation, but the practicality of doing so has not been established. The effect on change estimates of airframe mobilities without a rotating rotor in a vacuum is discussed in Appendix B.

The basic analytical testing equation is of the form

$$\{q'\} = \{q\} - [A]\{r\} \tag{13}$$

where q is the vector of complex motions (vibrations or strains) on the airframe measured in flight without a structural change, r is the vector of complex motions measured in flight at the coordinates of the structural change, q' is the vector of complex flight motions that result from the change and A is

a matrix function of measured airframe mobilities and mobilities of the structural change. If the structural change has negligible effect on the structural dynamics of the helicopter, the A matrix is nearly null and Ar is negligible; resulting flight vibrations and strains are virtually unchanged. If, on the other hand, the structural change has a significant effect on the dynamics such that the absolute values of the Ar terms are much greater than the absolute values of the q terms, then the change will make the flight vibrations and strains much higher. It is seen, therefore, that analytical testing is least sensitive to errors in mobilities or modeling of the structural change when: (1) the structural change has negligible effect on flight vibrations and strains; and (2) the structural change results in much higher flight vibrations and strains.

The practical consequence is that one does not need high precision mobilities or change modeling to filter out quite rapidly those structural changes which either do not significantly change flight vibrations or strains or those structural changes which will significantly worsen flight vibrations or strains. Since most changes contemplated in the life cycle of a military helicopter are for mission improvement, not dynamics or stress improvement, there is an obvious value in using approximate but not precise structural dynamics data to identify those changes which are likely to create serious flight structural problems before proceeding with flight testing the changes or with more expensive and more precise measures of analysis and test.

## APPLICATIONS OF ANALYTICAL TESTING

The following numerical illustrations of the analytical testing methodology utilize ground and flight vibration data obtained from an Army AH-1G test vehicle. The types of dynamic changes which are considered include mass, stiffness, absorber, and active suppressors. Except for the mass change example, the analytical testing illustrations are hypothetical. In addition, these results do not suggest applicability to the AH-1G or any specific helicopter.

## Test Vehicle and Test Conditions

The AH-1G is an armed helicopter that is configured with two-bladed, teetering main and tail rotors. Armaments include nose mounted and wing mounted weapons. A plan side view of the AH-1G is shown below.

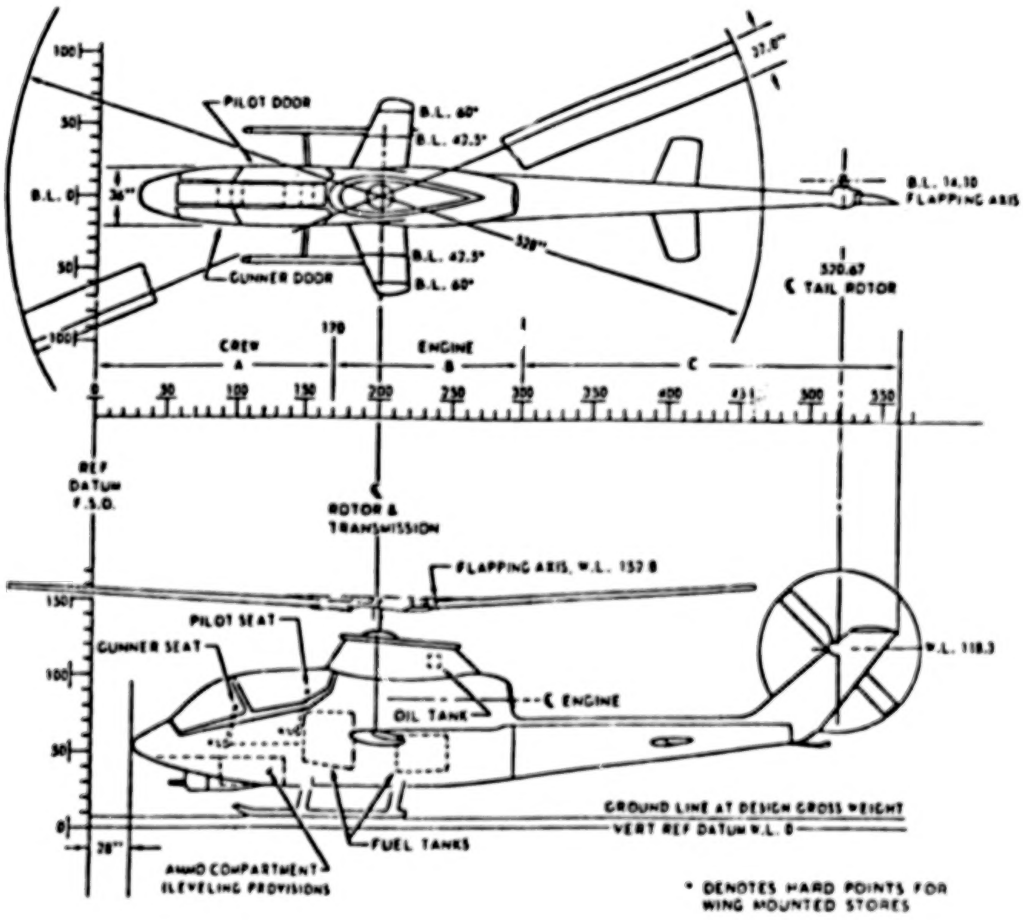


## Mass Changes

Any change of a structural nature in a helicopter can be described in terms of its attachment point mobilities which include the effects of stiffness, mass, and damping of the change. However, the most common changes can be described essentially as mass changes. Among these are external stores added to or taken from the aircraft as exemplified by rocket pods, bombs, missiles, guns, and

external fuel. There is often an extremely large number of possible combinations of external stores on helicopters because of the variety of missions. Cargo and transport helicopters have many variations in payload of a mass change nature. There are mass changes from fuel burn-off, depletion of ammunition, and firing of rockets or missiles.

In the continuing development of a helicopter it would be expeditious to predict the effects of flight stresses and vibration of such changes so that problem areas can be anticipated, engineering judgments can be made, and corrective action prepared with minimum trial-and-error testing. Allowing for flight data scatter, the engineer would make such predictions at several critical locations with analytical testing for critical classes of maneuvers. It is impractical to attempt precise predictions for every possible airspeed, gross weight, c.g. location, yaw rate, pitch rate, roll rate, power setting, air temperature, wind condition, altitude, etc., and for all the locations of interest on the helicopter. In a well developed helicopter analytical testing would be used for major changes, such as the contemplated addition of rocket pods, but in a helicopter in the early stages of development analytical testing would be applied to a wider variety of mass changes to aid in identifying possible problems.

## A Flight Example for Mass Changes

The AH-1G is used to illustrate the analytical testing methodology. Consider the hypothetical situation of an AH-1G which had never flown with rocket pods. An addition of rocket pods weighing 181 kg (400 lb) each to the outboard wing station is contemplated. This represents a 9.4 percent increase in the gross weight of the helicopter. The predictions are made from the clean configuration for classes of maneuvers without accounting for additional drag, fuel burnoff, or other causes of possible changes in external aerodynamic loading.

The following flight acceleration data were taken on an as-available basis from another project. No strain data were available. The clean configuration, without rocket pods, had a take-off gross weight of 3830 kg (8465 lb) and was

flown in ground winds of 5 to 7 knots, Outside Air Temperature (OAT) of 10°C (50°F) and 766 mm (30.17 in.) Hg barometric pressure. The flights with the rocket pods were made at 4106 kg (9075 lb) take-off gross weight with ground winds of 3 to 5 knots, OAT of 20°C (68°F) and 754 mm (29.68 in.) Hg barometric pressure. The c.g. was at FS 196.3 in both flights. Power and control settings were not necessarily matched in the flights. Data were analyzed for the condition of highest peak-to-peak vibration of a set of selected points, differing from flight to flight, in each class of flight condition with a harmonic analysis over five to eight rotor revolutions. Except for the unavailability of strains, this situation is representative of practical application of analytical testing.

The mobilities of the left and right wing stores positions for vertical motion constitute a 2 x 2 complex matrix. These are at Butt Lines ±60 and are identified as Z200L and Z200R.

$$\left[\ddot{Y}_{rr}\right] = \begin{bmatrix} .054/-8° & .012/14° \\ .012/14° & .040/8° \end{bmatrix} \frac{g}{1000\ N} \qquad (14)$$

Analytical testing predictions were made for nine motion coordinates shown in the sketch below.

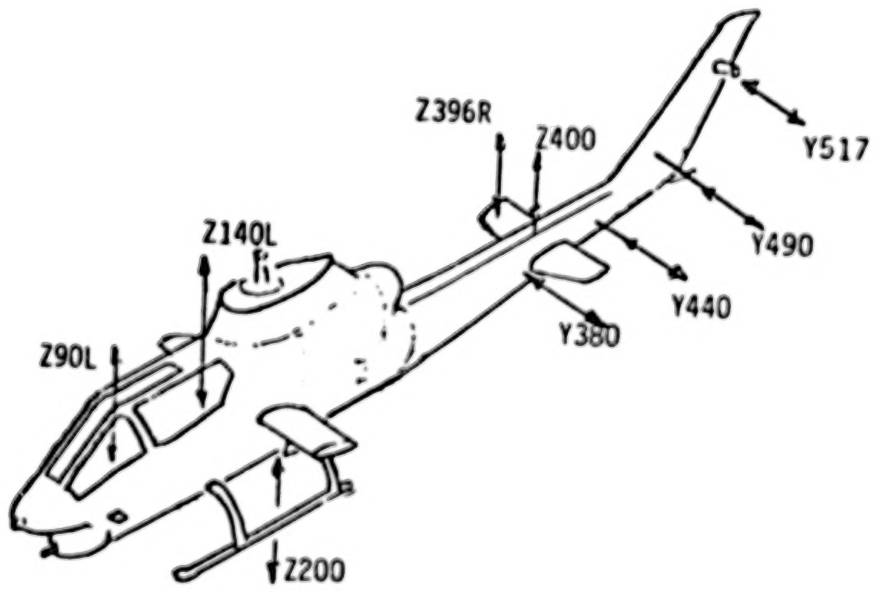

The matrix of mobilities for these nine coordinates relative to forcing at Z200L and Z200R is as follows:

$$\left[\ddot{Y}_{jr}\right] = \begin{array}{l} \\ \text{Z200} \\ \text{Z90L} \\ \text{Z140L} \\ \text{Z396R} \\ \text{Z400} \\ \text{Y380} \\ \text{Y440} \\ \text{Y490} \\ \text{Y517} \end{array} \begin{array}{c} \begin{array}{cc} \text{Z200L} & \text{Z200R} \end{array} \\ \begin{bmatrix} .033/-4° & .052/9° \\ .017/22° & .024/-140° \\ .046/5° & .018/-176° \\ .046/-19° & .068/11° \\ .100/-49° & .049/-97° \\ .193/144° & .208/-48° \\ .091/-167° & .086/8° \\ .065/77° & .084/-96° \\ .168/130° & .151/-53° \end{bmatrix} \end{array} \frac{g}{1000\ N} \qquad (15)$$

The vibration, in g units, resulting from the change is obtained from equation (11)

$$\left\{\ddot{q}'_j\right\} = \left\{\ddot{q}_j\right\} - \left[\ddot{Y}_{jr}\right] \left( \begin{bmatrix} \frac{1}{181kg} & 0 \\ 0 & \frac{1}{181kg} \end{bmatrix} \frac{1}{G} + \left[\ddot{Y}_{rr}\right] \right)^{-1} \left\{\ddot{q}_r\right\} \qquad (16)$$

where G is the gravitational acceleration. The effects of this mass change, using equation (16), on 2P(10.8 Hz) vibrations are summarized in the following discussions.

Level flights. - The effect of the pods at $.5V_H$, shown in Table I, is small. The aft tail lateral accelerations, which are sensitive to main rotor 2P forces on the vertical fin, are higher than predicted but still low. At $V_H$ the pods result in lower vertical vibration, as shown in Table II, but the change is not very great. The lateral vibration at FS Y380 was predicted to increase and showed a greater increase in the pod flight. The decrease in vibration at FS Y490 and FS Y517 was significantly greater than predicted. Whether the difference is due to inaccuracy of the method, the 181 kg (400 lb) weight difference, or the 8 knot air speed difference is not known but the general conclusions from the prediction are reflected in the flight with the pods. Gross weight difference results from fuel burnoff.

TABLE I. - 2P VIBRATION IN STRAIGHT AND LEVEL FLIGHT AT .5 $V_H$, g

| | Flight of clean configuration | Predicted for flight with pods | Flight with pods |
|---|---|---|---|
| | 3840 kg (8465 lb) gross weight | 4203 kg (9265 lb) gross weight | 4035 kg (8895 lb) gross weight |
| | 70 knots | | 67 knots |
| Z200 | .10/0° | .09/0° | .11/14° |
| Z90L | .03/83° | .02/73° | .03/100° |
| Z140L | .04/33° | .03/24° | .03/43° |
| Z396R | .25/-21° | .23/-22° | .21/-9° |
| Z400 | .22/-19° | .21/-16° | .20/-8° |
| Y380 | .07/262° | .12/85° | .10/119° |
| Y440 | .14/233° | .16/126° | .21/137° |
| Y490 | .18/22° | .17/133° | .26/148° |
| Y517 | .29/201° | .29/151° | .37/167° |

TABLE II. - 2P VIBRATION IN STRAIGHT AND LEVEL FLIGHT AT $V_H$, g

| | Flight of clean configuration | Predicted for flight with pods | Flight with pods |
|---|---|---|---|
| | 3840 kg (8465 lb) gross weight | 4203 kg (9265 lb) gross weight | 4017 kg (8855 lb) gross weight |
| | 144 knots | | 136 knots |
| Z200 | .20/73° | .18/73° | .15/85° |
| Z90L | .20/133° | .18/129° | .18/125° |
| Z140L | .18/114° | .15/109° | .16/104° |
| Z396R | .31/48° | .27/48° | .22/48° |
| Z400 | .34/44° | .32/45° | .31/46° |
| Y380 | .19/206° | .25/156° | .31/177° |
| Y440 | .61/-145° | .66/-152° | .64/-167° |
| Y490 | .88/-150° | .82/-152° | .50/-148° |
| Y517 | 1.66/-138° | 1.57/-142° | 1.15/-144° |

Gunnery runs. - The data for the flight of the clean aircraft were not necessarily taken for a portion of the rolling pullout comparable to that for which those data were taken on the flight with the pods. From the prediction of the effects of the pods, shown in Table III, the pods have little effect on the vibration at some locations and cause a decrease in the vibration at others in a high load factor rolling pullout to the left. The pod flight data leads to the same conclusion. The same situation pertains in a rolling pullout to the right, shown in Table IV. In this case the predictions for FS Z396R and FS Y517 showed reductions that were not seen in the pod flight as did the prediction for FS Y380 in Table III. However, considering the nature of the data samples, the conclusion of the prediction is reflected in the pod flight.

Sideward flight and landing. - The flight data in Table V are samples taken from sideward flight to the right to 35 knots with reversal and sideward flight to the left to 35 knots. There is no significant change in vibration due to the pods in sideward flight or in approach and landing. The phase angles of the data at very low g-levels, determined from harmonic analysis, are highly variable. In approach and landing with pods, Table VI, the data sample shows low vibration at FS 490 and FS 517, fin stations of large vibration scatter, and is most likely the result of the time sample chosen.

TABLE III. - 2P VIBRATION IN ROLLING PULLOUT TO LEFT, g

| | Flight of clean configuration | Predicted for flight with pods | Flight with pods |
|---|---|---|---|
| | 3645 kg (8035 lb) gross weight | 4130 kg (9105 lb) gross weight | 3966 kg (8744 lb) gross weight |
| | 187 knots 1.42 g load factor | | 186 knots 1.52 g load factor |
| Z200 | .53/85° | .52/89° | .58/84° |
| Z90L | .46/118° | .42/117° | .42/116° |
| Z140L | .47/105° | .42/103° | .40/104° |
| Z396R | .52/73° | .42/75° | .54/76° |
| Z400 | .94/68° | .83/70° | .79/66° |
| Y380 | .50/-126° | .32/-158° | .52/-157° |
| Y440 | 1.28/-115° | 1.25/-120° | 1.04/-141° |
| Y490 | 1.27/-116° | 1.19/-114° | .93/-121° |
| Y517 | 1.82/-91° | 1.60/-89° | 1.59/-92° |

TABLE IV. - 2P VIBRATION IN ROLLING PULLOUT TO RIGHT, g

| | Flight of clean configuration | Predicted for flight with pods | Flight with pods |
|---|---|---|---|
| | 3792 kg (8361 lb) gross weight | 4155 kg (9161 lb) gross weight | 4042 kg (8909 lb) gross weight |
| | 164 to 128 knots 1.78 to 1.5 g load factor | | 162 knots 1.23 g load factor |
| Z200 | .36/84° | .32/85° | .24/79° |
| Z90L | .49/129° | .44/128° | .31/117° |
| Z140L | .43/115° | .37/113° | .31/106° |
| Z396R | .33/55° | .26/56° | .47/71° |
| Z400 | .82/61° | .72/61° | .63/60° |
| Y380 | .47/-121° | .24/193° | .24/-167° |
| Y440 | .97/-114° | .94/-123° | .79/-158° |
| Y490 | .71/-121° | .61/-116° | .47/-144° |
| Y517 | .85/-106° | .58/-107° | .85/-123° |

TABLE V. - 2P VIBRATION IN SIDEWARD FLIGHT, g

| | Flight of clean configuration | Predicted for flight with pods | Flight with pods |
|---|---|---|---|
| | 3688 kg (8130 lb) gross weight | 4051 kg (8930 lb) gross weight | 3980 kg (8774 lb) gross weight |
| | 35 knots right to 35 knots left | | |
| Z200 | .23/142° | .20/143° | .25/130° |
| Z90L | .11/145° | .10/147° | .12/138° |
| Z140L | .13/144° | .12/144° | .12/138° |
| Z396R | .26/137° | .22/136° | .18/131° |
| Z400 | .25/132° | .22/140° | .23/125° |
| Y380 | .03/-46° | .01/-31° | .02/-52° |
| Y440 | .08/-43° | .06/-47° | .08/-82° |
| Y490 | .03/54° | .03/47° | .04/104° |
| Y517 | .02/45° | .04/73° | .01/-142° |

TABLE VI. 2P VIBRATION IN APPROACH AND LANDING, g

| | Flight of clean configuration | Predicted for flight with pods | Flight with pods |
|---|---|---|---|
| | 3613 kg (7966 lb) gross weight | 3976 kg (8766 lb) gross weight | 4002 kg (8824 lb) gross weight |
| Z200 | .14/-13° | .13/-13° | .14/-21° |
| Z90L | .10/31° | .09/29° | .07/24° |
| Z140L | .11/12° | .10/9° | 08/2° |
| Z396R | .24/-47° | .22/-49° | .20/-38° |
| Z400 | .27/-24° | .25/-20° | .25/-28° |
| Y380 | .10/126° | .10/82° | .08/111° |
| Y440 | .18/140° | .19/131° | .15/-121° |
| Y490 | .15/137° | .13/136° | .01/174° |
| Y517 | .24/-40° | .29/-33° | .05/-161° |

## Vibration Absorber Changes

All major helicopter manufacturers have used conventional spring-mass vibration absorbers with varying degrees of success. Except for in-plane centrifugal hub absorbers which are used to cancel (N-1)P and (N+1)P shears in the rotating system of helicopters, absorbers are customarily tuned to be coincident with the excitation frequency and placed at the airframe location where vibration reduction is needed. In limited applications, airframe absorbers have been remotely placed from points where low vibration is desired. The remote absorber has the advantage of providing vibration reduction at locations where conventional airframe absorbers are physically impractical. These remote absorbers have been trial-and-error tuned to be somewhat off resonance to achieve optimum vibration reduction.

Airspeed, gross weight, and center of gravity variations alter the relative magnitudes and phasings of airframe responses, thus absorber effectiveness varies. There are two situations in which the effects of absorbers are independent of the airspeed and flight maneuver of the helicopter. First, is the extreme situation with absorbers coincident to each vectorial coordinate of external forces and moments acting on the helicopter. In this case, the entire airframe has virtually zero vibration at all airspeeds and in all maneuvers. The second situation is at the attachment point of the absorbers along the absorber direction. Clearly, the dynamicist must consider the flight effects of a limited number of absorbers at airframe locations remote from the absorbers.

For single-point or discrete impedance changes, equations (11) and (12) reduce to simple scalar algebra equations for estimating the effects on vibrations or strains. The vibration absorber analytical testing equations become for acceleration, after simplifying equation (11),

$$\ddot{q}'_j = \ddot{q}_j - \frac{\ddot{Y}_{jr}\,\ddot{q}_r}{\ddot{Y}^c_{rr} + \ddot{Y}_{rr}} \tag{17}$$

and, for strain, after simplifying equation (12)

$$\varepsilon_j' = \varepsilon_j - \frac{\ddot{Y}_{jr}^{(\varepsilon)} \ddot{q}_r}{\ddot{Y}_{rr}^{c} + \ddot{Y}_{rr}} \tag{18}$$

where $\ddot{Y}_{rr}^{c}$ is the unrestrained driving-point acceleration mobility of the absorber at its attachment point r. For a structurally damped absorber, the unrestrained driving-point acceleration mobility is

$$\ddot{Y}_{rr}^{c} = \frac{1 - \omega^2/\Omega_T^2 + ig}{m(1+ig)} \tag{19}$$

where $\Omega_T$ is the tuning frequency, m is the absorber mass, and g is the nondimensional structural damping coefficient. Similarly, with viscous damping

$$\ddot{Y}_{rr}^{c} = \frac{1 - \omega^2/\Omega_T^2 + i2\zeta\omega/\Omega_T}{m(1+i2\zeta\omega/\Omega_T)} \tag{20}$$

where $\zeta$ is the viscous damping factor. As equations (17) and (18) show, the required absorber weight, tuning frequency (not necessarily equal to the excitation frequency), and damping (not necessarily zero) for minimum vibration or strain along the motion coordinate j are functions of the flight vibration at r, the flight vibration or strain at j, the r-j mobility, and the r-r mobility. A vibration absorber can be designed to minimize both vibrations and strains. For vibratory strains the required r-j mobility is defined as the strain mobility.

Vibration attenuation is a fundamental objective in dynamics and equation (17) can be written in a slightly different form as

$$\ddot{q}_j'/\ddot{q}_j = 1.0 - \frac{\ddot{Y}_{jr} \ddot{q}_r/\ddot{q}_j}{\ddot{Y}_{rr}^{c} + \ddot{Y}_{rr}} \tag{21}$$

The effects of tuning and damping on vibration at j can be examined by plotting the absolute value of $(\ddot{q}_j'/\ddot{q}_j)$ versus the tuning ratio, $\Omega_T/\omega$, for fixed values of damping. Interactive computer graphics offer the capability to investigate the effects at various critical airframe locations to select the tuning frequency for the optimum overall effect. A weighting factor can be assigned to

$|\ddot{q}'/\ddot{q}|$ for each station and one composite curve can be displayed for many stations.

Conventional absorbers are analyzed with regard to vibration at the absorber attachment point r. If j replaces r in equation (21), then the absorber transmissibility becomes

$$\ddot{q}'_r/\ddot{q}_r = \frac{\ddot{Y}^c_{rr}}{\ddot{Y}^c_{rr} + \ddot{Y}_{rr}} \tag{22}$$

or, after substituting for $\ddot{Y}^c_{rr}$ in equation (19),

$$\ddot{q}'_r/\ddot{q}_r = \frac{1 - \omega^2/\Omega_T^2 + ig}{1 - \frac{\omega^2}{\Omega_T^2} + \ddot{Y}^R_{rr}m - \ddot{Y}^I_{rr}mg + i\left(\ddot{Y}^I_{rr}m + mg\ddot{Y}^R_{rr} + g\right)} \tag{23}$$

The percentage reduction of vibration at the absorber attachment point is, of course, independent of the flight vibration. A conventional absorber with zero damping produces zero vibration when $\ddot{Y}^c_{rr}$ is zero or when the tuning frequency coincides with the excitation frequency. When the forcing frequency equals the tuning frequency, equation (23) gives

$$\ddot{q}'_r/\ddot{q}_r = \frac{g}{m}\left[\frac{i}{\ddot{Y}^R_{rr} - \ddot{Y}^I_{rr}\, g + i\left(\ddot{Y}^I_{rr} + g\,\ddot{Y}^R_{rr} + \frac{g}{m}\right)}\right] \tag{24}$$

Thus, for a given absorber damping the attachment point vibration ratio is inversely proportional to the absorber mass.

The imaginary part of the helicopter driving-point acceleration mobilities is necessarily positive, but the real part may be either positive or negative. Because helicopter structures do not have proportional damping the modes are, in general, complex and, even in the vicinity of a well separated mode with a high rr modal acceleration (residue), the real part of the driving-point mobility is not necessarily smaller just below resonance than just above a resonance

as in structures with classical modes. For structures with classical modes, the signs of the real parts of the driving-point mobilities may be the same just above and just below a resonance, due to coupling of other modes, and that sign may be positive or negative. Therefore, the resonance introduced by the addition of the absorber may occur above or below the driving-point antiresonant frequency created by the absorber. Because the driving-point mobility is a function of frequency it is necessary to examine equation (22) over a frequency spectrum to determine the absorber bandwidth, that is, the change in resultant vibration with variation in excitation frequency or rotor speed.

As seen from equation (24), the vibration ratio at the attachment point is, for small damping, directly proportional to the damping. This leads to the misconception that minimal absorber damping is desirable regardless of the location of the absorber and the point of concern on the helicopter.

Obtaining zero vibration. - In equation (21) let $\ddot{q}_j$ be zero. Then,

$$\ddot{Y}_{rr}^{c} = \ddot{Y}_{jr} \frac{\ddot{q}_r}{\ddot{q}_j} - \ddot{Y}_{rr} \tag{25}$$

The absorber mobility required for zero vibration along the j motion coordinate is a function of the in-flight vibration of the motion coordinate j and that of the absorber, r. The complex $\ddot{q}_r/\ddot{q}_j$ ratio will usually be different for each flight condition and zero vibration at j from an absorber at r is dependent on the flight condition. Since the driving-point imaginary acceleration mobility must be positive, it is necessary but not sufficient for the imaginary part of the right hand side of equation (25) to be positive for zero vibration. Through control of absorber damping zero vibration at a desired point can be achieved in any one flight condition only under certain circumstances.

## Examples of Absorber Analysis

The following examples are presented to illustrate the applicability of analytical testing for examining the effects of absorbers on AH-1G airframe vibrations. The absorber is a simple spring-mass device with hysteretic damping as discussed for equation (19). Equations (21) and (22) are used to determine the performance of the absorber at critical points on the airframe for several representative flight conditions.

Absorber at nose. - This example considers the effects on vertical vibration at the gunner's left (FS Z90L) and at the horizontal stabilizer (FS Z400). A vertical absorber, weighing 13.61 kg (30 lb), is located at the nose (FS Z50) of the AH-1G as shown in the sketch below.

The acceleration mobilities which were measured during the ground vibration test are

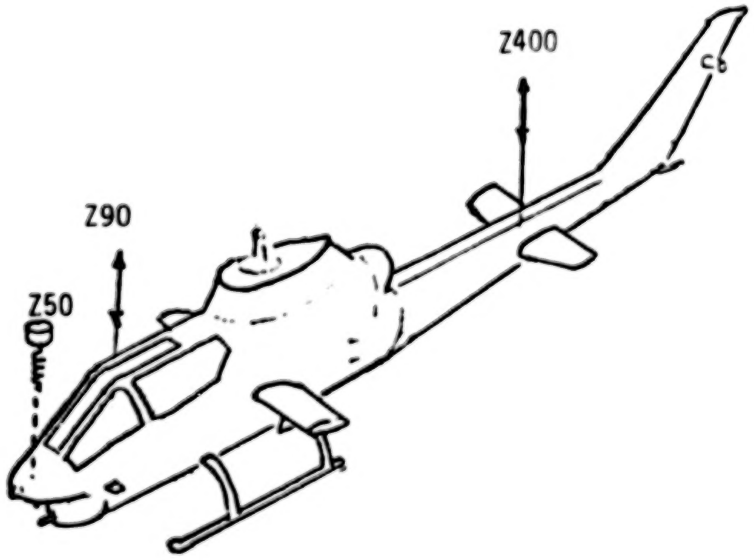


$$\begin{Bmatrix} \ddot{Y}\ (Z50,\ Z50) \\ \ddot{Y}\ (Z90,\ Z50) \\ \ddot{Y}\ (Z400,Z50) \end{Bmatrix} = \begin{Bmatrix} .100\ g/1000\ N\ (.044\ g/100\ lb)/10° \\ .09\ \ g/1000\ N\ (.040\ g/100\ lb)/8° \\ .232\ g/1000\ N\ (.103\ g/100\ lb)/123° \end{Bmatrix} \tag{26}$$

The vibrations measured in flight are shown in Table VII. The driving-point mobility at FS Z50 is nearly the same as the transfer mobility between Z50 and Z90L and the flight vibrations of these coordinates are only slightly different in magnitude, but significantly different in phase. The effect of the nose absorber on gunner vibration will not be the same as the effect of an absorber directly at the gunner station.

TABLE VII. - VERTICAL 2P (10.8 Hz) VIBRATIONS, g

| | Z50 Nose | Z90 Gunner's left | Z400 Horizontal stabilizer |
|---|---|---|---|
| 187 kts rolling pullout left | .426/150° | .464/118° | .938/68° |
| 161 kts rolling pullout right | .533/156° | .494/129° | .818/61° |
| 144 kts | .215/168° | .201/133° | .344/44° |
| 103 kts 45° turn | .121/162° | .131/116° | .237/92° |
| Sideward flight R & L to 35 kts | .106/152° | .113/145° | .249/132° |
| Approach and landing | .095/-69° | .100/-31° | .271/-24° |

Figure 1 shows the variation in vertical vibration at the gunner's left with variation in the tuning and damping of the nose absorber. The abscissa scale is not the same as an RPM sweep because the mobilities and the vibrations would change in an RPM sweep. It is impractical to do an RPM sweep in every maneuver. However, sensitivity to changes in the tuning frequency are indicative of bandwidth.

In most plots of Figure 1, a change in the absorber tuning of less than 1% causes a significant change in gunner's seat vibration, indicating an impractically narrow bandwidth. Note that 2% structural damping, not zero damping, in the absorber gives minimum gunner vibration at 144 knots and in a 103-knot turn, but in other maneuvers zero damping gives the minimum. In the rolling

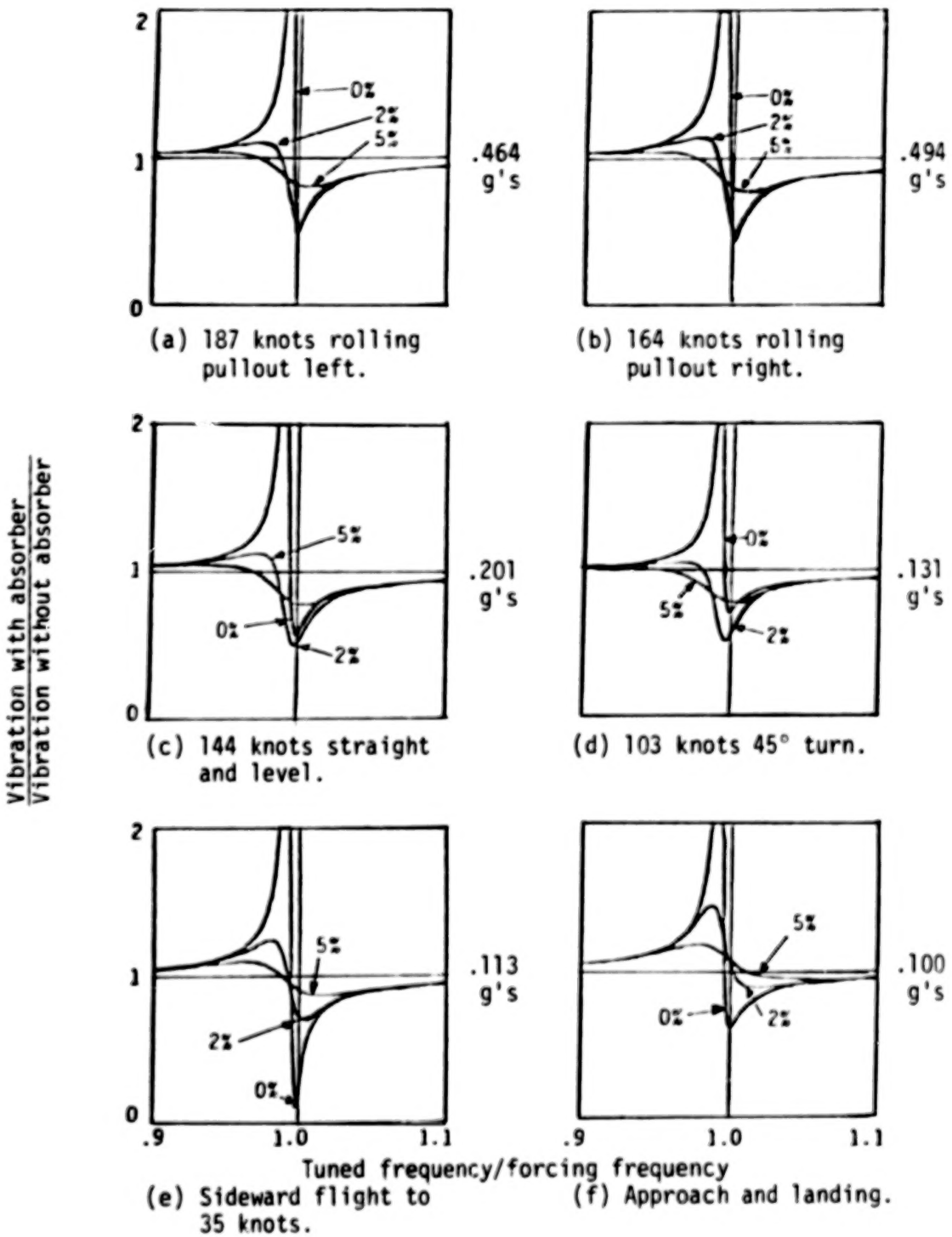


Figure 1. - Effect on gunner vertical (FS Z90) vibration of 13.61 kg (30 lbs) vertical absorber at nose (FS Z50) for 0%, 2%, and 5% absorber structural damping.

pullouts 2% damping reduces the peak of mistuning more than it raises the depth of the valley. The tuning ratio for minimum vibration is very close to 1.0 and for gunner's seat attenuation the absorber is tuned to 2P or 10.8 Hz.

The effect of the nose absorber on the vertical vibration at the horizontal stabilizer (FS Z400) is shown in Figure 2. The absorber frequency for minimum vibration shifts somewhat with maneuvers but is generally lower than 2P. Figure 2 also indicates that tuning the nose absorber to 2P (10.8 Hz) to minimize gunner vibration will increase the horizontal stabilizer vibration by a substantial amount in most flight conditions. The converse is true if the nose absorber is tuned to minimize horizontal stabilizer vertical vibration.

There is also a significant change in vibration between zero and 2% damping. The extreme sensitivity of vibration at the gunner's station and the horizontal stabilizer station to absorber tuning and absorber damping suggests that an absorber at the nose would have to weigh much more than 13.61 kg (30 lb) to be useful.

Absorber at the tail rotor. - The principal concern in this example is minimization of the lateral vibration at FS Y490, where the vertical stabilizer joins the tail boom. A lateral absorber, weighing 13.61 kg (30 lb), is located at the tail rotor gearbox as shown in the sketch on page 30.

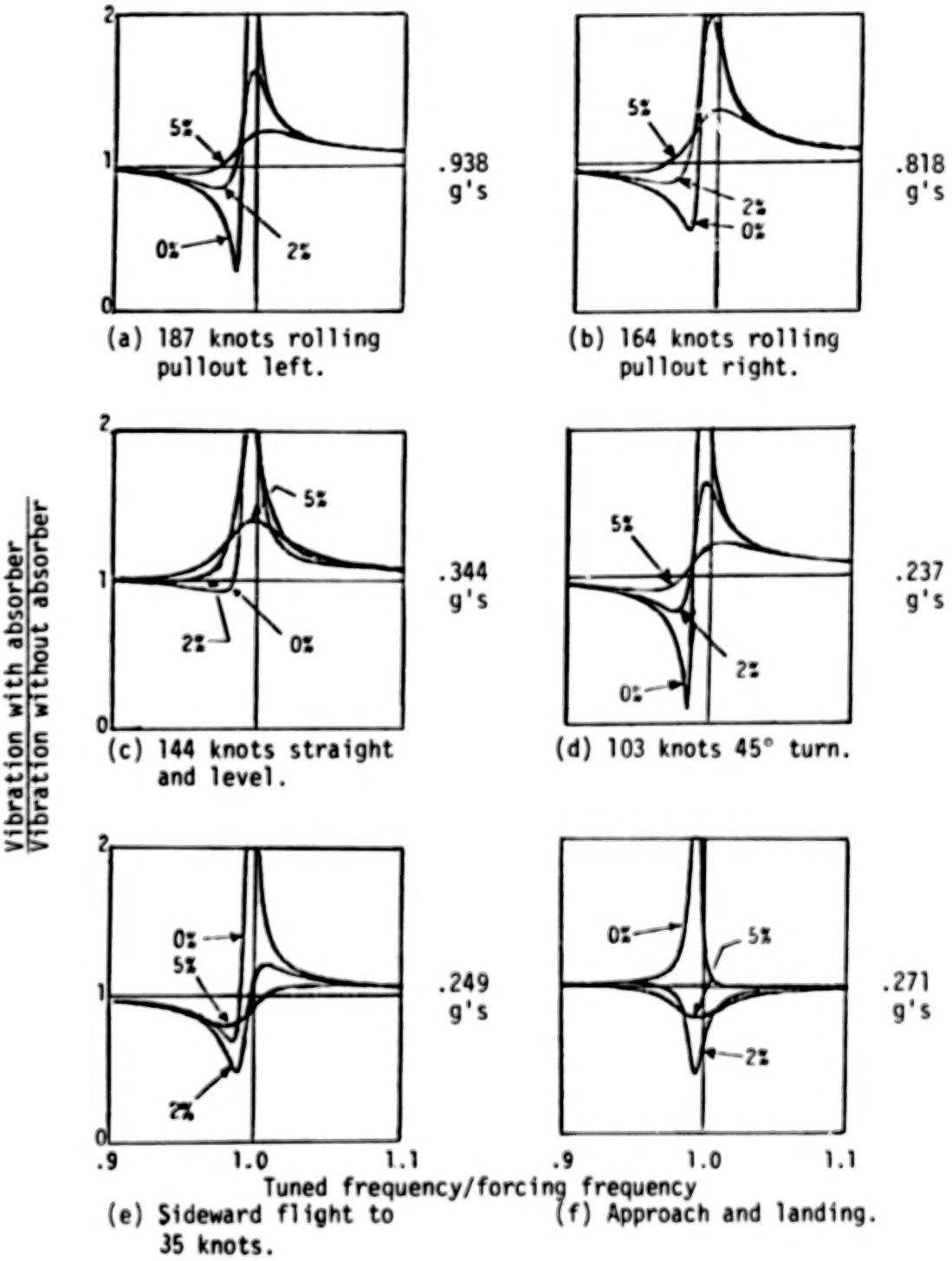


Figure 2. - Effect on stabilizer vertical (FS Z400) vibration of 13.61 kg (30 lb) vertical absorber at nose (FS Z50) for 0%, 2%, and 5% absorber structural damping.

The pertinent acceleration mobilities are

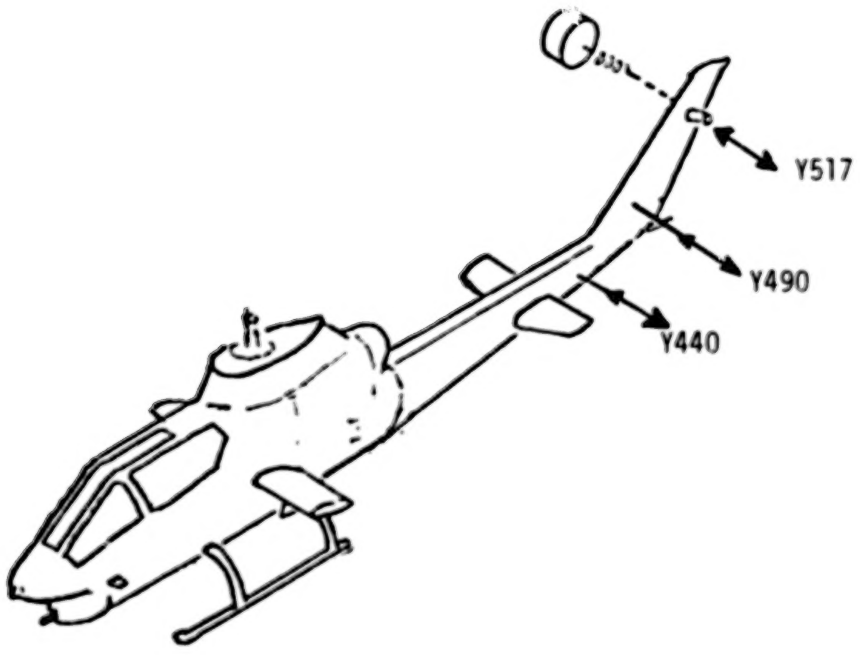


$$\begin{Bmatrix} \ddot{Y}(Y517,Y517) \\ \ddot{Y}(Y490,Y517) \\ \ddot{Y}(Y440,Y517) \end{Bmatrix} = \begin{bmatrix} 3.597\ g/1000\ N\ (1.583\ g/100\ lb)/17° \\ 1.576\ g/1000\ N\ (.693\ g/100\ lb)/20° \\ .535\ g/1000\ N\ (.235\ g/100\ lb)/2° \end{bmatrix} \quad (27)$$

and the flight accelerations are given in Table VIII.

The lateral response at the absorber attachment point, for 2% absorber damping is shown in Figure 3. Comparison of Figure 3 to Figures 1 and 2 (note abscissa scale change) shows that the tail rotor gearbox absorber is much less sensitive to the frequency ratio, indicating a broader bandwidth than the nose absorber. The high lateral driving-point mobility at the tail rotor gearbox explains this improvement. As seen from equation (22), the flight accelerations cancel at the absorber attachment point and Figure 3 is, therefore, the same for all flight conditions.

TABLE VIII. - LATERAL 2P (10.8 Hz) VIBRATIONS, g

| | Y517 | Y490 | Y440 |
|---|---|---|---|
| 187 kts rolling pullout left | 1.815/-91° | 1.266/-116° | 1.282/-115° |
| 164 kts rolling pullout right | .851/-106° | .710/-121° | 967/-114° |
| 144 kts | 1.797/-133° | .878/-150° | .611/-145° |
| 103 kts 45° turn | .405/171° | .233/175° | .118/-170° |
| Sideward flight R & L to 35 kts | .017/-45° | .031/-54° | .075/-43° |
| Approach and landing | .238/-40° | .150/137° | .184/140° |

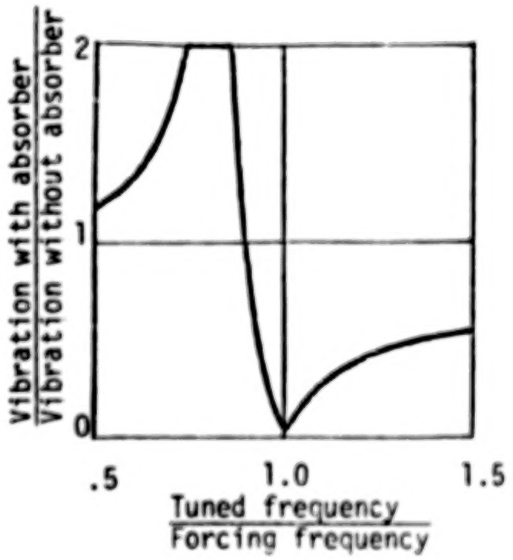


Figure 3. - Lateral response at the tail rotor gearbox (FS Y517) for 2% structural damping.

Comparing Figure 4 with Figures 1 and 2 shows that the tail rotor absorber effects on fin lateral vibration are much less sensitive to tuning and absorber damping than the nose absorber effects on vertical vibration at the gunner's station and stabilizer station. Although the variations in minimum vibration with damping are small in Figure 4, the minimum is lowest with zero damping, except in the 187-knot rolling pullout where 5% structural damping gives the lowest vibration. The absorber tuning frequency for the minimum vibration varies somewhat with flight condition but is near 90% of 2P in most cases. In this example a tuning frequency of about 9.7 Hz appears to be the best compromise. Such a selection, as seen from Figure 4, would result in much higher fin vibration in approach and landing. Referring to Figure 3, a tuning frequency of about 9.7 Hz gives almost the same vibration at the absorber attachment point. Figure 5 shows the vibration at FS Y440 for variation in tuning of the absorber with 2% absorber structural damping. The 9.7 Hz tuning frequency would have a minor effect at this location in most flight conditions.

The engineer must be cautious of the effects of RPM changes and as a first approximation the engineer, assuming the vibrations to remain constant with RPM change given no RPM sweep flight data, would utilize the mobility spectrum data to create plots similar to those of Figure 4 with an inverted abscissa parameter: i.e., variation in forcing frequency for the tuning frequency selected. This would be done on the interactive computer for all locations and directions of importance over the RPM range allowable in flight.

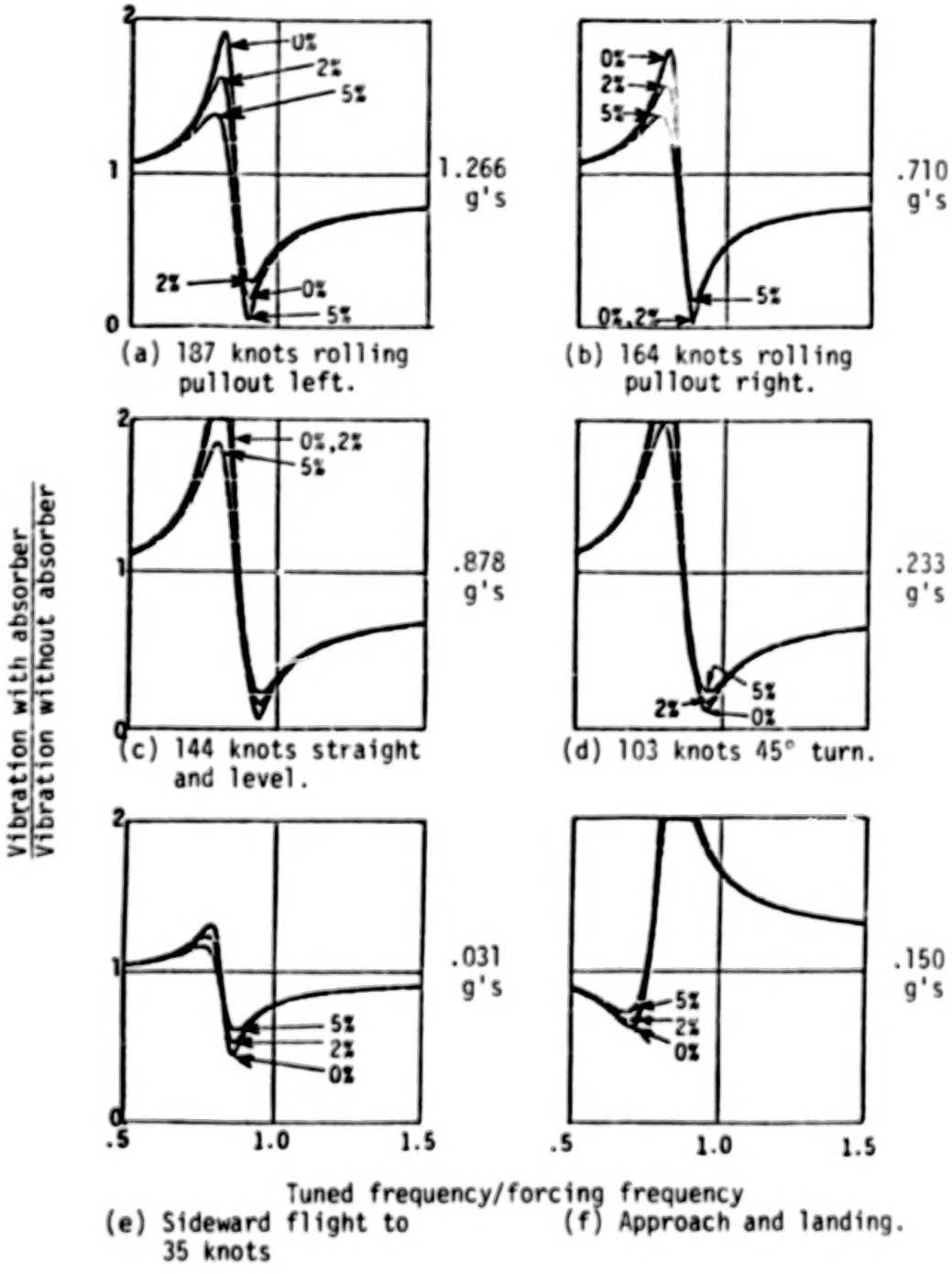


Figure 4. - Effect on fin lateral (FS Y490) of 13.61 kg (30 lb) lateral absorber at tail rotor for 0%, 2%, and 5% absorber structural damping.

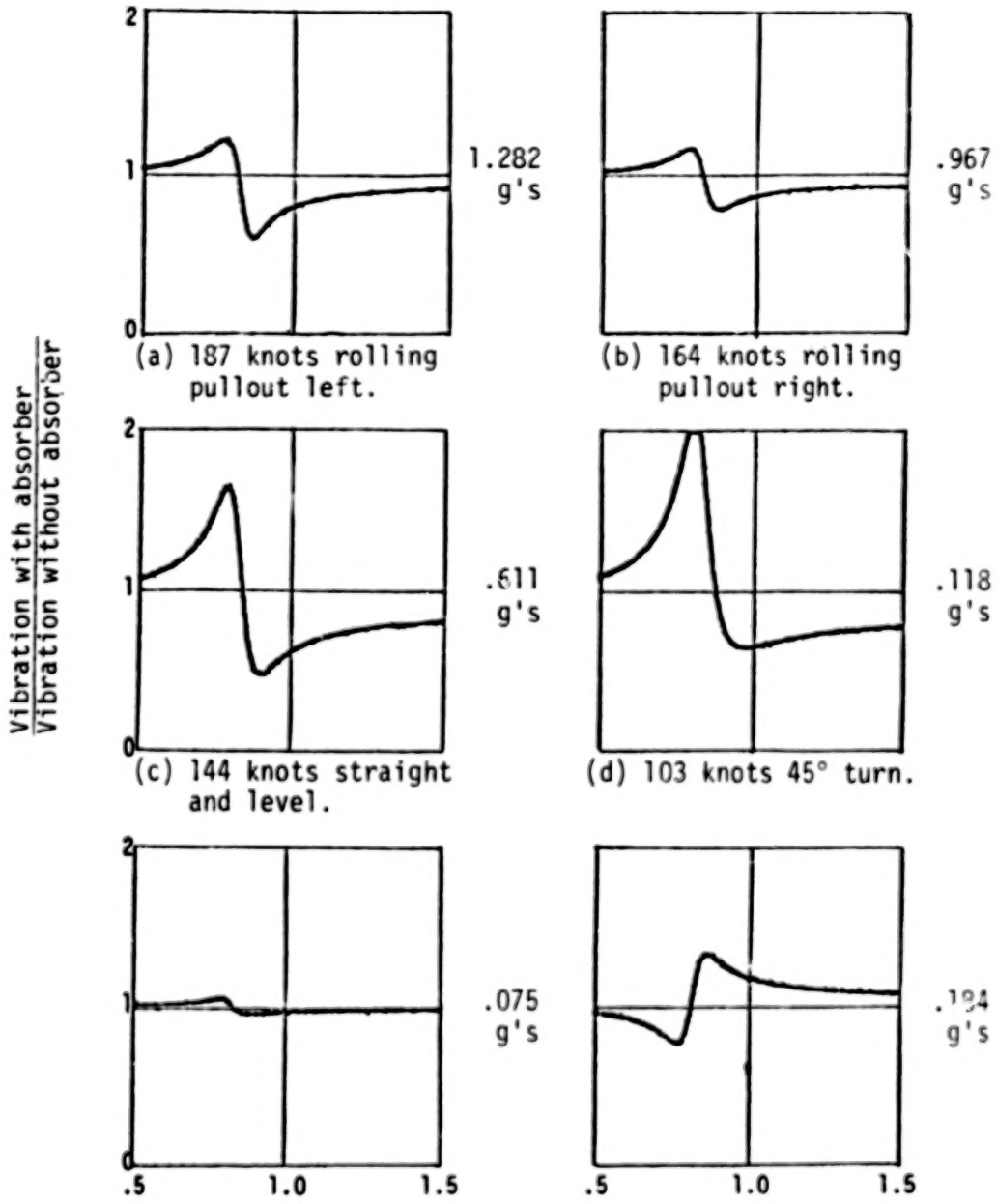


Figure 5. - Effect on boom lateral (FS Y440) of 13.61 kg (30 lb) lateral absorber at tail rotor for 2% absorber structural damping.

## Active Vibration Suppression

Vibration suppression and vibration isolation are distinguished by considering suppression to imply something other than separating (isolating) the externally excited structure. Active vibration suppression devices may be applied without consideration of the physical locations of the external exciting forces and moments. In this report the term active is used in the customary sense to indicate a powered device which creates an external force with magnitude and phase controlled by reference to a feedback signal of vibration or strain. The vibration or strain to be controlled will generally not be at the location of the active vibration suppressor.

Active vibration suppression with time-domain control has been highly effective in some applications at frequencies far below the lowest blade passage frequency in helicopters and continuing work in this specialized area may eventually be important at helicopter frequencies, but such matters are beyond the scope of this report. Frequency-domain control of active vibration suppressors, perhaps by minicomputers, is not as frequency limited as time-domain control and is close to the state-of-the-art of shaking hardware. For these reasons, frequency-domain control is implied in the considerations in this report. It is to be understood in the discussions following that any active vibration suppressor can, by the methods described for a given frequency, be simultaneously applied to other frequencies which are not necessarily limited to harmonics of main rotor blade passage frequency.

Minimizing the norm of a set of flight accelerations or strains. - Active vibration suppressors, R in number, can be used to minimize the sum of the squares of K, greater than R, accelerations or strains. Let the $f_r$ complex vector be that of the forces or moments applied by the R active vibration suppressors and the primed quantities be the resulting complex accelerations and strains. The matrix equation which defines this situation is

$$\begin{Bmatrix} \ddot{q}'_a \\ \hline \varepsilon'_s \end{Bmatrix} = \begin{Bmatrix} \ddot{q}_a \\ \hline \varepsilon_s \end{Bmatrix} + \begin{bmatrix} \ddot{Y}_{ar} \\ \hline Y^{(\varepsilon)}_{sr} \end{bmatrix} \{f_r\} \qquad (28)$$

K x 1 K x 1 K x R R x 1

or, more concisely,

$$\underset{K \times 1}{\left\{q_k'\right\}} = \underset{K \times 1}{\left\{q_k\right\}} + \underset{K \times R}{\left[Y_{kr}\right]} \underset{R \times 1}{\left\{f_r\right\}} \tag{29}$$

The sum of the squares (Euclidian norm) becomes

$$\left\{q_k'\right\}^{*T}\left\{q_k'\right\} = \left\{q_k\right\}^{*T}\left\{q_k\right\} + \left\{q_k\right\}^{*T}\left[Y_{kr}\right]\left\{f_r\right\} + \left\{f_r\right\}^{*T}\left[Y_{kr}\right]^{*T}\left[Y_{kr}\right]\left\{f_r\right\} + \left\{f_r\right\}^{*T}\left[Y_{kr}\right]^{*T}\left\{q_k\right\} \tag{30}$$

where * denotes the complex conjugate.

The left hand side of equation (30) is, of course, a real scalar and the minimum sum of the squares is obtained by setting the partial derivative of this complex scalar function with respect to the complex transpose of the $f_r$ vector to zero.

$$\frac{\partial\left\{q_k'\right\}^{*T}\left\{q_k'\right\}}{\partial\left\{f_r\right\}^{*T}} = 0 = 2\left[Y_{kr}\right]^{*T}\left\{q_k\right\} + 2\left[Y_{kr}\right]^{*T}\left[Y_{kr}\right]\left\{f_r\right\}^{(m)} \tag{31}$$

The complex forces from the R active vibration suppressors necessary to minimize the sum of the squares (the Euclidian norm or sum of the squares of the absolute values) of the K (greater than R) vibrations or strains in any flight condition are

$$\left\{f_r\right\}^{(m)} = -\left(\left[Y_{kr}^*\right]^T\left[Y_{kr}\right]\right)^{-1}\left[Y_{kr}^*\right]^T\left\{q_k\right\} \tag{32}$$

or

$$\left\{f_r\right\}^{(m)} = -\left[Y_{kr}\right]^{+}\left\{q_k\right\} \tag{33}$$

This process is, except for the minus sign, identical to that of Force Determination.[5]

If R were equal to K, then all K accelerations and strains would be zero. In this case it is necessary to examine the vibration or strain of each important motion coordinate which is not of the set of K = R because some of those of the nonnulled set could have been made much worse. When K is greater than R, it is necessary to check every significant motion coordinate, including those of the minimized set, because a reduction in the sum of the squares of the minimized set does not guarantee that some motion coordinates in the minimized set are not amplified beyond tolerable values. The changed vibration is determined from

$$\underset{1x1}{q'_j} = \underset{1x1}{q_j} + \underset{1xR}{[Y_{jr}]} \underset{Rx1}{\{f_r\}^{(m)}} \tag{34}$$

## Some Types of Active Vibration Suppressors

The following types of active vibration suppressors are discussed to illustrate the application of analytical testing to active vibration suppression. The list is not intended to be all inclusive and only a cursory examination of the practicality of the devices is presented.

Active mass. - The shaking of a reaction mass by an actuator attached to the airframe creates an external force on the airframe as shown below. The response, acceleration or strain, to be controlled will usually be remote from the active mass and may be in any spatial direction. The feedback to the

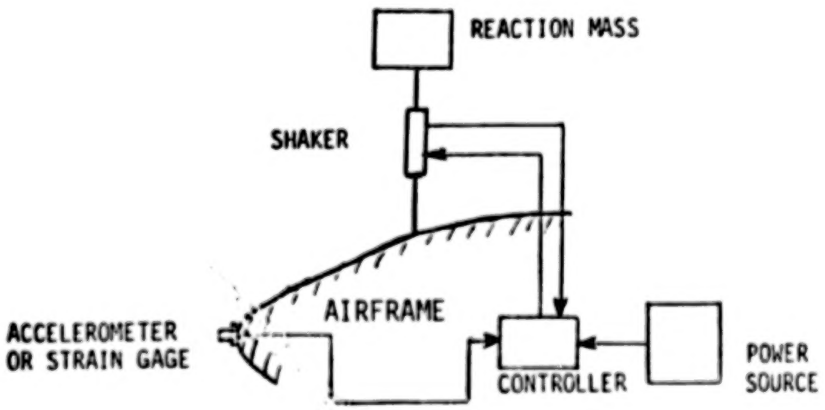

controller from the shaker may be both force magnitude and phase. To obtain the desired force level on the airframe with minimum reaction mass weight requires the reaction mass to move through a large displacement.

Active stiffness. - A shaker or actuator may be placed between two points on the structure as shown in the following sketch.

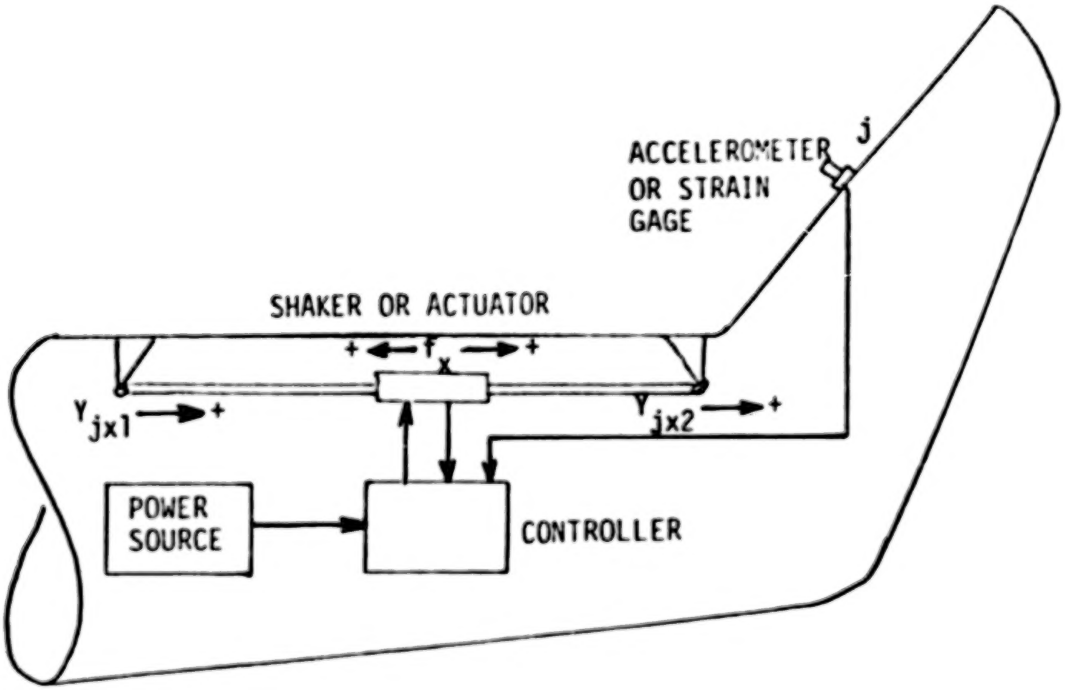


The response at j is given by

$$q'_j = q_j + (Y_{jx2} - Y_{jx1})\, f_x \tag{35}$$

where x1 and x2 must be colinear. Feedback from the shaker may be both force magnitude and force phase.

Control surface suppressor. - An aerodynamic surface, such as a canard or horizontal stabilizer, can be vibrated as shown in the following sketch to create an external force. Considering the control surface to be essentially rigid, one may obtain phase feedback. However, the actual external vibratory force produced may not be known accurately unless the suppressor can be test calibrated with a suitably placed strain gage or bending bridge because of the

difficulties in calculation of the force from unsteady aerodynamics and aerodynamic interferences.

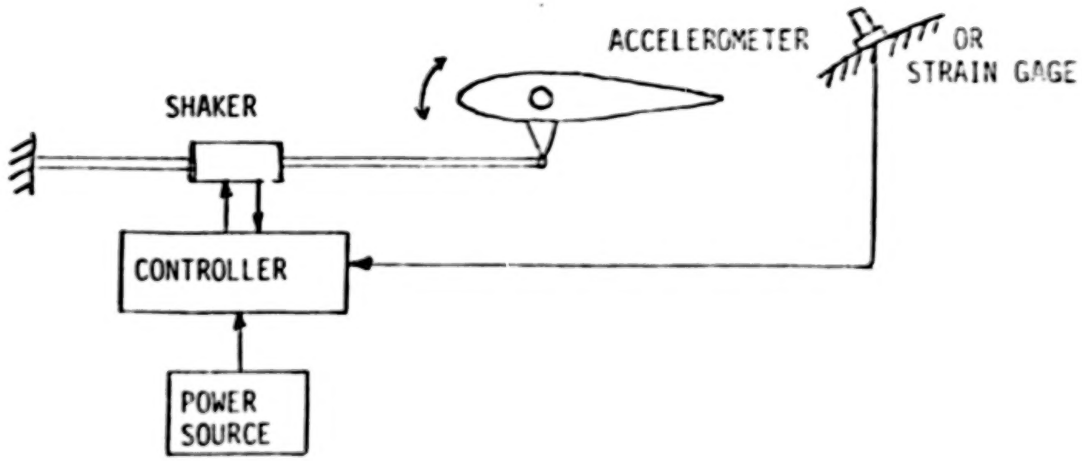


A disadvantage of using a fixed-system control surface as a vibration suppressor is airspeed dependence because the maximum force required may not be at the highest airspeed.

Rotor control suppression. - Variation in rotor pitch is another possible method of active vibration control. A schematic for vibratory tail rotor pitch is shown below.

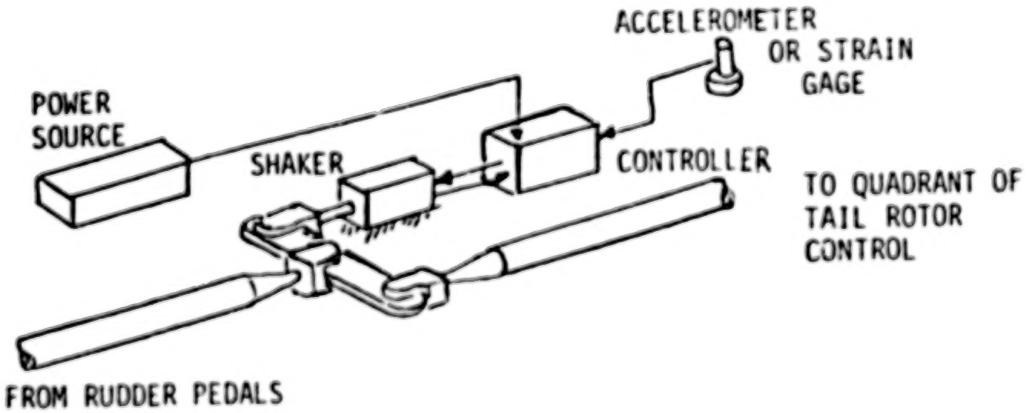


In some types of tail rotor installations the vibratory force magnitude and phase may be obtained from strain gages on the tail rotor shaft.

Active absorber. - The active absorber can be used to suppress vibration at a particular frequency. The major advantage of an active absorber is the reduction of the shaker size required for a given output force. Figure 6 depicts a conventional absorber with damping. The active absorber is simply a spring in parallel with the shaker, as shown in Figure 7.

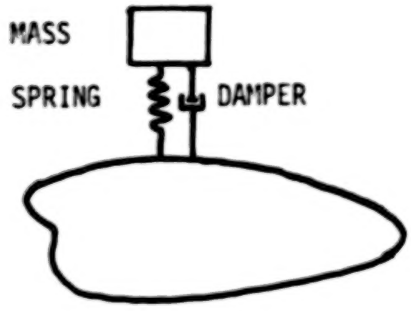


Figure 6. - Conventional absorber with damping.

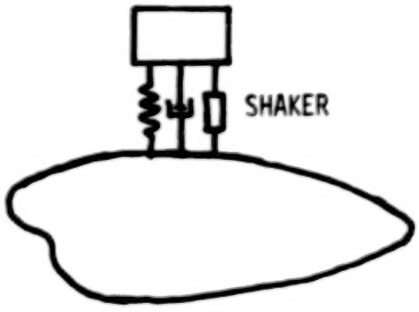


Figure 7. - Active absorber. Damping may be zero.

The displacements of the absorber mass and the fuselage are obtained from

$$\begin{Bmatrix} q'_a \\ q'_r \end{Bmatrix} = \begin{bmatrix} Y'_{aa} & Y'_{ar} \\ Y'_{ra} & Y'_{rr} \end{bmatrix} \begin{Bmatrix} 0 \\ f_r \end{Bmatrix} \tag{36}$$

where the elements of the matrix in equation (36) are displacement mobilities with the absorber on the fuselage. Substituting for the absorber parameters leads to the result

$$\begin{bmatrix} Y'_{aa} & Y'_{ar} \\ Y'_{ra} & Y'_{rr} \end{bmatrix} = \frac{1}{\Delta} \begin{bmatrix} K(1+ig) + Y_{rr}^{-1} & K(1+ig) \\ K(1+ig) & K(1+ig) - \omega^2 m \end{bmatrix} \tag{37}$$

where

$$\Delta = K(1+ig)(Y_{rr}^{-1} - \omega^2 m) - \omega^2 m\, Y_{rr}^{-1} \tag{38}$$

and $Y_{rr}$ is the driving-point mobility without the absorber. The spring stiffness, spring structural damping, and absorber mass are K, g, and m, respectively. The motion of the absorber mass is obtained from equation (36) and, after eliminating $f_r$, becomes

$$q'_a = \frac{Y'_{ar}\, q'_r}{Y'_{rr}} \tag{39}$$

For a shaker force f on the absorber mass and -f on the fuselage, equation (28) determines the displacement of the absorber mass as

$$q''_a = \frac{Y'_{ar}}{Y'_{rr}}\, q'_r + \left(Y'_{aa} - Y'_{ar}\right) f \tag{40}$$

and the displacement of the fuselage as

$$q''_r = q'_r - \left(Y'_{rr} - Y'_{ar}\right) f \tag{41}$$

then

$$q''_a - q''_r = \left(\frac{Y'_{ar}}{Y'_{rr}} - 1\right) q'_r + \left(Y'_{aa} + Y'_{rr} - 2\, Y'_{ar}\right) f \tag{42}$$

Substituting for the driving-point displacement mobility of the absorber, equation (22) leads to the result

$$q'_r = q_r \frac{[K(1+ig) - \omega^2 m]}{[K(1+ig) - \omega^2 m - Y_{rr}\, K(1+ig)\, \omega^2 m]} \tag{43}$$

where $q_r$ is the motion of the fuselage without the absorber.

Equation (42) can then be written as

$$q''_a - q''_r = \frac{\omega^2 m q_r + (1 - \omega^2 m\, Y_{rr})\, f}{K(1+ig)\,(1 - \omega^2 m\, Y_{rr}) - \omega^2 m} \tag{44}$$

The force on the fuselage is

$$f_r = K(1+ig)\,(q''_a - q''_r) - f \tag{45}$$

or

$$f_r = \frac{\omega^2 m \left[f + q_r K(1 + ig)\right]}{K(1 + ig)(1 - Y_{rr}\omega^2 m) - \omega^2 m} \tag{46}$$

and in terms of acceleration

$$f_r = \frac{-\ddot{q}_r m(1 + ig) + \frac{\omega^2}{\Omega_T^2} f}{1 - \frac{\omega^2}{\Omega_T^2} + m\left(\ddot{Y}_{rr}^R - g\ddot{Y}_{rr}^I\right) + im\left(\ddot{Y}_{rr}^I + g\ddot{Y}_{rr}^R\right) + ig} \tag{47}$$

where $\Omega_T$ is the antiresonant frequency at r created by the absorber.

To minimize the denominator with tuning, let

$$\frac{\omega^2}{\Omega_T^2} = m\left(\ddot{Y}_{rr}^R - g\ddot{Y}_{rr}^I\right) + 1 \tag{48}$$

which sets the real part of the denominator of equation (47) to zero. The tuning of the active absorber is independent of flight vibrations at the attachment point and the response point whereas the tuning of a conventional absorber is not. With the tuning condition of equation (48), equation (47) becomes

$$f_r = i\,\frac{\ddot{q}_r m\,(1 + ig) - f\,\omega^2/\Omega_T^2}{m\left(\ddot{Y}_{rr}^I + g\ddot{Y}_{rr}^R\right) + g} \tag{49}$$

From equation (48) the tuning frequency of the active absorber is

$$\Omega_T = \frac{\omega}{\sqrt{1 + m\left(\ddot{Y}_{rr}^R - g\ddot{Y}_{rr}^I\right)}} \tag{50}$$

In operation, the minicomputer controller determines the magnitude and phase required of the shaker from

$$f = \frac{\Omega_T^2}{\omega^2}\left[|f_r|\left\{m\left(\ddot{Y}_{rr}^I + g\ddot{Y}_{rr}^I\right) + g\right\}/\left(\phi_f + 90^\circ\right) + |\ddot{q}_r|\, m\left(1 + g^2\right)/\phi_r + \tan^{-1} g\right] \tag{51}$$

The force on the fuselage at r, $f_r$, for zero vibration at j is determined from

$$f_r = - \frac{\ddot{q}_j}{\ddot{Y}_{jr}} \tag{52}$$

There are two feedback signals to the controller of the active absorber: the acceleration at the attachment point and the vibration (strain or acceleration) of the motion coordinate to be nulled.

## Examples of Active Vibration Suppression

The applicability of analytical testing for examining the effects of active vibration suppressors on airframe vibration is illustrated using AH-1G ground and flight test vibration data. Equations (33) and (34) are used to determine the required control forces and the changed vibrations.

Horizontal stabilizer aerodynamic suppressor. - This example considers the effects on vertical vibration for 2P excitation of the horizontal stabilizer. As shown in the following sketch, the horizontal stabilizer is vibrated in pitch with sufficient force magnitude and phase to give zero vertical vibration at the pilot's seat (FS Z140). The effects at FS Z90, FS Z400, and FS Z540 are also examined. The vertical acceleration mobilities at these four locations are shown in Table IX. Table X presents the flight vertical accelerations for four flight conditions.

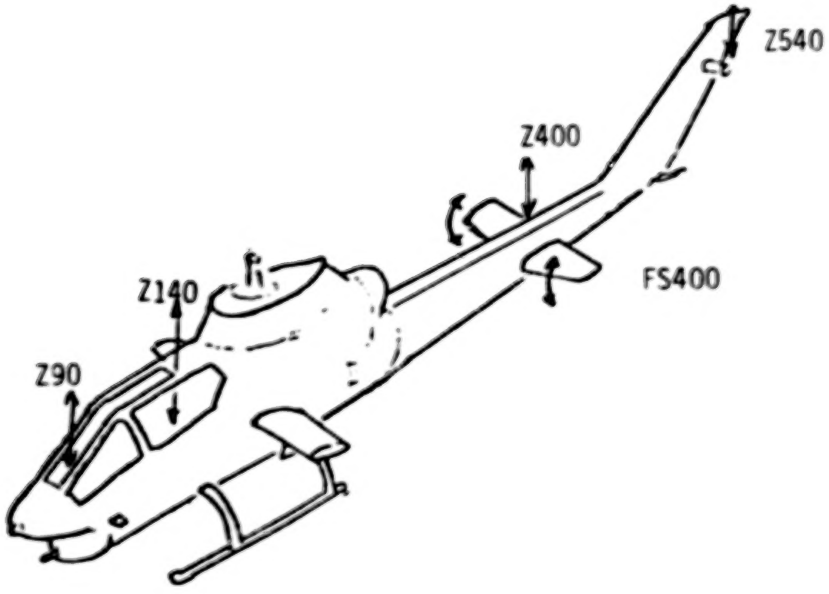


At 187 knots, the required force is

$$f_r = - \frac{\ddot{q}(Z140)}{\ddot{Y}(Z400,Z140)} = - \frac{.147g's/124°}{(.065g's/1000\ N)/-84°} \tag{53}$$

$$= - 2261\ N(-510\ lb)/208°$$

and similarly for other flight conditions. The vibration at any point is obtained from equation (34) as

$$\ddot{q}'_j = \ddot{q}_j + \ddot{Y}_{jr}\, f_r \tag{54}$$

and the results are shown in Table XI.

TABLE IX. - ACCELERATION MOBILITIES AT 10.8 HZ, g/1000 N (g/100 lb)

| | Z90 | Z140 | Z400 | Z540 |
|---|---|---|---|---|
| Z90 | .103/10° (.046) | .070/6° (.031) | .038/-138° (.017) | .288/9° (.128) |
| Z140 | .070/6° (.031) | .052/5° (.023) | .065/-84° (.029) | .124/25° (.055) |
| Z400 | .038/-138° (.017) | .065/-84° (.029) | .072/64° (.320) | .672/-32° (.299) |
| Z540 | .288/9° (.128) | .124/25° (.055) | .672/-32° (.299) | 2.855/-8° (1.270) |

TABLE X. - FLIGHT ACCELERATIONS AT 10.8 HZ, g

| | 187 Knots rolling pullout left | 164 Knots rolling pullout right | 144 Knots straight and level | 103 Knots 45° turn |
|---|---|---|---|---|
| Z90 | .335/120° | .322/134° | .118/120° | .064/124° |
| Z140 | .147/124° | .274/114° | .114/99° | .078/95° |
| Z400 | .938/68° | .818/61° | .344/44° | .237/92° |
| Z540 | 1.992/-118° | 1.454/-131° | .769/-131° | .684/-167° |

Assume that the horizontal stabilizer is vibrated in pitch with sufficient force magnitude and phase to give zero vertical vibration at the pilot's seat, as shown by the previous sketch.

TABLE XI. VERTICAL VIBRATION AT 10.8 HZ WITH AND WITHOUT HORIZONTAL STABILIZER AERODYNAMIC SUPPRESSOR, g

| | 187 Knots rolling pullout left | | 164 Knots rolling pullout right | | 144 Knots straight and level | | 103 Knots 45° turn | |
|---|---|---|---|---|---|---|---|---|
| Force at Z400 | -2255 N/208° (-507 lb) | | -4204 N/198° (-945 lb) | | -1748 N/183° (-393 lb) | | -1197 N/179° (-269 lb) | |
| | With | Without | With | Without | With | Without | With | Without |
| Z 90 | .287 | .335 | .316 | .322 | .120 | .118 | .074 | .064 |
| Z140 | 0 | .147 | 0 | .274 | 0 | .114 | 0 | .078 |
| Z400 | 2.51 | .938 | 3.798 | .818 | 1.58 | .344 | 1.074 | .237 |
| Z540 | 1.95 | 1.992 | 2.523 | 1.454 | 1.263 | .769 | .592 | .684 |

The pilot's seat vibration is zero in all flight conditions with a large increase in vertical vibration at the horizontal stabilizer station on the boom. The forces required are very large, however.

For purposes of illustration let it be assumed that the horizontal stabilizer has an area of approximately 1 square meter and that trim requirements would permit a 2P pitch vibration of $\pm$ 3° maximum producing a vertical force of 1112 N (250 lb) at 187 knots airspeed. With the maximum force proportional to the square of the airspeed, the vibrations obtainable with this arrangement are given in Table XII.

Even with the very large forces of Table XI, zero vibration at the pilot's seat from an active vibration suppressor at the horizontal stabilizer station is obtained at the expense of large increases in tail boom vibration with negligible changes in gunner's seat vibration. The reduction in vibration at the pilot's seat and gunner's seat using the horizontal stabilizer as an aerodynamic suppressor, as shown in Table XII, are not impressive.

TABLE XII. - HORIZONTAL STABILIZER FORCED AT 10.8 HZ TO MINIMIZE PILOT'S SEAT VIBRATION

| | 187 knots rolling pullout left | | 164 knots rolling pullout right | | 144 knots straight and level | | 103 knots 45° turn | |
|---|---|---|---|---|---|---|---|---|
| Force at FS Z400 | -1112 N/208° (-250 lb) | | -854 N/198° (-192 lb) | | -658 N/183° (-148 lb) | | -338 N/179° (-76 lb) | |
| Vertical vibration with and without suppression, g | | | | | | | | |
| | With | Without | With | Without | With | Without | With | Without |
| Z90 | .309 | .335 | .315 | .322 | .114 | .118 | .064 | .064 |
| Z140 | .075 | .147 | .218 | .274 | .071 | .114 | .056 | .078 |
| Z400 | 1.700 | .938 | 1.409 | .818 | .802 | .344 | .465 | .237 |
| Z540 | 1.821 | 1.992 | 1.298 | 1.454 | .804 | .769 | .551 | .684 |

T-tail aerodynamic suppressor. - The effects on vertical vibration for 2P excitation of the T-tail, as shown below, are illustrated in this example.

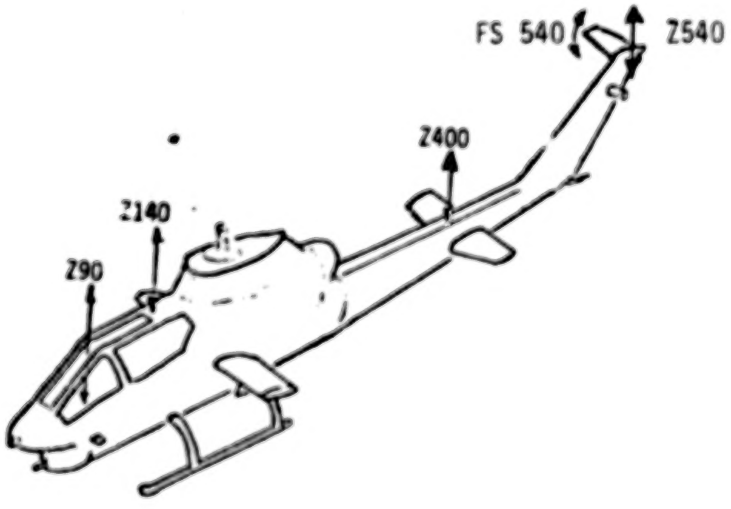


The principal objective is to give zero vertical vibration at the gunner's seat (FS Z90). The airframe locations and flight conditions are identical to the previous example. The T-tail horizontal control surface is not required for

trim and can be operated at higher 2P vibratory angles of incidence than the horizontal stabilizer (FS Z400). Therefore, assuming a T-tail area of approximately 0.4 square meter, a vibratory force of about 1200 N (270 lb) at 164 knots can be generated.

The results of using the T-tail aerodynamic suppressor to null the gunners' seat vibration are shown in Table XIII. With the 164 knot presumption, the required forces are well within the airspeed-squared requirement. The T-tail is outside the path of the main rotor tip vortex indicating that it may not be the source of increased external loads at main rotor 2P.

Significant vibration reductions result at the pilot's seat and tail boom with zero vibration at the gunner's seat. Whether the increase in vibration at the tip of the fin (FS Z540) is structurally significant and whether the lateral offset of the T-tail force is detrimental or beneficial to fin bending are questions that would be answered by further analsis using analytical testing.

TABLE XIII. - VERTICAL VIBRATION AT 10.8 HZ WITH AND WITHOUT T-TAIL AERODYNAMIC SUPPRESSOR, g

| | 187 Knots rolling pullout left | | 164 Knots rolling pullout right | | 144 Knots straight and level | | 103 Knots 45° turn | |
|---|---|---|---|---|---|---|---|---|
| Force at FS Z540 | -1164 N/111° (-261.7 lb) | | -1119 N/125° (-251.6 lb) | | -410 N/111° (-92.2 lb) | | -222.4 N/115° (-50 lb) | |
| | With | Without | With | Without | With | Without | With | Without |
| Z 90 | 0 | .335 | 0 | .322 | 0 | .118 | 0 | .064 |
| Z140 | .031 | .147 | .181 | .274 | .080 | .114 | .062 | .078 |
| Z400 | .226 | .938 | .437 | .818 | .197 | .344 | .092 | .237 |
| Z540 | 5.000 | 1.992 | 3.975 | 1.454 | 1.740 | .769 | 1.295 | .684 |

Active absorber at the gunner's seat. - An active vertical absorber at the gunner's seat (FS Z90) is controlled to provide zero vertical vibration at the pilot's seat (FS Z140). The effects on vibrations were calculated at the locations shown in the sketch below for four flight conditions. The required acceleration mobilities and flight accelerations are given in Tables IX and X, respectively.

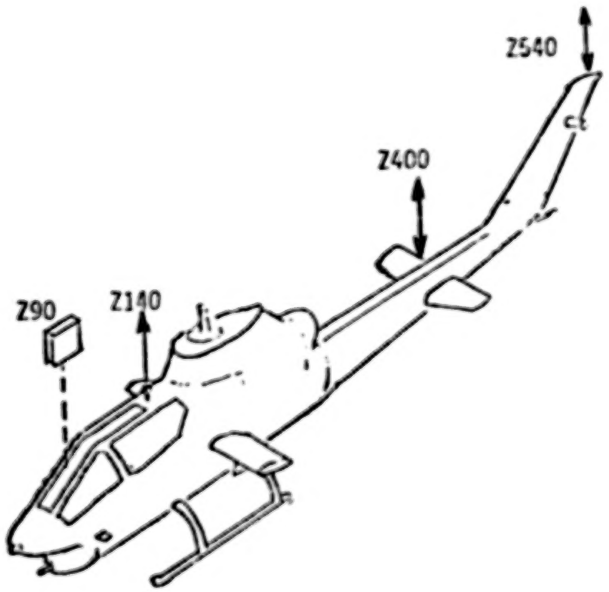


The results presented in Table XIV indicate that the pilot's seat (FS Z140) vertical vibration is zero for all flight conditions. The gunner's seat (FS Z90) vertical vibration remains the same in the 103-knot turn but is reduced in the other maneuvers. The horizontal stabilizer (FS Z400) vertical vibration does not change appreciably and the fin (FS Z540) vertical vibration is increased.

The active absorber parameters are calculated from equations (50), (51), and (52). At 187 knots the suppressor force is -2100 N (-472 lb)/118° acting through .335 g/120° at 10.8 Hz. The output power is the real part of the product of force and velocity which gives 33.08 Nm/s (.044 hp) consumed in the suppression. For a 4.536 kg (10 lb) reaction mass, the required tuning frequency is 10.78 Hz and the required shaker force is 65.5 N (14.8 lb)/41.1°, assuming 3 percent hysteretic damping in the absorber.

TABLE XIV. - VERTICAL VIBRATION AT 10.8 HZ WITH AND WITHOUT ACTIVE ABSORBER AT GUNNER'S STATION, g

| | 187 Knots rolling pullout left | | 164 Knots rolling pullout right | | 144 Knots straight and level | | 103 Knots 45° turn | |
|---|---|---|---|---|---|---|---|---|
| Force at FS Z90 | -2108 N/118° (-474 lb) | | -3732 N/108° (-839 lb) | | -1637 N/93° (-368 lb) | | -1121 N/89° (-252 lb) | |
| | With | Without | With | Without | With | Without | With | Without |
| Z90 | .123 | .335 | .132 | .322 | .066 | .118 | .064 | .064 |
| Z140 | .000 | .147 | .000 | .274 | .000 | .114 | .000 | .078 |
| Z400 | .939 | .938 | .834 | .818 | .349 | .344 | .272 | .237 |
| Z540 | 2.315 | 1.992 | 2.151 | 1.454 | 1.117 | .769 | .781 | .684 |

Active absorber at the tail rotor. - In this example the objective is to produce zero lateral vibration on the fin (FS Y490) at 10.8 Hz. An active lateral absorber at the tail rotor gearbox was selected as the vibration suppressor, although excitation of tail rotor pitch is an alternative. The preference of harmonic control of the tail rotor or an active absorber depends on many factors among which are tail rotor blade loads. Main rotor 2P excitation of the tail rotor may increase or decrease tail rotor fatigue life and this requires additional investigation. The effects on lateral flight accelerations were calculated at the locations shown in the following sketch for four flight conditions. The required acceleration mobilities and flight accelerations are shown in Tables XV and XVI, respectively. The flight conditions are identical to the previous example.

The results shown in Table XVII indicate that the tail rotor gearbox vibration is negligibly affected in the rolling pullouts, but significantly reduced in 144-knot level flight and in the 103-knot turn. The vibration at FS Y440 is reduced substantially in the 187-knot left rolling pullout and at 144-knot level flight, reduced somewhat in the 164-knot right rolling pullout, and increased in the 103-knot turn. Changes in pilot and gunner vibration are not significant. As expected, the fin (FS Y490) vibration is zero for all flight conditions. A

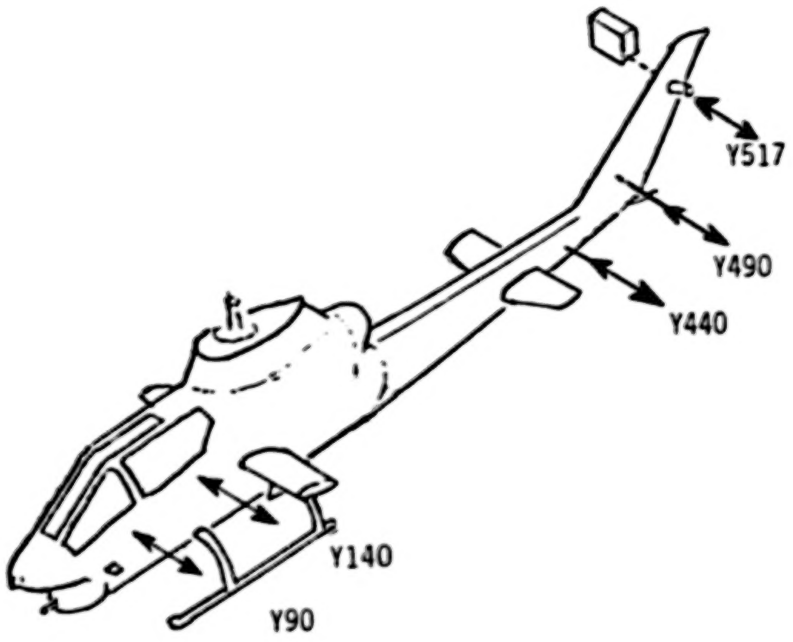


TABLE XV. - ACCELERATION MOBILITIES AT 10.8 HZ RELATIVE TO FS Y517 (TAIL ROTOR LATERAL), g/1000 N (g/100 lb)

| Fuselage stations | | | | |
|---|---|---|---|---|
| Y517 | Y490 | Y440 | Y140 | Y90 |
| 3.597/17° (1.600) | 1.576/20° (.701) | .535/2° (.238) | .178/103° (.079) | .339/84° (.151) |

TABLE XVI. - LATERAL FLIGHT VIBRATION, g

| Airspeed | Fuselage stations | | | | |
|---|---|---|---|---|---|
| | Y517 | Y490 | Y440 | Y140 | Y90 |
| 187 kts | 1.815/-91° | 1.266/-116° | 1.282/-115° | .123/-96° | .191/-94° |
| 164 kts | .851/-106° | .710/-121° | .967/-114° | .118/-89° | .147/-83° |
| 144 kts | 1.637/-138° | .878/-150° | .611/-145° | .055/-114° | .103/-120° |
| 103 kts | .405/171° | .233/175° | .048/-95° | .048/-95° | .072/-105° |

TABLE XVII. - LATERAL VIBRATION AT 10.8 HZ WITH AND WITHOUT ACTIVE ABSORBER AT TAIL ROTOR GEARBOX, g

| | 187 Knots rolling pullout left | | 164 Knots rolling pullout right | | 144 Knots straight and level | | 103 Knots 45° turn | |
|---|---|---|---|---|---|---|---|---|
| Force at FS Y517 | -803 N/-136° (-181 lb) | | -450 N/-141° (-101 lb) | | -557 N/-170° (-125 lb) | | -148 N/155° (-33 lb) | |
| | With | Without | With | Without | With | Without | With | Without |
| Y517 | 1.552 | 1.815 | .857 | .851 | .602 | 1.657 | .127 | .405 |
| Y490 | 0 | 1.266 | 0 | .710 | 0 | .878 | 0 | .233 |
| Y440 | .297 | 1.282 | .755 | .967 | .356 | .611 | .104 | .048 |
| Y140 | .140 | .123 | .092 | .118 | .073 | .055 | .022 | .048 |
| Y 90 | .183 | .191 | .068 | .147 | .119 | .103 | .027 | .072 |

comparison of the tail boom (FS Y440) vibration reduction given in Table XVII to Figure 5 shows that the active absorber behaves quite differently from the conventional absorber at stations other than that suppressed.

The active absorber parameters are calculated from equations (50), (51), and (52). At 187 knots the suppressor force is -803 N (-181 lb)/-136° acting through 1.815 g/-91° at 10.8 Hz which gives 172 Nm/s (.229 hp) consumed in the suppression. For a 2.27 kg (5.0 lb) reaction mass, the required tuning frequency is 10.41 Hz and the required shaker force is 38.9 N (8.76 lb)/174°, assuming 5 percent hysteretic damping in the absorber.

## Stiffness Changes

Skin and plate changes. - The basic equation for a stiffness change is obtained by combining equations (11) and (12)

$$\left\{\begin{array}{c}\ddot{q}_k' \\ \hline \epsilon_j'\end{array}\right\} = \left\{\begin{array}{c}\ddot{q}_k \\ \hline \epsilon_j\end{array}\right\} - \left[\begin{array}{c}\ddot{Y}_{kr} \\ \hline Y_{kr}(\epsilon)\end{array}\right] \left( [I] + [K_{rr}][Y_{rr}] \right)^{-1} [K_{rr}] \{q_r\} \qquad (55)$$

where $[K_{rr}]$ is the stiffness matrix of the skin section as a free body, $\{q_r\}$ is the vector of flight displacements at the change coordinates and $[Y_{rr}]$ is the matrix of displacement mobilities of the airframe at the change coordinates. A skin, as opposed to a plate, has negligible transverse stiffness and the coordinates, $\{q_r\}$, are on the surface of the airframe. The differences among the coordinates, $\{q_r\}$, are most important in a stiffness change. It would be impractical in most cases to obtain $\{q_r\}$ from flight accelerometers alone because of the small difference between large numbers. This problem, however, is resolved using strain gages.

Figure 8 shows a skin section and the rectangular coordinates of the relevant stiffness matrix. The skin may be of nonhomogeneous materials with nonconstant thickness, such as a two dimensionally tapered composite, with directional modulii of elasticity or a simple metal sheet. Only the stiffness matrix needs to be known in applying equation (55). The effects of proportional or nonproportional damping may be included in equation (55) by replacing $[K_{rr}]$ with a complex matrix which is the sum of the real stiffness matrix and an imaginary damping matrix, frequency dependent for viscous damping and frequency independent for hysteretic damping.

It is immaterial to the analytical testing approach whether the surface of the helicopter at which the skin or plate change is to be made is flat or curved.

For n nodes on a skin there are 2n rectangular coordinates and the stiffness matrix (the matrix of the partial derivatives of force to displacement) is a square matrix of order 2n and rank 2n - 3. For practical flight and shake test measurements the skin section may be modeled in terms of 2n - 3 strain coordinates as shown in Figure 9.

The displacement mobility matrix for the strain coordinates of, for example, the skin section of Figure 9 may be determined as shown in Figure 10 where equal and opposite forces are applied across a distance $\delta$. This type of displacement mobility (influence coefficient) matrix becomes

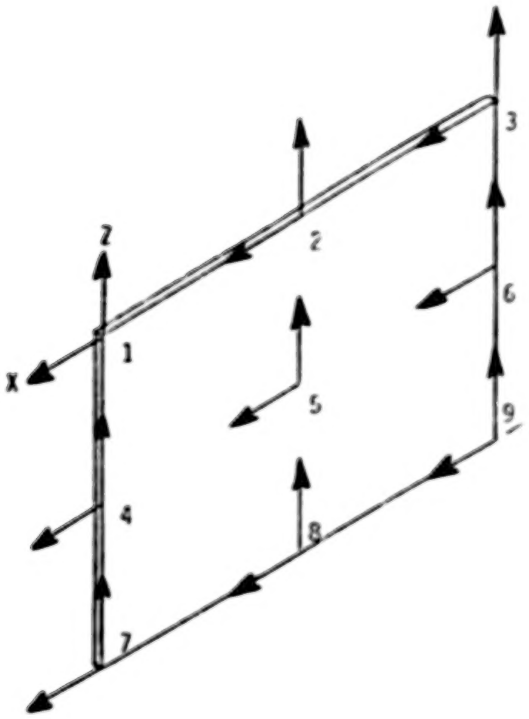


Figure 8. - Rectangular coordinates of a skin section with nine nodes.

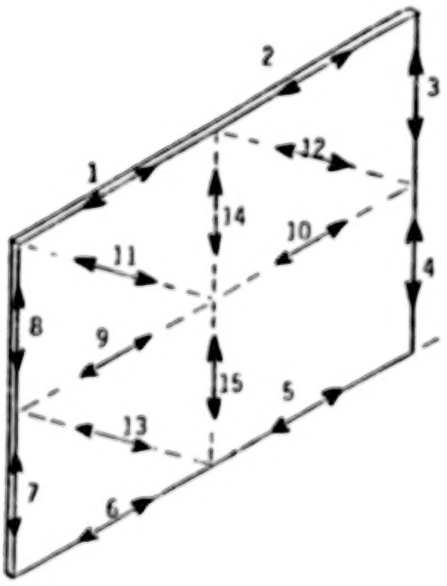


Figure 9. - Strain coordinates of a skin section with nine nodes.

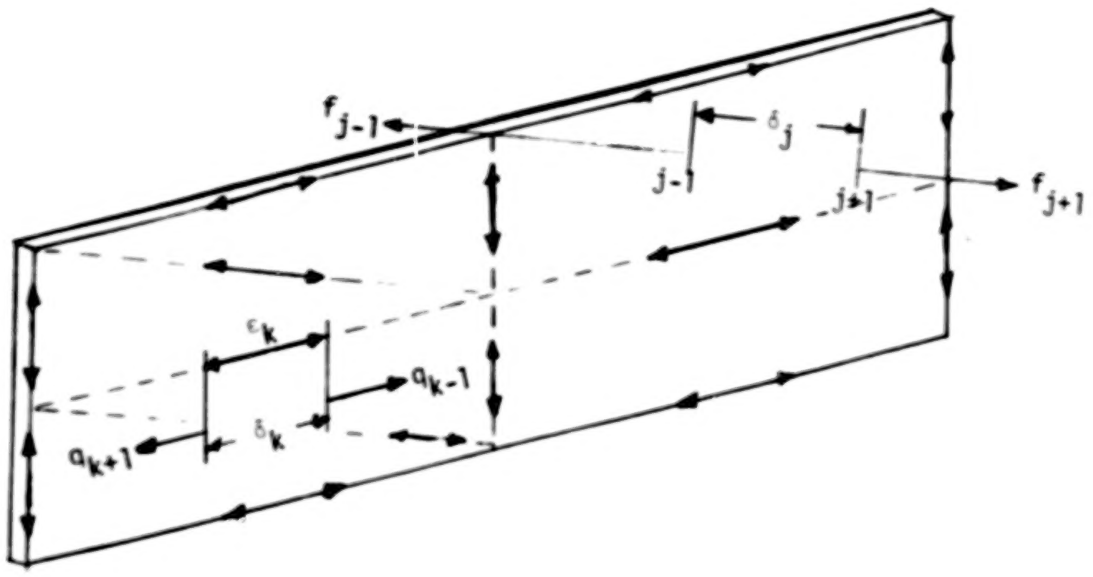


Figure 10. - The jkth element of the strain stiffness matrix is $\frac{\partial(f_{j+1} - f_{j-1})}{\partial(q_{k+1} - q_{k-1})}$.

$$\left[\gamma(c)\right] = \frac{\partial \Delta q_k}{\partial \Delta f_j} \tag{56}$$

which is, of course, nonsingular and may be inverted to give a stiffness matrix

$$\left[\gamma(c)\right]^{-1} \equiv [k] = \left[\frac{\partial \Delta f_j}{\partial \Delta q_k}\right] \tag{57}$$

where

$$\Delta f_j = \frac{1}{2}(f_{j+1} - f_{j-1})$$

and

$$\Delta q_k = q_{k+1} - q_{k-1}$$

If, on the other hand, the conventional type 2n x 2n stiffness matrix K is available the strain type stiffness matrix k may be found using a coordinate transformation. Note that

$$[K] \equiv \left[\frac{\partial f_r}{\partial q_r}\right] \tag{58}$$

A transformation matrix [T] exists such that

$$\underset{(2n-3)x1}{\{\Delta q\}} = \underset{(2n-3)x2n}{[T]} \underset{2nx1}{\{q\}} \tag{59}$$

where

$$[T] = \left[\frac{\partial \Delta q}{\partial q}\right] \tag{60}$$

Let

$$\underset{3}{\overset{2n}{\left[\phi^{(R)} \vdots \phi\right]}}$$

be the eigenvectors of K where the superscript R indicates the rigid body modes, those of zero eigenvalues.

$$[K]\,[\phi] = [\phi]\,[\lambda] \tag{61}$$

and

$$[\phi]^T[K]\,[\phi] = [K^*]$$

for nonzero eigenvalues. The inverse of K may be expressed as

$$[K]^{-1} = \left[\phi^R \vdots \phi\right] \begin{bmatrix} 0 & \vdots & 0 \\ \cdots & \ddots & \cdots \\ 0 & \vdots & \frac{1}{K^*} \end{bmatrix} \left[\phi^R \vdots \phi\right]^T \tag{62}$$

This matrix is singular because of the three reciprocal of zero terms in the diagonal matrix. The 2n x 2n eigenvector matrix is necessarily nonsingular. A coordinate transformation of equation (62) using equation (60) yields

$$[k]^{-1} = \left[\frac{\partial \Delta q}{\partial \Delta f}\right] = [T] \left[\phi^R \vdots \phi\right] \begin{bmatrix} 0 & \vdots & 0 \\ \cdots & \ddots & \cdots \\ 0 & \vdots & \frac{1}{K^*} \end{bmatrix} \left[\phi^R \vdots \phi\right]^T [T]^T \tag{63}$$

which is a (2n-3) x (2n-3) matrix. The transformation of equation (60) applied to a rigid body mode is necessarily zero. Therefore,

$$[k]^{-1} = \left[0 \;\vdots\; T\phi\right] \begin{bmatrix} \frac{1}{0} & \vdots & 0 \\ \cdots & \cdots & \cdots \\ 0 & \vdots & \frac{1}{K^*_n} \end{bmatrix} \left[0 \;\vdots\; T\phi\right]^T \tag{64}$$

The 0 x 0/0 indeterminant terms in the product are zero and equation (64) may be written as

$$\left[Y^{(c)}_{rr}\right] \equiv [k]^{-1} = [T][\phi] \left[\frac{1}{K^*_n}\right] [\phi]^T[T]^T$$

from which it follows that k, a nonsingular matrix of order (2n-3), is given by

$$\left[\frac{\partial \Delta f}{\partial \Delta q}\right] \equiv [k] = \left([T][\phi]\right)^{-T} [K^*_n] \left([T][\phi]\right)^{-1}$$

$$= \left([T][\phi]\right)^{-T} [\phi]^T[K][\phi] \left([T][\phi]\right)^{-1} \tag{65}$$

It is also necessary to establish the types of mobility measurements which are practical in an actual airframe.

For forces $f_{j+1}$ and $f_{j-1}$ only in Figure 9,

$$\Delta q_k = \frac{\partial q_{k+1}}{\partial f_{j+1}} f_{j+1} + \frac{\partial q_{k+1}}{\partial f_{j-1}} f_{j-1} - \frac{\partial q_{k-1}}{\partial f_{j+1}} f_{j+1} - \frac{\partial q_{k-1}}{\partial f_{j-1}} f_{j-1} \tag{66}$$

But, $-f_{j-1} = f_{j+1} = \Delta f_j$. Therefore

$$\frac{\Delta q_k}{\Delta f_j} = \frac{\partial q_{k+1}}{\partial f_{j+1}} - \frac{\partial q_{k+1}}{\partial f_{j-1}} - \frac{\partial q_{k-1}}{\partial f_{j+1}} + \frac{\partial q_{k-1}}{\partial f_{j-1}}$$

$$= \sum_{i=1}^{N} \left( \Psi_{k+1,i}\, \Psi_{j+1,i} - \Psi_{k+1,i}\, \Psi_{j-1,i} - \Psi_{k-1,i}\, \Psi_{j+1,i} + \Psi_{k-1,i}\, \Psi_{j-1,i} \right) F_i$$

$$= \sum_{i=1}^{N} \left( \Psi_{k+1,i} - \Psi_{k-1,i} \right) \left( \Psi_{j+1,i} - \Psi_{j-1,i} \right) F_i \tag{67}$$

For forces only at j

$$\frac{\Delta q_k}{\Delta f_j} = \sum_{i=1}^{N} \left( \frac{\Psi_{k+1,i} - \Psi_{k-1,i}}{\delta_k} \right) \left( \frac{\Psi_{j+1,i} - \Psi_{j-1,i}}{\delta_j} \right) \delta_j \, \delta_k \, F_i \tag{68}$$

or, for any number of forces,

$$\left[ \gamma_{rr} \right] = \left[ \frac{\partial \Delta q_k}{\partial \Delta f_j} \right] = \left[ \sum_{i=1}^{N} \Psi_{ki}^{(\epsilon)} \, \Psi_{ji}^{(\epsilon)} \, \delta_j \, \delta_k \, F_i \right] \tag{69}$$

Similarly,

$$\frac{\partial \ddot{q}_k}{\partial \Delta f_r} = \sum_{i-1}^{N} \Psi_{ki} \; \Psi_{ri}^{(\epsilon)} \, \delta_r \, \ddot{F}_i \tag{70}$$

With a strain stiffness matrix, equation (55) becomes

$$\begin{Bmatrix} \ddot{q}'_k \\ \hline \epsilon'_j \end{Bmatrix} = \begin{Bmatrix} \ddot{q}_k \\ \hline \epsilon_j \end{Bmatrix} - \begin{bmatrix} \partial \ddot{q}_k / \Delta f_r \\ \hline \partial \epsilon_j \\ \overline{\partial \Delta f_r} \end{bmatrix} \left( [I] + \left[ k_{rr} \right] \left[ \frac{\partial \Delta q_r}{\partial \Delta f_r} \right] \right)^{-1} \left[ k_{rr} \right] \left\{ \epsilon_r \, \delta_r \right\} \tag{71}$$

In the case of a plate, there is transverse stiffness and nonnegligible mass. The aircraft is tested with n accelerometers perpendicular to the surface, for n attachment points, in addition to the strain gages, as shown in Figure 11.

Numerical example of a transformation to a strain stiffness. - The six pinned rods of Figure 12 provide a simple illustration of the transformation from a stiffness matrix with rectangular coordinates to one with strain coordinates.

In the stiffness matrix with rectangular coordinates, shown following Figures 11 and 12, the k terms are axial spring rates subscripted with the terminal positions of the rods.

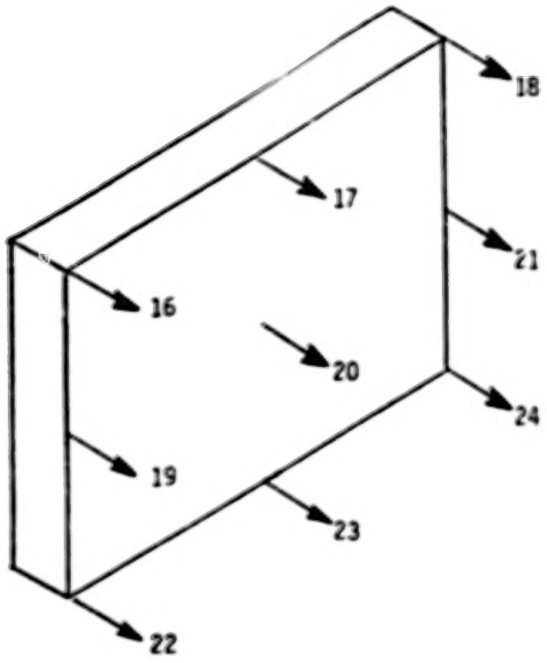


Figure 11. - A plate change with nine attachment points.

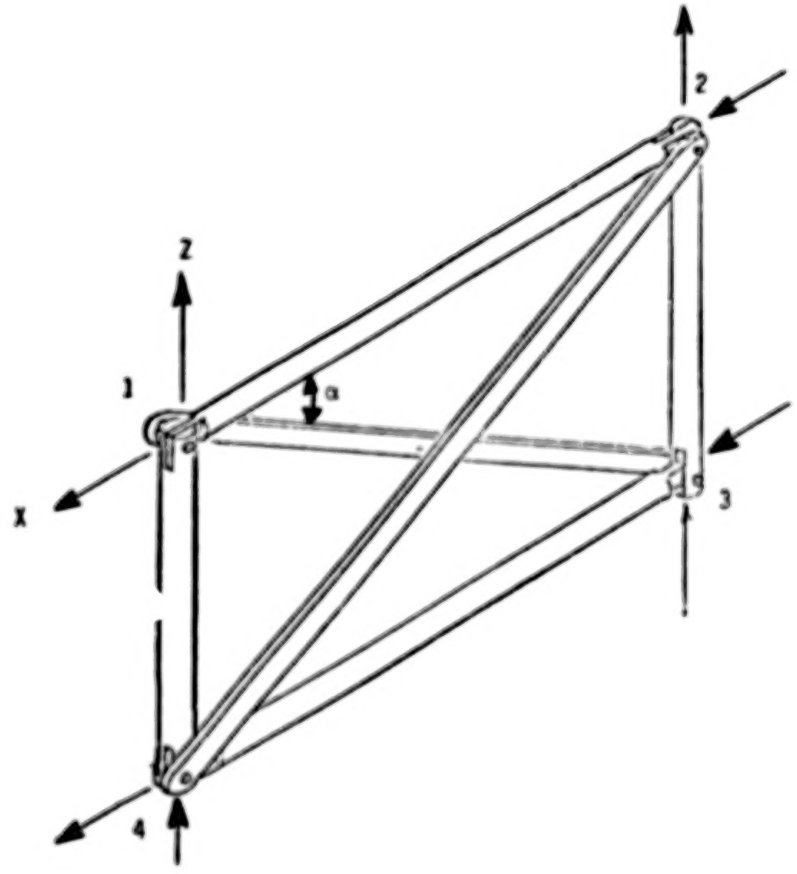


Figure 12. - Simple bar truss with rectangular coordinates.

$$[K] = \begin{bmatrix}
k_{12}+k_{13}\cos^2\alpha & -k_{12} & -k_{13}\cos^2\alpha & 0 & k_{13}\cos\alpha\sin\alpha & 0 & -k_{13}\sin\alpha\cos\alpha & 0 \\
-k_{12} & k_{24}\cos^2\alpha+k_{12} & 0 & -k_{24}\cos^2\alpha & 0 & -k_{24}\cos\alpha\sin\alpha & 0 & k_{24}\sin\alpha\cos\alpha \\
-k_{13}\cos^2\alpha & 0 & k_{34}+k_{13}\cos^2\alpha & -k_{34} & -k_{13}\sin\alpha\cos\alpha & 0 & k_{13}\sin\alpha\cos\alpha & 0 \\
0 & -k_{24}\cos^2\alpha & -k_{34} & k_{24}\cos^2\alpha+k_{34} & 0 & k_{24}\sin\alpha\cos\alpha & 0 & -k_{24}\sin\alpha\cos\alpha \\
k_{13}\sin\alpha\cos\alpha & 0 & -k_{13}\sin\alpha\cos\alpha & 0 & k_{14}+k_{13}\sin^2\alpha & 0 & -k_{13}\sin^2\alpha & -k_{14} \\
0 & -k_{24}\sin\alpha\cos\alpha & 0 & k_{24}\sin\alpha\cos\alpha & 0 & k_{23}+k_{24}\sin^2\alpha & -k_{23} & -k_{24}\sin^2\alpha \\
-k_{13}\sin\alpha\cos\alpha & 0 & k_{13}\sin\alpha\cos\alpha & 0 & -k_{13}\sin^2\alpha & -k_{23} & k_{23}+k_{13}\sin^2\alpha & 0 \\
0 & k_{24}\sin\alpha & 0 & -k_{24}\sin\alpha\cos\alpha & -k_{14} & -k_{24}\sin^2\alpha & 0 & k_{14}+k_{24}\sin^2\alpha \\
x_1 & x_2 & x_3 & x_4 & z_1 & z_2 & z_3 & z_4
\end{bmatrix} \quad (72)$$

This matrix has a degeneracy of three since the null vector is equal to the product of the K matrix and the transpose of the following independent vectors:

$$\begin{bmatrix} 1 & 1 & 1 & 1 & 0 & 0 & 0 & 0 \end{bmatrix}$$

representing x translation,

$$\begin{bmatrix} 0 & 0 & 0 & 0 & 1 & 1 & 1 & 1 \end{bmatrix}$$

representing z translation and

$$\begin{bmatrix} 0 & 0 & -\sin\alpha & -\sin\alpha & 0 & \cos\alpha & \cos\alpha & 0 \end{bmatrix}$$

representing a rotation.

The coordinate transformation equation in this case is

$$\begin{Bmatrix} x_1 - x_2 \\ x_4 - x_3 \\ z_1 - z_4 \\ z_2 - z_3 \\ D_1 - D_3 \end{Bmatrix} = \begin{bmatrix} 1 & -1 & 0 & 0 & 0 & 0 & 0 & 0 \\ 0 & 0 & -1 & 1 & 0 & 0 & 0 & 0 \\ 0 & 0 & 0 & 0 & 1 & 0 & 0 & -1 \\ 0 & 0 & 0 & 0 & 0 & 1 & -1 & 0 \\ \cos\alpha & 0 & -\cos\alpha & 0 & \sin\alpha & 0 & -\sin\alpha & 0 \end{bmatrix} \begin{Bmatrix} x_1 \\ x_2 \\ x_3 \\ x_4 \\ z_1 \\ z_2 \\ z_3 \\ z_4 \end{Bmatrix} \qquad (73)$$

or

$$\{\Delta q\} = [T]\ \{q\}$$

Let the spring rates, force/deflection, in Figure 12 be

$$k_{12} = k_{34} = 3 \times 10^5$$

$$k_{14} = k_{23} = 2 \times 10^5$$

$$k_{13} = k_{24} = 5 \times 10^5$$

The stiffness matrix, K, in the X and Z coordinates is

$$[K] = \begin{bmatrix} 700000 & -300000 & -400000 & 0 & 200000 & 0 & -200000 & 0 \\ -300000 & 700000 & 0 & -400000 & 0 & -200000 & 0 & 200000 \\ -400000 & 0 & 700000 & -300000 & -200000 & 0 & 200000 & 0 \\ 0 & -400000 & -300000 & 700000 & 0 & 200000 & 0 & -200000 \\ 200000 & 0 & -200000 & 0 & 300000 & 0 & -100000 & -200000 \\ 0 & -200000 & 0 & 200000 & 0 & 300000 & -200000 & -100000 \\ -200000 & 0 & 200000 & 0 & -100000 & -200000 & 300000 & 0 \\ 0 & 200000 & 0 & -200000 & -200000 & -100000 & 0 & 300000 \end{bmatrix} \qquad (74)$$

The transformation matrix is

$$[T] = \begin{bmatrix} 1 & -1 & 0 & 0 & 0 & 0 & 0 & 0 \\ 0 & 0 & -1 & 1 & 0 & 0 & 0 & 0 \\ 0 & 0 & 0 & 0 & 1 & 0 & 0 & -1 \\ 0 & 0 & 0 & 0 & 0 & 1 & -1 & 0 \\ .894427 & 0 & -.894427 & 0 & .447214 & 0 & -.447214 & 0 \end{bmatrix} \quad (75)$$

The eigenvectors of nonzero eigenvalues of K are

$$[\phi] = \begin{bmatrix} -1 & -1 & 1 & \sqrt{2}-1 & 0 \\ 1 & -1 & -1 & 1-\sqrt{2} & 0 \\ 1 & 1 & 1 & 1-\sqrt{2} & 0 \\ -1 & 1 & -1 & \sqrt{2}-1 & 0 \\ 1-\sqrt{2} & -1/2 & 0 & -1 & -1 \\ 1-\sqrt{2} & 1/2 & 0 & -1 & 1 \\ \sqrt{2}-1 & 1/2 & 0 & 1 & -1 \\ \sqrt{2}-1 & -1/2 & 0 & 1 & 1 \end{bmatrix} \quad (76)$$

The eigenvectors of K are orthogonal because K is symmetrical. The strain stiffness matrix, k, which is the matrix of $\partial\Delta q_k / \partial\Delta f_j$, is found using equation (65).

$$[k] = \begin{bmatrix} 675781.2 & 375781.2 & 187890.6 & 187890.6 & -419262.7 \\ 375781.2 & 675781.3 & 187890.6 & 187890.6 & -419262.7 \\ 187890.6 & 187890.6 & 293945.3 & 293945.3 & -209631.4 \\ 187890.6 & 187890.6 & 293945.3 & 293945.3 & -209631.4 \\ -419262.7 & -419262.7 & -209631.4 & -209631.4 & 1E+06 \end{bmatrix} \quad (77)$$

The inverse of the above k matrix is a strain mobility matrix which is the same as a strain influence coefficient matrix and is shown on the following page.

$$[k]^{-1} = \begin{bmatrix} 2.54902E\text{-}06 & -7.843137E\text{-}07 & -5.882353E\text{-}07 & -5.882353E\text{-}07 & 4.932503E\text{-}07 \\ -7.843137E\text{-}07 & 2.54902E\text{-}06 & -5.882353E\text{-}07 & -5.882353E\text{-}07 & 4.932503E\text{-}07 \\ -5.882353E\text{-}07 & -5.882353E\text{-}07 & 4.558823E\text{-}06 & -4.411764E\text{-}07 & 3.699378E\text{-}07 \\ -5.882353E\text{-}07 & -5.882353E\text{-}07 & -4.411764E\text{-}07 & 4.558823E\text{-}06 & 3.699377E\text{-}07 \\ 4.932503E\text{-}07 & 4.932503E\text{-}07 & 3.699378E\text{-}07 & 3.699377E\text{-}07 & 1.568704E\text{-}06 \end{bmatrix} \tag{78}$$

As shown by this simple illustration, the coordinates conventionally used in finite element analyses for skin stiffness changes of any number of nodes can be changed by matrix transformations to accommodate strain instrumentation only, a matter of critical importance in practice where differential colinear displacements along a fuselage surface are very small.

Application of analytical testing to a skin change. - From equation (71), it is seen that the flight accelerations with the skin change are

$$\left\{q_k'\right\} = \left\{q_k\right\} - \left[\partial q_k / \partial \Delta f_r\right] \left( [I] + \left[k_{rr}\right] \left[\frac{\partial \Delta q_r}{\partial \Delta f_r}\right] \right)^{-1} \left[k_{rr}\right] \left\{\varepsilon_r \ \delta_r\right\} \tag{79}$$

and the flight strains with the change are

$$\left\{\varepsilon_j'\right\} = \left\{\varepsilon_j\right\} - \left[\partial \Delta q_j / \partial \Delta f_r\right] \left( [I] + \left[k_{rr}\right] \left[\frac{\partial \Delta q_r}{\partial \Delta f_r}\right] \right)^{-1} \left[k_{rr}\right] \left\{\varepsilon_r \ \delta_r\right\} \tag{80}$$

Define

$$\left\{F_r\right\} = \left( [I] + \left[k_{rr}\right] \left[\frac{\partial \Delta q_r}{\partial \Delta f_r}\right] \right)^{-1} \left[k_{rr}\right] \left\{\varepsilon_r \ \delta_r\right\} \tag{81}$$

For analytical purposes, this may be thought of as a new set of external forces operating on the aircraft and caused by the skin change. In this case, these are tensile forces, as illustrated in Figure 10. Equations (79) and (80) may be written

$$\left\{q_k'\right\} = \left\{q_k\right\} - \left[\frac{\partial q_k}{\partial \Delta f_r}\right] \left\{F_r\right\} \tag{82}$$

and

$$\left\{\varepsilon_j'\right\} = \left\{\varepsilon_j\right\} - \left[\frac{\partial \varepsilon_j}{\partial \Delta f_r}\right] \left\{F_r\right\} \tag{83}$$

The strain stiffness matrix, $k_{rr}$, of the contemplated skin change is obtained from a finite element analysis as discussed above. From flight tests of the baseline aircraft, the accelerations $\{q_k\}$ and the strains $\{\varepsilon_j\}$ at coordinates of interest are known. From modal shake testing (or finite element analysis) of the baseline aircraft the orthonormal modes $[\Psi_k]$ and $\left[\Psi_j^{(\varepsilon)}\right]$ and the frequency function [F] are known.

The nonflying shake test aircraft is instrumented with strain gages as shown in Figure 13 for a nine node change and a modal analysis test is done to obtain the orthonormal modal elements of $\left[\Psi_r^{(\varepsilon)}\right]$. The distance between nodes should be as large as possible to avoid large orthonormal strain mode elements at very high frequencies which occur when there is negligible inertial effect at a node. Long gage strain gages are preferred to minimize local effects.

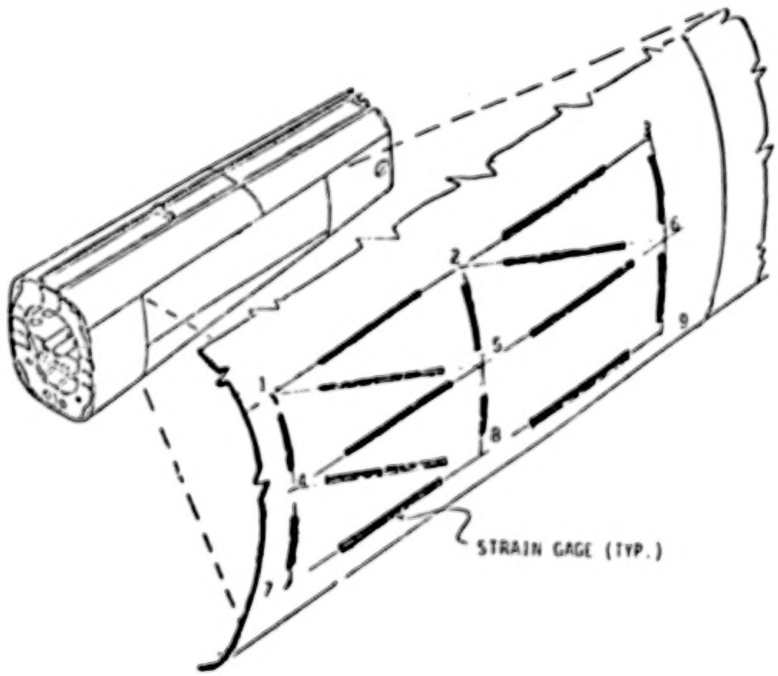


Figure 13. - Strain gages on the fuselage for flight and shake tests.

In equation (82)

$$\left[\frac{\partial \ddot{q}_k}{\partial \Delta f_r}\right] = \left[\Psi_k\right] \left[\ddot{F}\right] \left[\Psi_r^{(\epsilon)}\right]^T \left[\delta_r\right] \tag{84}$$

and in equation (83)

$$\left[\frac{\partial \epsilon_j}{\partial \Delta f_r}\right] = \left[\Psi_j^{(\epsilon)}\right] \left[F\right] \left[\Psi_r^{(\epsilon)}\right]^T \left[\delta_r\right] \tag{85}$$

A certain amount of engineering judgment must be applied to the mobilities and stiffnesses used in the equations when dealing with high load factor maneuvers in which the skin buckling might occur before reaching limit load. An approach to further investigations of this problem might be to consider an approximate strain stiffness matrix of the estimated decrease in skin stiffness with buckling, $\tilde{k}_{rr}$, and formulate

$$\left[\frac{\partial \epsilon_j}{\partial \Delta f_r}\right]_{\text{buckled}} = \left[\frac{\partial \epsilon_j}{\partial \Delta f_r}\right] \left\{\left[I\right] + \left(\left[I\right] - \left[\tilde{k}_{rr}\right] \left[\frac{\partial \Delta q_r}{\partial \Delta f_r}\right]\right)^{-1} \left[\tilde{k}_{rr}\right] \left[\frac{\partial \Delta q_r}{\partial \Delta f_r}\right]\right\} \tag{86}$$

If the $k_{rr}$ matrix of equation (81) is multiplied by a constant factor, c, the equation may be expressed as

$$\left\{F_r\right\} = \left(\left[\frac{1}{c}\right] + \left[k_{rr}\right] \left[\frac{\partial \Delta q_r}{\partial \Delta f_r}\right]\right)^{-1} \left[K_{rr}\right] \left\{\epsilon_r \delta_r\right\} \tag{86a}$$

That is, the unit matrix is simply replaced by a diagonal matrix of the reciprocal of the change factor c. The acceleration change along k

$$\frac{\ddot{q}_k'}{\ddot{q}_k} = 1 - \left[\partial \ddot{q}_k / \partial \Delta f_r\right] \left(\left[\frac{1}{c}\right] + \left[k_{rr}\right] \left[\frac{\partial \Delta q_r}{\partial \Delta f_r}\right]\right)^{-1} \left[k_{rr}\right] \left\{\frac{\epsilon_r \delta_r}{\ddot{q}_k}\right\} \tag{87}$$

and the strain change along j

$$\frac{\epsilon_j'}{\epsilon_j} = 1 - \left[\partial\Delta q_k / \partial\Delta f_r\right] \left( \left[\frac{1}{c_j}\right] + \left[k_{rr}\right] \left[\frac{\partial\Delta q_r}{\partial\Delta f_r}\right] \right)^{-1} \left[k_{rr}\right] \left\{\frac{\epsilon_r \delta_r}{\epsilon_j \delta_j}\right\} \qquad (88)$$

for any flight condition.

Equation (88) may be displayed as a function of c, the change factor, as shown in Figure 14. In a skin change, c would be the proportionality of skin thickness of the change. In this manner, the effects of the contemplated change at many different fuselage locations in a variety of maneuvers can be systematically evaluated to select the most suitable compromise of thickness factor.

Strap, Stringer and Strut Changes. - For a stringer or strap change, as shown in Figure 15, the stiffness matrix of equation (71) is diagonal with each element being the axial stiffness of the corresponding section of the strap. Equation (71) may then be expressed as

$$\left\{\begin{array}{c} \ddot{q}_k' \\ \hline \epsilon_j' \end{array}\right\} = \left\{\begin{array}{c} \ddot{q}_k \\ \hline \epsilon_j \end{array}\right\} - \left[\begin{array}{c} \partial\ddot{q}_k / \partial\Delta f_r \\ \hline \partial\epsilon_j / \partial\Delta f_r \end{array}\right] \left( \left[\frac{1}{k_{rr}}\right] + \left[\frac{\partial\Delta q_r}{\partial\Delta f_r}\right] \right)^{-1} \left\{\delta_r \ \epsilon_r\right\} \qquad (89)$$

In evaluating the effects of a possible strut addition where there is no strut at present, as in Figure 16, there is no existing surface on which to place strain gages. A pin-ended tube can be put in the position of the strut to activate a differential motion transducer such as a linear differential voltage transducer or potentiometer. The term $k_{rr}$ is the axial stiffness of the strut in equation (89) which may be written

$$\left\{\begin{array}{c} \ddot{q}_k' \\ \hline \epsilon_j' \end{array}\right\} = \left\{\begin{array}{c} \ddot{q}_k \\ \hline \epsilon_j \end{array}\right\} - \left\{\begin{array}{c} \partial\ddot{q}_k / \partial\Delta f_r \\ \hline \partial\epsilon_j / \partial\Delta f_r \end{array}\right\} \frac{\epsilon_r \delta_r}{1/k_{rr} + \partial\Delta q_r / \partial\Delta f_r} \qquad (90)$$

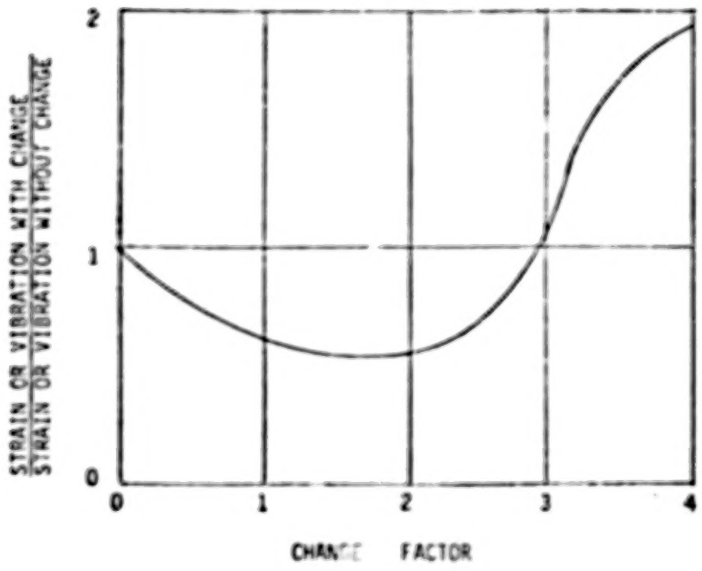


Figure 14. - The change in flight response of any coordinate in any maneuver displayed as a function of a change factor, such as skin thickness.

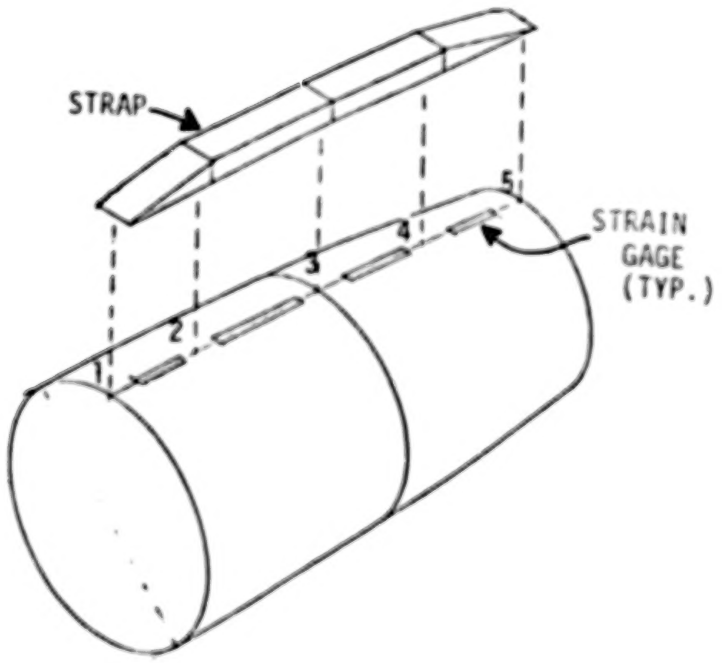


Figure 15. - A strap change of stiffness.

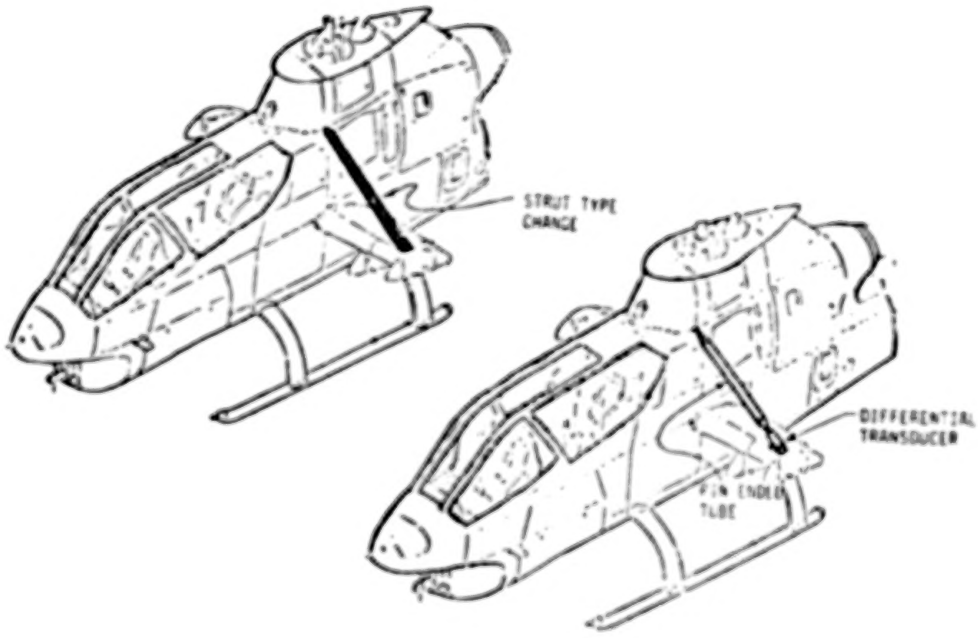


Figure 16. - A strut type change and differential transducer instrumentation in shake test.

# TECHNIQUES AND PROCEDURES FOR VIBRATION TESTING OF THE AH-1G HELICOPTER

The development of effective techniques for shaking the AH-1G and analyzing the acquired vibration data constituted a major part of the research work associated with analytical testing. The validity of the methods employed rests heavily upon the consistency between the measured structural mobilities and the theoretical models for which these mobilities are derived. This consistency is critical since the measured mobilities are used not only for obtaining the global modal parameters of the test vehicle, but also to derive mobilities which were not measured directly.

Digital signal analyzers have made it possible to measure the response of structures to any physically realizable excitation. However, the interpretation of measured structure to specified excitation forces is subject to the mathematical model used in the process of analyzing the data. The model may be more or less sophisticated, depending on the test data. The dynamic testing of a structure like the helicopter poses a number of specific problems. These problems are associated with: (1) the size and complexity of structure; (2) nonuniform distribution of mass, stiffness, and damping; and (3) the correct application of linear vibration theory to the process of data acquisition and analysis.

It has been implied that the techniques adopted for the structural dynamic testing are closely related with the theory underlying the vibration analysis. A discussion of the specific test procedures must necessarily be preceded by a brief summary of the theoretical considerations. This chapter addresses: (1) the theory of the generalized linear structure; (2) the principal characteristics of acceleration mobility data; (3) testing procedures for global parameters and the estimation of these parameters; (4) testing procedures for obtaining mode shapes and the method of calculating mode shapes; and (5) methods for deriving mobilities from modal data.

## Theory of the Generalized Linear Structure

The dynamic properties of any structure can always be characterized by a relationship between a selected set of motion coordinates and the set of externally applied forces, i.e.:

$$\begin{Bmatrix}\text{Motion}\\ \text{Vector}\end{Bmatrix} = \left|\begin{matrix}\text{Character of}\\ \text{Structure}\end{matrix}\right| \times \begin{Bmatrix}\text{Force}\\ \text{Vector}\end{Bmatrix} \tag{91}$$

The character of the structure implied in equation (91) will be termed mobility. If the motion vector is a vector of displacements/velocities/accelerations, the character of the structure is termed displacement/velocity/acceleration mobility, respectively.

The central phenomenon of vibration theory is cyclic oscillation, hence the quantities that go into equation (91) are generally sought in the frequency domain; for example, in acceleration measurements:

$$\{\ddot{y}(\omega)\} = [\ddot{Y}(\omega)]\{f(\omega)\} \tag{92}$$

where $\{\ddot{y}(\omega)\}$ is the Fourier transform of the accelerations; $[\ddot{Y}(\omega)]$ is the acceleration mobility matrix; and $\{f(\omega)\}$ is the Fourier transform of the vector of generalized forces, compatible with the selected set of coordinates.

From a measurement standpoint, the jkth element of the matrix $[\ddot{Y}(\omega)]$ relates the acceleration measured along the jth coordinate when the only force acting on the structure is that applied along the kth coordinate; i.e.:

$$\ddot{y}_j(\omega) = \ddot{Y}_{jk}(\omega)\ f_k(\omega) \qquad \text{when } f_{i \neq k} = 0 \tag{93}$$

Linear vibration response of a structure may be characterized by the following conditions: (1) the response of the structure to random forcing is stationary in time (i.e., forced vibrations are steady); (2) the elements of the matrix $[\ddot{Y}(\omega)]$ are functions of frequency only, and depend on neither the motion coordinates, nor the forcing vector; and (3) the mobility matrix $[\ddot{Y}(\omega)]$ is symmetric; i.e., $\ddot{Y}_{jk} = \ddot{Y}_{kj}$.

The foregoing conditions have specific practical implications in vibration testing and analysis. The first condition is necessary for any structure to survive continuous operation under arbitrary dynamic excitation. The second condition more or less stipulates the type of shake test data that is adequate for analysis based on a linear model of the structure. If the mobility functions measured for different force levels are not the same, the assumption of linearity is not satisfied. This is usually the case when only part of the structure may be participating in the response. As the force level is increased, more and more of the relevant motion coordinates of the structure start to participate in the response. The range of linear response is reached only when the measured mobility remains unchanged with changing force levels. The third requirement is that of reciprocity. If the shaking and measurement stations are interchanged, the same mobility should be recorded, otherwise the [Y] matrix will not be symmetric, as required by the linear model.

It is important to note that, in the foregoing characterization of a linear system, no assumptions are made about the nature of the damping mechanisms occurring in the structures. All the conditions required for linear modeling can be verified in the process of the actual shake test of the structure.

The relationship between the Fourier transform of the force vector and that of the displacement vector of a steadily vibrating undamped multiple degree of freedom system can be written as:

$$\left(-\omega^2 [M] + [K]\right)(y(\omega)) = f(\omega) \tag{94}$$

where [M] and [K] are real, symmetric mass and stiffness matrices, respectively. Thus, the displacement mobility matrix for an undamped system is simply:

$$[Y(\omega)]_U = \left(-\omega^2 [M] + [K]\right)^{-1} \tag{95}$$

The presence of damping in its most general form can be modeled by introducing a frequency dependent complex damping matrix into equation (95), i.e.:

$$[Y(\omega)]_D = \left(-\omega^2 [M] + [K] + [D^R(\omega)] + i[D^I(\omega)]\right)^{-1} \tag{96}$$

It is to be carefully noted that this analytical development has meaning only in the frequency domain for the general case of damping. This is mainly because the physical quantities that can be used to characterize the arbitrary damping of a structure are related to the energy dissipated per cycle of oscillation. In cases where the time domain, force/motion relationship, representing the damping mechanism is known, the damped equations of motion can be developed in the time domain and then Fourier transformed into the frequency domain. However, taking the inverse Fourier transform of the frequency-domain equations that may adequately describe an arbitrarily damped system may not yield a time-domain system of equations that makes physical sense. In other words, arbitrary damping mechanisms may not be susceptible to a time-domain description. Mathematical models, developed from time-domain equations of motion, usually fail to identify global characteristics of structures with significant damping.

In general, the elements of $[D^R(\omega)]$ are small, compared to those of the [K] matrix. Also, in order for reciprocity conditions to be met and for energy to be dissipated, the damping matrix must be symmetric and non-negative definite over the entire frequency range.

For a damped system, then:

$$\left([K] + i[D(\omega)] - \omega^2 [M]\right) \{y(\omega)\} = \{f(\omega)\} \tag{97}$$

Consider the complex, frequency dependent characteristic value problem:

$$\left([K] + i[D(\omega)]\right)\{\phi\} = \lambda(\omega)[M]\{\phi\} \tag{98}$$

where $\{\phi\} = \{\phi^R\} + i\{\phi^I\}$ is the complex characteristic vector which can be assumed to be frequency independent; $\lambda(\omega) = \lambda^R(\omega) + i\lambda^I(\omega)$ is the frequency dependent complex eigenvalue.

If combinations of $\left(\lambda_j(\omega), \{\phi\}_j\right)$ and $\left(\lambda_k(\omega), \{\phi\}_k\right)$ exist, which satisfy equation (98), then:

$$\{\phi\}_k^T \left([K] + i[D(\omega)]\right)\{\phi\}_j = \lambda_j(\omega)\{\phi\}_k^T [M]\{\phi\}_j \tag{99}$$

and

$$\{\phi\}_j^T \left([K] + i[D(\omega)]\right)\{\phi\}_k = \lambda_k(\omega)\{\phi\}_j^T [M]\{\phi\}_k \tag{100}$$

$\{\phi\}^T$ denotes the transpose of $\{\phi\}$. By virtue of the symmetry of the [K], [M], and $[D(\omega)]$ matrices, equations (99) and (100) lead to the following orthogonality relationships:

$$\{\phi\}_j^T [M] \{\phi\}_k = m_j \delta_{jk} \tag{101}$$

and

$$\{\phi\}_j^T \left([K] + i[D(\omega)]\right)\{\phi\}_k = \left(k_j + id_j(\omega)\right) \delta_{jk} \tag{102}$$

where:

$$m_j = \{\phi\}_j^T [M] \{\phi\}_j \tag{103}$$

$$k_j = \{\phi\}_j^T [K] \{\phi\}_j \tag{104}$$

$$d_j(\omega) = \{\phi\}_j^T [D(\omega)] \{\phi\}_j \tag{105}$$

$$\delta_{jk} = \begin{matrix} 0 & j \neq k \\ 1 & j = k \end{matrix} \tag{106}$$

It follows that:

$$\begin{aligned} \{\phi\}_j^T \left([K] - \omega^2 [M] + i[D(\omega)]\right)\{\phi\}_k &= \left(k_j - \omega^2 m_j + id_j(\omega)\right)\delta_{jk} \\ &= \left(\lambda_j(\omega) - \omega^2\right)m_j \delta_{jk} \end{aligned} \tag{107}$$

If the vectors $\{\phi\}_j$ exist, it can easily be verified that only the imaginary parts of $\lambda_j(\omega)$ need be frequency dependent. So that:

$$\lambda_j(\omega) = \lambda_j^R + i\,\lambda_j^I(\omega) \tag{108}$$

Indeed, by post-multiplying the transpose of equation (98) by $\{\phi\}_j^*$, which is the complex conjugate of $\{\phi\}_j$, the following equation is obtained:

$$\{\phi\}_j^T \left([K] + i[D(\omega)]\right)\{\phi\}_j^* = \lambda_j(\omega)\ \{\phi\}_j^T [M]\ \{\phi\}_j^* \tag{109}$$

Similarly, the complex conjugate of equation (98) can be premultiplied by $\{\phi\}_j^T$ to get:

$$\{\phi\}_j^T \left([K] - i[D(\omega)]\right)\{\phi\}_j^* = \lambda_j^*(\omega)\ \{\phi\}_j^T [M]\ \{\phi\}_j^* \tag{110}$$

From equations (109) and (110);

$$\lambda_j(\omega) + \lambda_j^*(\omega) = 2\ \{\phi\}_j^T [K]\ \{\phi\}_j^* / \{\phi\}_j^T [M]\ \{\phi\}_j^* \tag{111}$$

and

$$\lambda_j(\omega) - \lambda_j^*(\omega) = 2i\ \{\phi\}_j^T [D(\omega)]\{\phi\}_j^* / \{\phi\}_j^T [M]\{\phi\}_j^* \tag{112}$$

The right hand side of equation (111) is a frequency independent quantity. However, the right hand side of equation (112) is frequency dependent, establishing the validity of the claim made in equation (108).

A complex L x N modal matrix $[\phi]$ can be defined such that its jth column is the L x 1 vector $\{\phi\}_j$; j = 1, 2, ...N, where L is the number of coordinates chosen to describe the system and N is the number of modes of the system. In principle, N is infinite; in practice, over a given frequency range, only a finite number of system modes are necessary.

Equation (97) can be rewritten to give,

$$\{y(\omega)\} = [\phi]\left[[\phi]^T\left([K] - \omega^2[M] + i[D(\omega)]\right)[\phi]\right]^{-1}[\phi]^T\{f(\omega)\} \qquad (113)$$

and, using the orthogonality relationships, leads to the results,

$$\{y(\omega)\} = [\phi]\left[\frac{1}{\left((\lambda_j^R - \omega^2) + i\lambda_j^I(\omega)\right) m_j}\right][\phi]^T\{f(\omega)\} \qquad (114)$$

By definition: $\{y(\omega)\} = [Y(\omega)]\{f(\omega)\}$ ; hence,

$$[Y(\omega)] = \sum_{n=1}^{N}\left[\frac{\{\phi\}_n\{\phi\}_n^T}{m_n}\right]\frac{1}{(\lambda_n^R - \omega^2) + i\,\lambda_n^I(\omega)} \qquad (115)$$

$\lambda_n^R$ and $\lambda_n^I(\omega)$ have units of (frequency)$^2$ and, from physical considerations, both $\lambda_n^R$ and $\lambda_n^I(\omega)$ are positive. It is, therefore, possible to define:

$$\lambda_n^R \equiv \Omega_n^2 \qquad (116)$$

and

$$\lambda_n^I(\omega) \equiv g_n(\omega)\Omega_n^2 \qquad (117)$$

The matrix of modal acceleration coefficients of the nth mode is defined as:

$$[A]_n \equiv \frac{1}{m_n}\{\phi\}_n\{\phi\}_n^T \qquad (118)$$

The acceleration mobility matrix and the displacement mobility matrix are related by:

$$[\ddot{Y}(\omega)] = -\omega^2[Y(\omega)] \qquad (119)$$

Making use of equations (116), (117), (118), and (119), the jkth acceleration mobility can be written as:

$$\ddot{Y}_{jk}(\omega) = - \sum_{n=1}^{N} A_{jkn} \frac{\omega^2/\Omega_n^2}{(1 - \omega^2/\Omega_n^2) + ig_n(\omega)} \tag{120}$$

In the most general case, the dependence of $g_n(\omega)$ on frequency may not be known. However, it is expedient to take advantage of the fact that the $ig_n(\omega)$ term in equation (120) is dominant only in the frequency range where $\omega^2/\Omega_n^2 = 1$, i.e., near the natural frequency of the nth mode. Thus, any suitable representation of $g_n(\omega)$ which matches the correct value in the neighborhood of $\omega = \Omega_n$ may be assumed.

The general form of the jkth element of the acceleration mobility matrix can be written as:

$$\ddot{Y}_{jk} = \ddot{Y}^R_{jk} + i\ddot{Y}^I_{jk} = E^R_{jk} + iE^I_{jk} - \sum_{n=1}^{N} A_{jkn} \frac{\omega^2/\Omega_n^2}{(1 - \omega^2/\Omega^2_n) + ig_n(\omega)} \tag{121}$$

where $E^R_{jk} + iE^I_{jk}$ represents the rigid body acceleration coefficients ($E^I_{jk}$ is usually very small compared to the rest of the terms in the series and is often neglected); $A_{jkn} = A^R_{jkn} + iA^I_{jkn}$ is the jkth complex element of the matrix of modal accelerations for the nth mode; $\Omega_n$ and $g_n$ are the natural frequencies and damping coefficients of the nth mode, respectively; $\omega$ is frequency.

## Characteristics of Acceleration Mobility Data

### Mode frequency functions

The real and imaginary parts of $\ddot{Y}_{jk}$ can be written as:

$$\ddot{Y}^R_{jk} = E^R_{jk} - \sum_{n=1}^{N} \left[ A^R_{jkn} \ddot{F}^R_n (\omega) - A^I_{jkn} \ddot{F}^I_n (\omega) \right] \tag{122}$$

and

$$\ddot{Y}^I_{jk} = E^I_{jk} - \sum_{n=1}^{N} \left[ A^I_{jkn} \ddot{F}^R_n (\omega) + A^R_{jkn} \ddot{F}^I_n (\omega) \right] \tag{123}$$

or:

$$\ddot{Y}_{jk} = E^R_{jk} + iE^I_{jk} - \sum_{n=1}^{N} A_{jkn} \ddot{F}_n (\omega) \tag{124}$$

where the mode frequency functions are defined as:

$$\ddot{F}^R_n (\omega) \equiv \frac{\omega^2/\Omega_n^2 \, (\omega^2/\Omega_n^2 - 1)}{(\omega^2/\Omega_n^2 - 1)^2 + g_n^2} \tag{125}$$

$$\ddot{F}^I_n (\omega) \equiv \frac{g_n \, \omega^2/\Omega_n^2}{(\omega^2/\Omega_n^2 - 1)^2 + g_n^2} \tag{126}$$

and

$$\ddot{F}_n (\omega) \equiv \ddot{F}^R_n (\omega) + i\ddot{F}^I_n (\omega) \tag{127}$$

Equations (122), (123), and (124) represent the measured acceleration mobility as a linear combination of the mode functions. It is, therefore, important to acquire a familiarity with the basic characteristics of the mode functions of damped systems and the essential features of their linear combinations. Plots of $\ddot{F}^R (\omega)$ and $\ddot{F}^I (\omega)$ as functions of frequency ratio for three values of the damping coefficient are shown in Figure 17. The polar plots of the complex $\ddot{F} (\omega)$ functions are shown in Figure 18.

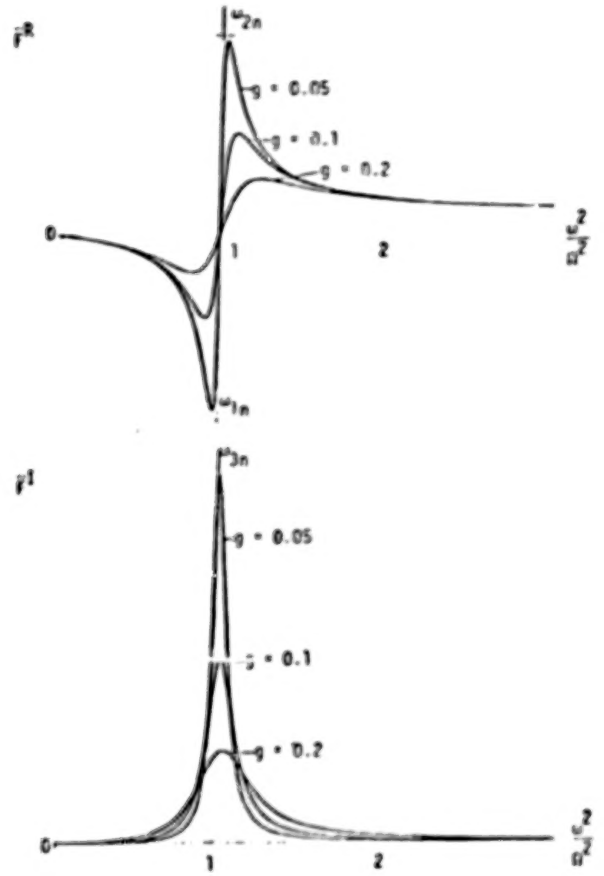


Figure 17. - Real ($\ddot{F}^R$) and imaginary ($\ddot{F}^I$) parts of the complex "mode" function $\ddot{F}(\omega)$.

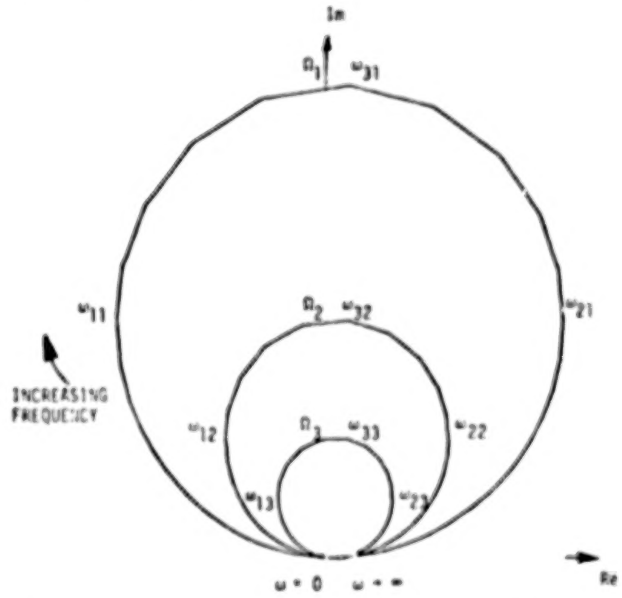


Figure 18. - Polar plot of the complex $\ddot{F}(\omega)$ function.

The $\ddot{F}^R(\omega)$ function is characterized by two peaks at

$$\omega_{1n} = \Omega_n \sqrt{1 + g_n^2} - g_n \sqrt{1 + g_n^2} \tag{128}$$

and

$$\omega_{2n} = \Omega_n \sqrt{1 + g_n^2} + g_n \sqrt{1 + g_n^2} \tag{129}$$

while the $\ddot{F}^I(\omega)$ function has only one peak at $\omega_{3n} = \Omega_n \sqrt{1 + g_n^2}$. Note that,

$$\frac{\omega_{2n}^2 - \omega_{1n}^2}{\Omega_n^2} = 2g_n \sqrt{1 + g_n^2} \tag{130}$$

which increases with increasing damping.

From the plots in Figure 17, it is seen that linear combinations of $\ddot{F}^R$ and $\ddot{F}^I$ vary rapidly in the vicinity of the natural frequency, and are either negligible or slowly varying with frequency in the regions away from the natural frequency.

Separated Modes. - Equation (121) carries the basic implication that the effects of the structure's modes occurring at different frequencies on the measured mobility are additive in the frequency domain. If a mode occurs at a frequency, in the neighborhood of which the contributions from the other modes of the structure are either negligible or are weakly varying with frequency, such a mode is said to be well separated. The nature of the measured mobility in this frequency range will be dominated by that particular mode.

Classical Modes. - In the case of a classical mode, i.e., when the system mode shape is the same for the damped system as it would be for the undamped system the $A_{jkn}$ is a real number, i.e., $A^I_{jkn} = 0$, and the real part of the measured acceleration mobility will show two turning points for each separated mode and the imaginary part will show a single turning point only. For a classical mode, equation (130) can be approximated to give an estimate of the damping coefficient: $g_n = (\omega_{2n} - \omega_{1n})/\Omega_n$.

Figures 19 and 20 show acceleration mobility measurements obtained from a helicopter structure. Two close, but distinguishable modes are present. The dominant mode can be seen to be very nearly classical, with double turning points in the real, and a single turning point in the imaginary mobilities.

Complex Modes. - For the general case of nonclassical or complex modes, both $A^R_{jkn}$ and $A^I_{jkn}$ are significant. The measured real and imaginary mobilities of a well separated mode contain linear combinations of both $F^R(\omega)$ and $F^I(\omega)$ in proportions given in equations (122) and (123). In particular, if $A^I_{jkn} >> A^R_{jkn}$, it is the imaginary part of the acceleration mobility which will show two turning points, while the real part will show a single turning point only. Figures 21 and 22 show an example of this occurrence in the data measured from the AH-1G (the shaking coordinate was vertical at the tail, and the measurement coordinate was vertical at the nose) between 40 Hz and 50 Hz.

Coupled Modes. - System modes, occurring in frequency ranges such that their mutual contributions to the measured mobility in this frequency range are rapidly varying functions of frequency, are said to be coupled.

Mode Clusters. - A mode cluster (or a cluster of modes) is characterized by a group of system modes which are coupled together by virtue of the proximity of their resonances. Mode clusters are usually separated by regions of negligible or slowly varying mobility values in the frequency domain.

Mode clusters generally have the appearance of single modes in wideband, low frequency resolution mobility measurements. Higher resolution data usually helps to reveal the modal content of a particular mode cluster. Figure 23 shows broad band (0 - 200 Hz) mobility of a helicopter vertical tail shake, measuring vertical acceleration at the nose. Between mode clusters, measured mobility is seen to vary slowly close to the zero value. In fact, what appears to be a single mode in the 0 - 10 Hz frequency range is actually a cluster of two modes as figures 19 and 20 (which are higher resolution measurements of the same mobility in the 5 - 10 Hz range) show.

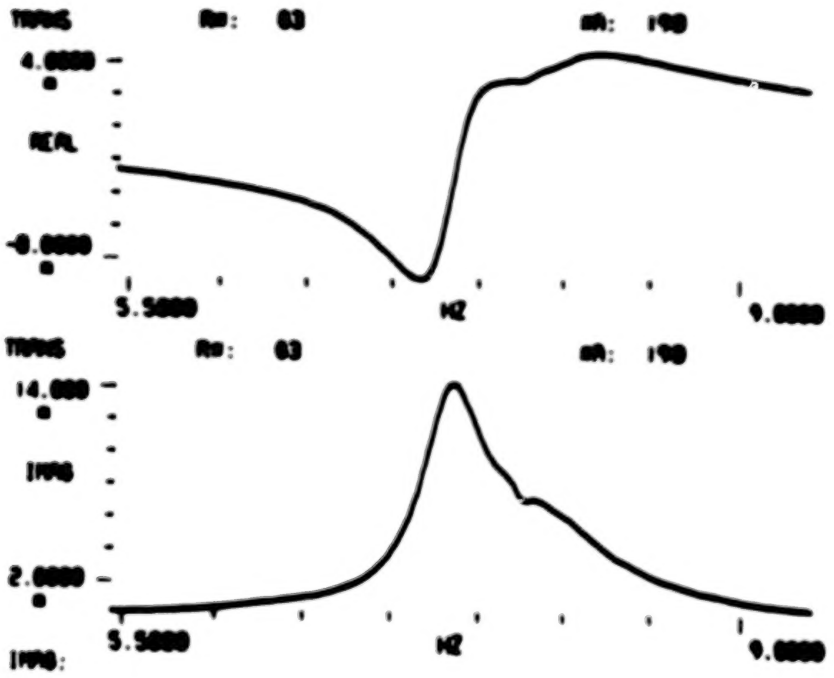

Figure 19. - Measured acceleration mobility of a helicopter between 5.5 and 10 Hz. (Shaking vertically at the tail, measuring vertical acceleration at the nose.)

Figure 20. - Data of Figure 19 plotted on the Argand Plane.

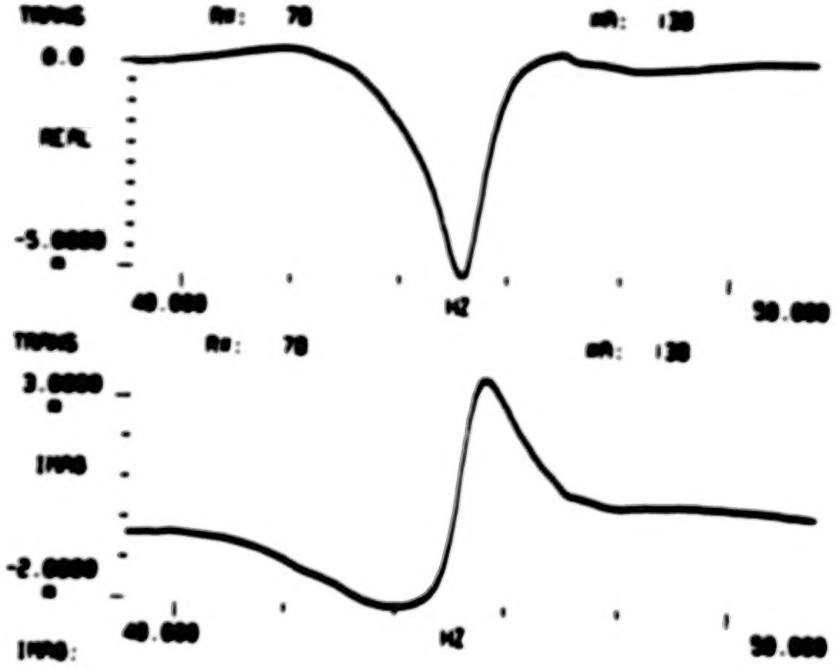

Figure 21. - Measured acceleration mobility of a helicopter between 38 Hz and 52 Hz. (Shaking vertically at the tail, measuring vertical acceleration at the nose.)

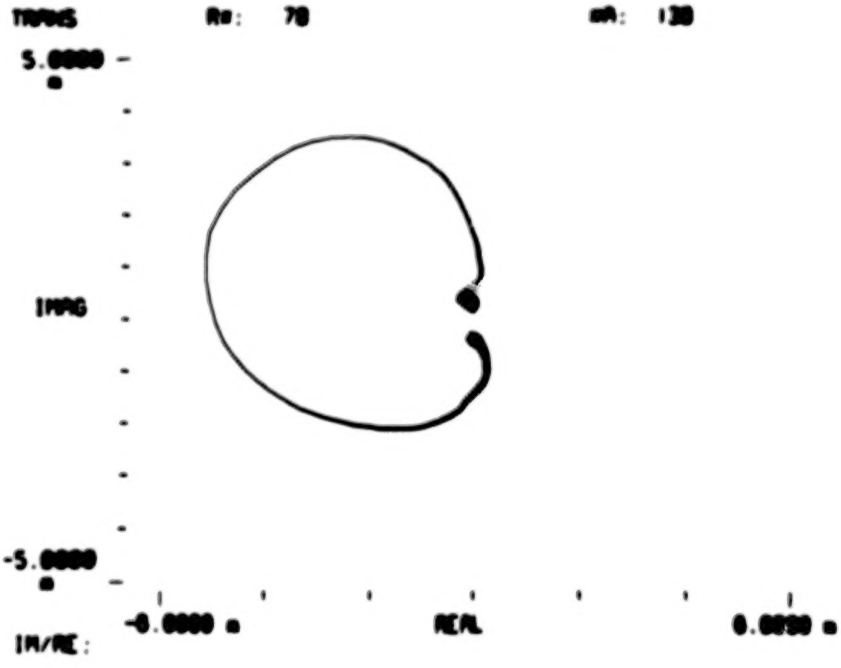

Figure 22. - Data of Figure 21 plotted on the Argand Plane.

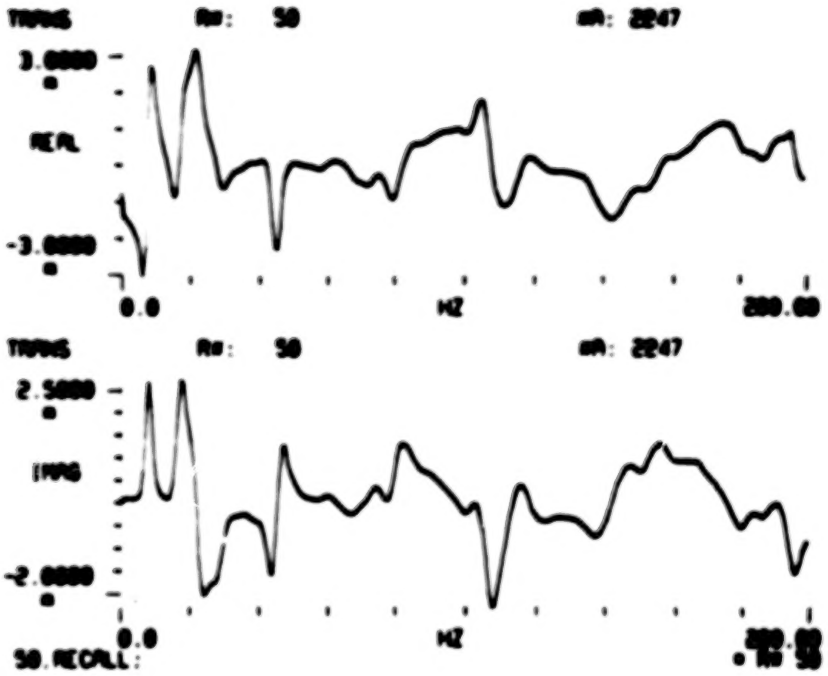

Figure 23. - Measured acceleration mobility of a helicopter between 2 Hz and 200 Hz. (Shaking vertically at the tail, measuring vertical acceleration at the nose.)

Identification of mode clusters is useful in determining which modes should be included when truncating equation (121), since the contributions of the remaining modes are either negligible or frequency independent. It also helps in identifying frequency segments for higher resolution data acquisition.

## Shake Testing for Global Parameters

Each elastic mode of the structure is characterized by a natural frequency $\Omega_{f_n}$ and a damping coefficient $g_n$ which are global properties of the structure. These are the only constants that enter into the mode frequency functions. They are the same for a given mode, regardless of the response coordinate. The first stage of modal testing is to determine the global parameters of the dominant elastic modes which occur inside the frequency range of interest.

The experimental data required for determining the global parameters are the continuous frequency plots of a number of mobilities which are considered to represent the global vibrational behavior of the structure. For a selected set of shaking locations, e.g., tail vertical, tail rotor gearbox lateral, etc., the transfer functions between the response coordinate and the shaking coordinate are measured over the determined frequency range. Typical response coordinates for such measurements are: (1) nose vertical; (2) wing (right and/or left) vertical; (3) center of gravity vertical; (4) tail vertical; and (5) horizontal stabilizer vertical.

The test set up for measuring frequency dependent mobility functions is shown in Figure 24. The helicopter is suspended as a free body by soft rubber bungee chords. The configuration shown has the shaker located vertically at the tail and the response accelerometer at the horizontal stabilizer vertical. Signals for driving the electromagnetic shaker originate from the signal generator. A force gage, installed at the point of force application generates voltage signals which are proportional to the applied force. These signals are inputs to the dual channel digital signal analyzer. The accelerometer at the response coordinate generates voltage signals, proportional to the response acceleration, which are also inputs to the digital signal analyzer.

The signal analyzer is capable of sampling the time-domain force and response signals, digitizing these samples and computing the real-time Fourier transforms of the data. It also computes the least squares estimate of the frequency-domain transfer function between the input and output spectra, which is the mobility between the response and forcing coordinates. All the frequency functions computed by the analyzer over the specified frequency interval can be stored on cassette tapes for future restoration and analysis. The oscilloscope allows the monitoring of the time-domain signals emanating from the force and response transducers. The frequency counter is used to precisely measure the frequencies of harmonic signals when required.

The accuracy with which the global parameters can be estimated is critically dependent on the quality of the data acquired for this purpose. For each pair of force and response locations, a random shake is done with the frequency

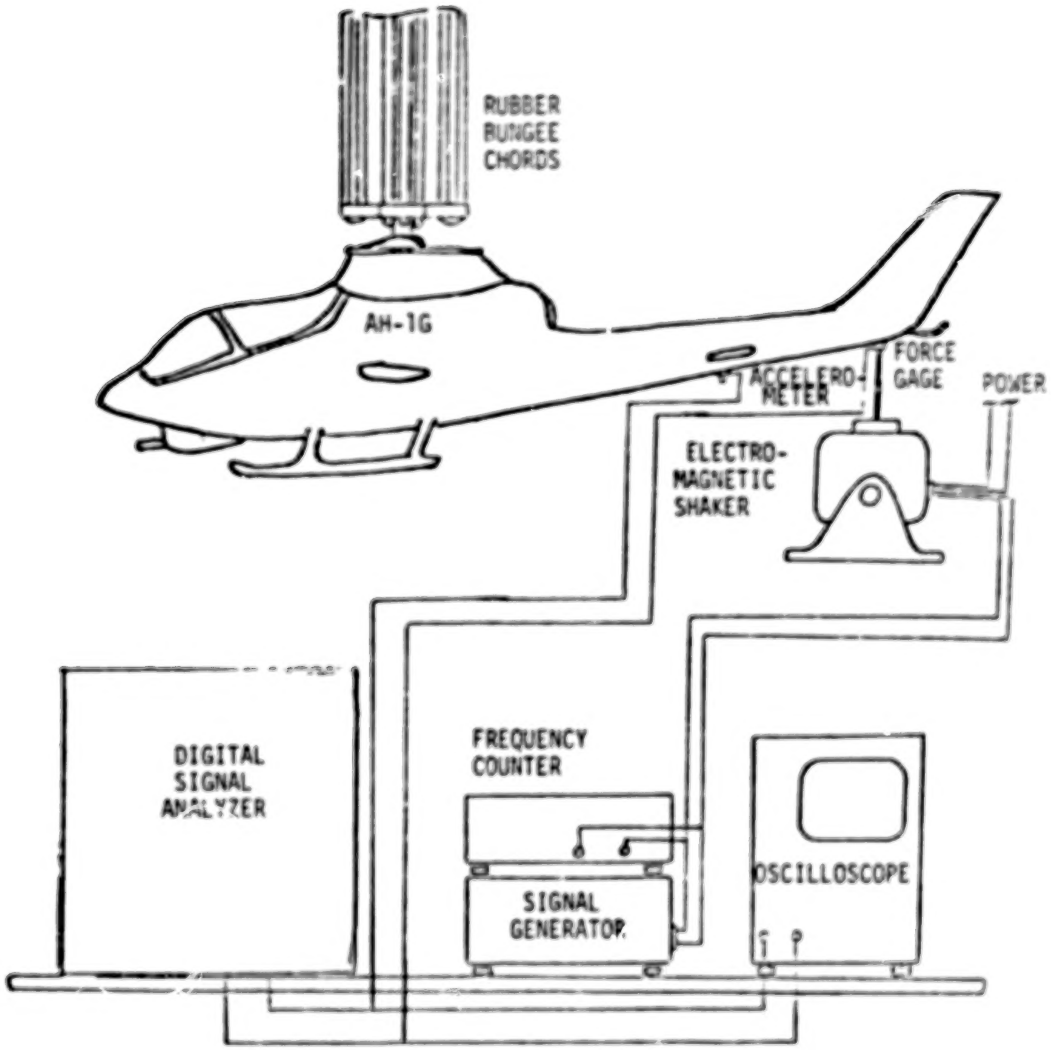


Figure 24. - Schematic of test set-up for global parameter testing.

bandwidth set to span twice the frequency range of interest (in this case, 0 - 200 Hz, since the modes of interest are between 2 - 100 Hz). This is done to insure that the modes up to 100 Hz are not coupled to modes occurring beyond 100 Hz, as may be the case when a local mode is present. For each new shaking station, several force levels are tested until the range of applied force is reached where the mobility plots do not depend on the force level anymore. This is one of the linearity requirements on the mobility plots. Having established the required force level and the absence of local coupling modes at higher frequency, another random shake is done, this time with the bandwidth set at 2 - 100 Hz. The above procedure is repeated for all the accelerometers which have been selected for global parameter testing.

The ratio of modal acceleration coefficient to damping ($A_{jkn}/g_n$) varies not only from mode to mode, but also from mobility to mobility, for a given mode, and the prominence of the various modes of the structure will be different in each of the mobilities recorded. That is to say, a given mode i occurring at $\Omega_i$ may appear very prominently on mobility $\ddot{Y}_{jk}(\omega)$, while the same mode may not be so significant in the mobility $\ddot{Y}_{j\ell}(\omega)$, where $\ell$ designates a response coordinate different from k. This will especially be the case if the mode shape associated with mode i has a much larger mode element at coordinate k than coordinate $\ell$. The prominence of a mode may also be due to light damping. Thus, by examining the set of broadband mobilities recorded, it is possible to associate each mode i with the mobility where the mode most prominently appears.

Although it is possible to obtain rough estimates of the natural frequencies and damping of the structural elastic modes from these broadband mobility plots especially when damping is very light (e.g., peaks of the imaginary mobility plots, and frequency separation of the peaks in the real mobility plots), there are a number of specific considerations why broadband mobility data is not suitable for global parameter extraction. Among these considerations are:

Measurement Accuracy. - The low frequency resolution associated with broadband mobility measurements tends to introduce errors into the measured mobility values due to the phenomenon of leakage. Leakage has to do with a spreading

of the energy contained at each discrete frequency over a relatively narrow band nearby. Although considerable effort is exerted into reducing leakage effects (e.g., by appropriately windowing) by the equipment manufacturers, the phenomenon still has to be reckoned with when the frequency resolution gets below certain limits. For acceptable measurements, bandwidths of about 25% of the center frequency have been recommended.

Parameter Extraction Accuracy. - Also associated with low frequency resolution are inaccuracies in the parameter extraction methods due to the frequency spacing between successive data points. The polar plot of mobilities, (see Figure 18) in the vicinity of a mode, describes a circular arc. Most methods for extracting natural frequencies, damping and modal acceleration coefficients are based on fitting a continuous circle through measured data and in some cases computing the rate of change of the arc length with frequency. Since the frequency data is discrete, arcs of the circle are necessarily approximated by segments. The error incurred by approximating a circular arc by a straight line segment increases as the frequency spacing between successive data points increases. Narrow band data, with bandwidth less than 25% of the natural frequency of a given mode, have been found to yield sufficiently accurate results. Initial estimates of the natural frequencies can be obtained from the broadband data.

For sufficient frequency resolution and to minimize leakage, the following bandwidths are recommended for use in narrow band testing using the HP5420A signal analyzer.

| Natural Frequency, $\Omega_i$ (Hz) | | Bandwidth (Hz) |
|---|---|---|
| Equal to or greater than | But less than | |
| 2 | 3 | .5 |
| 3 | 4 | .781 |
| 4 | 6 | 1.000 |
| 6 | 8 | 1.5625 |
| 8 | 12 | 2.000 |
| 12 | 16 | 3.125 |
| 16 | 25 | 4.000 |
| 25 | 32 | 6.250 |
| 32 | 50 | 8.000 |
| 50 | 64 | 12.500 |
| 64 | 100 | 16.000 |

In cases of g greater than .25 use a broader bandwidth. In all cases use the natural frequency as the center frequency.

## Swept Sine Testing

For all the narrow band mobility measurements, the excitation was achieved by applying pure sine wave signals to the electromagnetic shaker and varying the frequency of the sine waves over the range spanned by the bandwidth. This so-called swept sine technique was preferred to other excitation techniques over a narrow frequency band. Among other reasons for choosing the swept sine technique are that:

1. The energy input into each measurement frequency is maximum.
2. By choosing the right sweep speed (see sketch on following page), the steady state sinusoidal response of the structure is achieved at each measurement frequency. This is one of the assumptions made in the derivation of the generalized linear model.
3. Measurements are more accurate and reproducible.
4. The sampling frequencies and the adequate number of averages are more easily determined.

5. Good linearity and reciprocity checks were obtained.

6. High resolution of close modes can be achieved by selecting the right sweep speed.

Consider an undamped single degree of freedom linear system, described by the following equation of forced vibrations:

$$m\ddot{x} + kx = Fe^{i\omega t} \tag{131}$$

If the forcing frequency coincides with the undamped natural frequency, i.e., $\omega = \sqrt{\frac{k}{m}}$ , the response of the system is secular, and grows linearly with time.

Schematically:

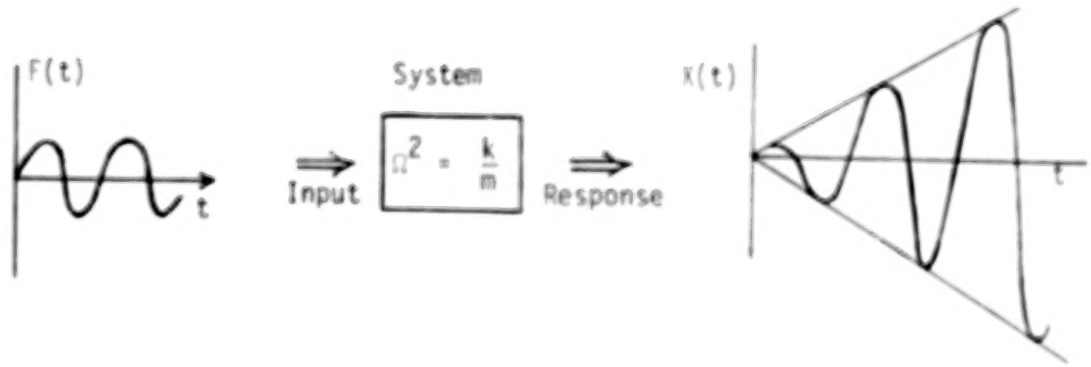


The undamped steady state response is governed by

$$\ddot{x} + \Omega^2 x = \frac{F}{m} e^{i\Omega t} \tag{132}$$

or,

$$x(t) = -i \frac{Ft}{2m\Omega} e^{i\Omega t} \tag{133}$$

However, because of the various dissipative mechanisms which constitute damping, the oscillations reach a limiting amplitude after some characteristic time .

TABLE OF CONTENTS

TABLE OF CONTENTS (continued)

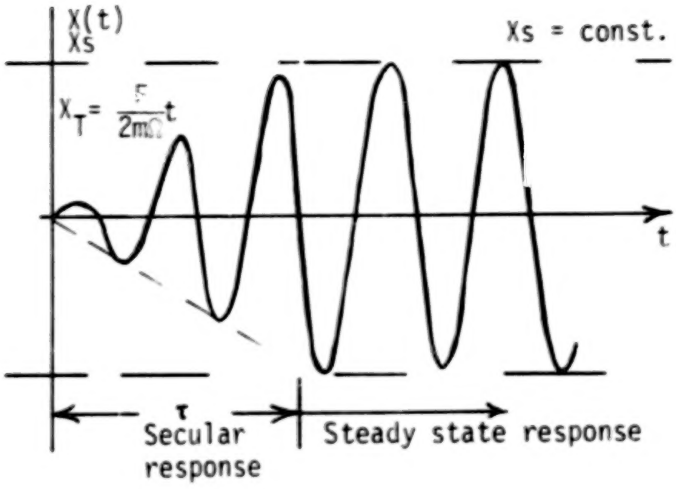


For damped hysteretic damping, g, the steady state response is governed by

$$\ddot{x} + (1 + ig)\Omega^2 x = \frac{F}{m} e^{i\Omega t} \tag{134}$$

or,

$$x(t) = -\frac{F}{mg\Omega^2} e^{i\Omega t} \tag{135}$$

The steady state amplitude is given by

$$Xs = \frac{F}{mg\Omega^2} \tag{136}$$

and the characteristic time for reaching steady state response can be estimated by equating,

$$X_T(\tau) = Xs \tag{137}$$

which gives,

$$\frac{F}{2m\Omega} \tau = \frac{F}{mg\Omega^2} \tag{138}$$

thus:

$$\tau = \frac{2}{g\Omega} = \frac{1}{\pi g f} \tag{139}$$

Suppose there are two neighboring structural modes with the natural frequencies separated by $\Delta f$ Hz. To resolve these two close modes, the speed at which the excitation frequency is changing must be of the order of:

$$v = V\Delta_f = \pi g f \ \Delta_f \quad \text{Hz/sec} \tag{140}$$

where $g$ = damping coefficient (lower bound)

$f$ = frequency in Hz

$\Delta_f$ = mode resolution in Hz.

If an estimate of the lower bound of the damping coefficient and the required mode resolution are available, the sweep speed required for swept sine shake testing is directly proportional to the frequency,

i.e. $$\frac{V(\Delta_f)}{f} = \text{const} \tag{141}$$

The relationship between the linear scale and the logarithmic scale on the signal generator is:

$$f_{dec} = \log_{10} \frac{f_{hz}}{f_0} \tag{142}$$

where

$f_{hz}$ = frequency in Hertz; $(f_0 \leq f_{hz} \leq 10 f_0)$

$f_{dec}$ = frequency in decades; $(0 \leq f_{dec} \leq 1.0)$

$f_0$ = base frequency on the scale.

From equation (142)

$$f_{hz} = f_0 \times 10^{f_{dec}} \tag{143}$$

$$\text{Sweep speed } v = \frac{df_{hz}}{df_{dec}} = \frac{df_{hz}}{df_{dec}} \times \frac{df_{dec}}{dt} \text{ Hz/sec.} \tag{144}$$

From equation (143)

$$\frac{df_{hz}}{df_{dec}} = (f_0 \ln 10) \times 10^{f_{dec}} = f_{hz} \ln 10 \tag{145}$$

and

$$\frac{v}{f_{hz}} = \frac{df_{dec}}{dt} \ln 10 \tag{146}$$

Thus, by selecting a constant logarithmic sweep speed ($df_{dec}/dt$ = const. = $\alpha$), equation (141) is automatically satisfied.

The constant $\alpha$ is determined by substituting the desired value of $\frac{v}{f_{hz}}$ into equation (146). For example, if at 2 hz we desire a sweep rate of 0.01 Hz/sec, then

$$\alpha = \frac{0.01(60)}{2 \ln 10} \text{ dec/min} = .13 \text{ dec/min} \tag{147}$$

## Estimation of Global Parameters

Various techniques have been developed for estimating the natural frequencies and damping coefficients of the elastic modes of a structure from mobility data. In all cases, certain assumptions have to be made about these modes. The simplest case is when the mode is well separated and lightly damped. For such modes, the natural frequency can be approximated by the peak of the imaginary displacement mobility. The damping coefficient can be estimated as:

$$g_n \simeq \frac{1}{2} \frac{\omega_2^2 - \omega_1^2}{\Omega_n^2} \simeq \frac{\omega_2 - \omega_1}{\Omega_n} \tag{148}$$

where $\omega_2$ and $\omega_1$ are the turning point frequencies in the real displacement mobility. The above simple case is almost exclusively reserved for simple structures with uniform distribution of mass, stiffness, and damping. Very few of the modes of the helicopter can be treated this way.

The ds/df$^2$ method of Kennedy and Pancu[9]. - The following is a more general approach which has been found to work well for both classical and complex, close or separated modes. By analogy with equations (122) through (127), the jkth displacement mobility can be expressed as:

$$Y_{jk} = \frac{E_{jk}}{-\omega^2} + \sum_{n=1}^{N} \left\{ \left( A^R_{jkn} F^R_n - A^I_{jkn} F^I_n \right) + i \left( A^R_{jkn} F^I_n + A^I_{jkn} F^R_n \right) \right\} \tag{149}$$

where, $A_{jkn} = A^R_{jkn} + iA^I_{jkn}$, is the jkth modal acceleration coefficient of nth mode and $E_{jk}$ is the contribution from the rigid body modes.

Recall that

$$F_n(\omega) = F^R_n(\omega) + i\, F^I_n(\omega) = \frac{-1}{\omega^2} \ddot{F}_n(\omega) \tag{150}$$

which gives

$$F^R_n(\omega) = \frac{1}{\Omega^2_n} \frac{1 - \omega^2/\Omega^2_n}{\left(1 - \omega^2/\Omega^2_n\right)^2 + g^2_n} \tag{151}$$

and

$$F^I_n(\omega) = \frac{1}{\Omega^2_n} \frac{-g_n}{\left(1 - \omega^2/\Omega^2_n\right)^2 + g^2_n} \tag{152}$$

In the immediate vicinity of the nth natural frequency, the displacement mobility can be approximated by:

$$Y_{jk}(\omega \approx \Omega_n) = \left\{ A^R_{jkn} F^R_n(\omega) - A^I_{jkn} F^I_n(\omega) + C^R_n \frac{\omega^2}{\Omega^2_n} + d^R_n \right\}$$

$$+ i \left\{ A^R_{jkn} F^I_n(\omega) + A^I_{jkn} F^R_n(\omega) + C^I_n \frac{\omega^2}{\Omega^2_n} + d^I_n \right\} \tag{153}$$

In equation (153), the sum of the contributions from all other modes has been represented by a complex straight line:

$$\left( C^R_n + i\, C^I_n \right) \frac{\omega^2}{\Omega^2_n} + d^R_n + i\, d^I_n$$

Dropping the subscripts j, k, n and writing the real and imaginary parts of the displacement mobility separately, gives

$$Y^R(\omega \approx \Omega) \approx A^R F^R(\omega) - A^I F^I(\omega) + C^R \frac{\omega^2}{\Omega^2} + d^R \tag{154}$$

$$Y^I(\omega \approx \Omega) \approx A^R F^I(\omega) + A^I F^R(\omega) + C^I \frac{\omega^2}{\Omega^2} + d^I \tag{155}$$

If the nth mode is classical and well separated, the imaginary part of the modal acceleration coefficient vanishes and the contributions from other modes are nearly independent of frequency. In other words, $A^I$, $C^R$, and $C^I$ vanish. Thus,

$$Y^R(\omega \approx \Omega) \approx A^R F^R(\omega) + d^R \tag{156}$$

$$Y^I(\omega \approx \Omega) \approx A^R F^I(\omega) + d^I \tag{157}$$

The peak of the imaginary mobility occurs when

$$\frac{dY^I}{d\omega^2} = 0 = A^R \frac{d}{d\omega^2} \left\{ F^I(\omega) \right\} \tag{158}$$

or,

$$\frac{A^R}{\Omega^2} \frac{2/\Omega^2 \; g \left[ 1 - \omega^2/\Omega^2 \right]}{\left[ \left( 1 - \omega^2/\Omega^2 \right)^2 + g^2 \right]^2} = 0 \tag{159}$$

which is when $\omega^2/\Omega^2 = 1$, as stated previously.

The peaks of the real displacement mobility occur when,

$$\frac{dY^R}{d\omega^2} = 0 = A^R \frac{d}{d\omega^2}\left[F^R(\omega)\right] , \tag{160}$$

or,

$$\frac{A^R}{\Omega^4} \frac{\left[\left(1 - \omega^2/\Omega^2\right)^2 - g^2\right]}{\left[\left(1 - \omega^2/\Omega^2\right)^2 + g^2\right]^2} = 0 \tag{161}$$

which gives peaks at

$$\frac{\omega_1^2}{\Omega^2} = 1 - g \tag{162}$$

and

$$\frac{\omega_2^2}{\Omega^2} = 1 + g \tag{163}$$

or,

$$g = \frac{1}{2} \frac{\omega_2^2 - \omega_1^2}{\Omega^2} \approx \frac{\omega_2 - \omega_1}{\Omega} \tag{164}$$

as stated previously.

When the mode is complex, equations (154) and (155) indicate that both the real and imaginary parts of the displacement mobility contain linear combinations of $F^R(\omega)$, $F^I(\omega)$, $\omega^2$, and constants. The peaks in the mobilities in the general case may not be simply related to the natural frequency and damping coefficients. Naturally, different degrees of approximations are feasible, depending on how complicated the situation really is.

A general technique, which has been found applicable to the majority of modes encountered on the AH-1G helicopter is based on the rate of change of the arc length of the modal curve (plotted on the complex plane, i.e., the plot of the $Y^I$ against $Y^R$ with frequency as a parameter).

$$\frac{ds}{d(\omega^2)} = \sqrt{\left[\frac{dY^R}{d(\omega^2)}\right]^2 + \left[\frac{dY^I}{d(\omega^2)}\right]^2} \tag{165}$$

where s is the arc length.

The rate of change of the arc length with respect to the square of frequency is stationary when

$$\frac{d^2s}{d(\omega^2)^2} = 0 = \frac{\frac{dY^R}{d(\omega^2)}\frac{d^2Y^R}{d(\omega^2)^2} + \frac{dY^I}{d(\omega^2)}\frac{d^2Y^I}{d(\omega^2)^2}}{\sqrt{\left[\frac{dY^R}{d(\omega^2)}\right]^2 + \left[\frac{dY^I}{d(\omega^2)}\right]^2}} \tag{166}$$

or

$$\frac{dY^R}{d(\omega^2)}\frac{d^2Y^R}{d(\omega^2)^2} + \frac{dY^I}{d(\omega^2)}\frac{d^2Y^I}{d(\omega^2)^2} = 0 \tag{167}$$

Upon substitution of equations (154) and (155) into equation (167) and simplifying, the following condition for the peak of the $\frac{ds}{d(\omega)^2}$ plot is obtained:

$$|A|^2 \frac{d}{d(\omega^2)}\left\{\left[\frac{dF^R}{d(\omega^2)}\right]^2 + \left[\frac{dF^I}{d(\omega^2)}\right]^2\right\} + \frac{C^R}{2}\left\{A^R\frac{d^2F^R}{d(\omega^2)^2} - A^I\frac{d^2F^I}{d(\omega^2)^2}\right\}$$

$$+ \frac{C^I}{2}\left\{A^R\frac{d^2F^I}{d(\omega^2)^2} + A^I\frac{d^2F^R}{d(\omega^2)^2}\right\} = 0 \tag{168}$$

where $|A|^2 = (A^R)^2 + (A^I)^2$.

For a well separated mode, the constants $C^R$ and $C^I$ will be nearly zero and equation (168) gives

$$\frac{d}{d(\omega^2)}\left\{\left[\frac{dF^R}{d(\omega^2)}\right]^2+\left[\frac{dF^I}{d(\omega^2)}\right]^2\right\}=0 \tag{169}$$

Equation (169) does not involve the modal acceleration coefficients $A^R$ and $A^I$. Thus, the condition for the peaking of the rate of change of the arc length with respect to frequency squared, holds true regardless of how complex the mode is, as long as it is well separated.

Equation (169) can be expanded, making use of equations (151) and (152), and the result is:

$$\frac{d}{d(\omega^2)}\left[\frac{\left[\left[\left(1-\frac{\omega^2}{\Omega^2}\right)^2-g^2\right]^2+4g^2\left[1-\frac{\omega^2}{\Omega^2}\right]^2\right]}{\Omega^8\left[\left[\left(1-\frac{\omega^2}{\Omega^2}\right)^2+g^2\right]^4\right.}\right]=0 \tag{170}$$

Equation (170) can be evaluated to yield

$$\frac{d}{d(\omega^2)}\left[\frac{1}{\Omega^8\left[\left(1-\frac{\omega^2}{\Omega^2}\right)^2+g^2\right]^2}\right]=\frac{4}{\Omega^{10}}\frac{\left[1-\frac{\omega^2}{\Omega^2}\right]}{\left[\left(1-\frac{\omega^2}{\Omega^2}\right)+g^2\right]^3}=0 \tag{171}$$

Thus, for a well separated mode, the peak of the $\frac{ds}{d(\omega^2)}$ plot will occur at the natural frequency, regardless of whether the mode is complex or classical. Any suitable finite difference scheme can be used to compute $\frac{ds}{d(\omega^2)}$ from measured data using equation (165).

It turns out that even for modes that are not well separated, the peaks of the $\frac{ds}{d(\omega^2)}$ plot still give good approximations to the natural frequencies. To establish why this is so, consider equation (168) term by term. The first term vanishes at the natural frequency, as we have already seen. The remaining terms can be rearranged as:

$$\frac{1}{\Omega^2}\frac{d^2F^R}{d(\omega^2)^2}\left(C^RA^R + C^IA^I\right) + \frac{1}{\Omega^2}\frac{d^2F^I}{d(\omega^2)^2}\left(C^IA^R - C^RA^I\right) \tag{172}$$

At the natural frequency

$$\frac{d^2F^R}{d(\omega^2)^2} = 0 \tag{173}$$

the remaining term becomes

$$-\frac{2}{\Omega^8 g^3}\left(C^IA^R - C^RA^I\right)$$

Lightly damped modes generally tend to be classical and well separated. This is understandable, since in the limit of zero damping, a classical undamped mode results. Thus, the low damping which will tend to drive $2/\Omega^8 g^3$ up, also drives $\left(C^IA^R - C^RA^I\right)$ down, effectively neutralizing the expression. This consequently reduces the error incurred by approximating the natural frequency by the peak of the $ds/d(\omega^2)$ plot. Experience has shown that modes which are too close to be resolved by the $ds/d(\omega^2)$ routine may not be resolvable by any other method presently known.

The diameter of the modal circle that fits the curvature of the displacement mobility plot (on the polar plane) in the vicinity of the natural frequency is:

$$D = \frac{|A|}{g\Omega^2} \tag{174}$$

At the natural frequency;

$$\left.\frac{dY^R}{d(\omega^2)}\right|_{\omega=\Omega} = -\frac{A^R}{g^2\Omega^4} + \frac{C^R}{\Omega^2} \tag{175}$$

and

$$\left.\frac{d\gamma^I}{d(\omega^2)}\right|_{\omega=\Omega} = \frac{-A^I}{g^2\Omega^4} + \frac{C^I}{\Omega^2} \tag{176}$$

Substituting equations (175) and (176) into equation (165) gives

$$\left.\frac{ds}{d(\omega^2)}\right|_{\omega=\Omega} = \frac{|A|}{g^2\Omega^4} + \text{Error of approximation} \tag{177}$$

The plot of arc length s against $\omega^2$ has a characteristic S shape, as shown by the sketch, below:

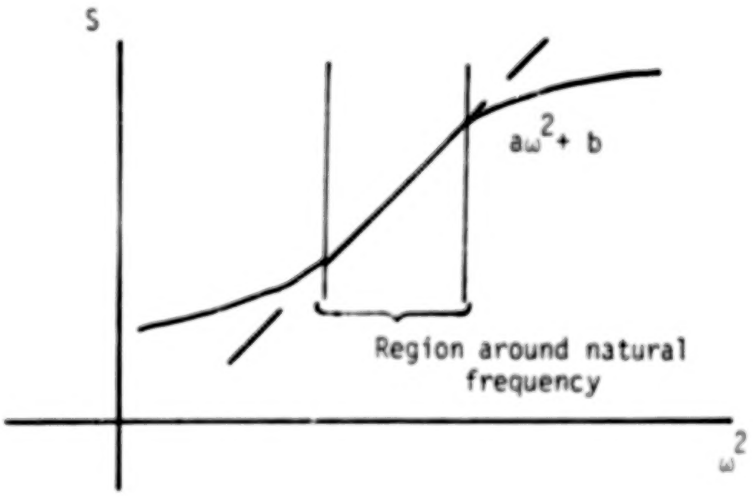


By fitting the best straight line to the inflection region of the S curve, one obtains a, the gradient of this line.

$$a = |A|/g^2\Omega^4 \tag{178}$$

From equations (174) and (178), the damping coefficient is evaluated as:

$$g = D/a\Omega^2 \tag{179}$$

where D is the diameter of the circle fit to the mobility data, a is the gradient of the line fit to the S plot and $\Omega$ is the natural frequency.

## Testing for Orthonormal Modes and Mode Shapes

The mode shapes of any structure are related to the modal acceleration coefficients as shown in equation (118); i.e.,

$$A_{jkn} = \frac{1}{m_n} \phi_{jn} \phi_{kn} \tag{180}$$

where $\phi_{jn}$ and $\phi_{kn}$ are mode shape elements at the jth and kth coordinates of the nth mode; $m_n$ is the generalized mass of the nth mode. There are two basic types of orthonormal modes which can be distinguished by considering the nature of the response and the excitation. The ordinary vibration orthonormal mode element, $\psi$, has units of $(1/\text{mass})^{1/2}$. The products of the jth and kth orthonormal mode elements and the mode frequency function summed over the modes defines the jk vibration mobility. On the other hand, the strain orthonormal mode element, $\psi^{(\epsilon)}$, has units of the square root of the reciprocal of force x seconds$^2$ x length. The products of the jth strain and kth vibration orthonormal mode elements and the mode frequency function summed over the modes defines the jk strain mobility. The types of orthonormal modes used in analytical testing and the corresponding types of mobilities are summarized in Table XVIII.

TABLE XVIII. - SUMMARY OF MOBILITY AND ORTHONORMAL MODE ELEMENTS

| Mobility | Modal acceleration (Residue) | Units of modal acceleration |
|---|---|---|
| $\frac{\partial q_j}{\partial f_k}$ | $- \psi_j \psi_k / \Omega^2$ | length/force |
| $\frac{\partial \epsilon_j}{\partial f_k}$ | $- \psi_j^{(\epsilon)} \psi_k / \Omega^2$ | 1/force |
| $\frac{\partial \Delta q_j}{\partial \Delta f_k}$ | $\frac{-1}{\Omega^2} \psi_j^{(\epsilon)} \psi_k^{(\epsilon)} \delta_k \delta_j$ | length/force |
| $\frac{\partial q_j}{\partial \Delta f_k}$ | $- \frac{1}{\Omega^2} \psi_j \psi_k^{(\epsilon)} \delta_k$ | length/force |

The orthonormal mode elements are defined as:

$$\Psi_{jn} = \frac{1}{\sqrt{m_n}} \phi_{jn} \tag{181}$$

and

$$\Psi_{kn} = \frac{1}{\sqrt{m_n}} \phi_{kn} \tag{182}$$

Thus,

$$A_{jkn} = \Psi_{jn} \Psi_{kn} \tag{183}$$

and

$$A_{jjn} = (\Psi_{jn})^2 \tag{184}$$

It follows from equations (183) and (184) that

$$\Psi_{kn} = \frac{A_{jkn}}{\sqrt{A_{jjn}}} \tag{185}$$

It can also be deduced that

$$\Psi_{kn} = \pm \sqrt{\frac{A_{jkn} A_{ikn}}{A_{ijn}}} \tag{186}$$

The choice of using either equation (185) or equation (186) to determine $\Psi_{kn}$ depends on the accessibility of the modal acceleration coefficients involved. Note that two shaking stations are involved in equation (186), whereas only one shaking station is involved in equation (185). It may turn out that the driving-point data that yields $A_{jjn}$ are such that accurate estimations of the $A_{jjn}$ for a number of the modes are not easy. This may in part be due to a strong local mode coupling, or a residual effect. In cases where this is so, it may be better to shake at a number of coordinates, and then use schemes similar to that in equation (186).

Consistency of the phase angle in equation (186) is achieved in the following manner. For an orthonormal mode element, in the nth mode, of large magnitude, say $\Psi_{kn}$, let

$$\Psi_{kn} = \left| \sqrt{\frac{A_{jkn} \cdot A_{\ell kn}}{A_{\ell jn}}} \right| \angle \frac{1}{2} (\phi_{jkn} + \phi_{\ell kn} - \phi_{\ell jn}) \tag{187}$$

where $\phi$ is phase angle. For any other orthonormal mode element, say p,

$$\Psi_{pn} = \left| \sqrt{\frac{A_{jpn} \cdot A_{\ell pn}}{A_{\ell jn}}} \right| \angle (\phi_{pkn} - \phi_{kn}) \tag{188}$$

Mode shapes of the structure, normalized with respect to the highest mode element can be obtained directly from the modal acceleration coefficients as:

$$\{\phi_n\} = \frac{1}{A_{j,max,n}} \begin{Bmatrix} A_{j1n} \\ A_{j2n} \\ \vdots \\ A_{jNn} \end{Bmatrix} \tag{189}$$

where $A_{j,max,n}$ is the modal acceleration coefficient with the maximum amplitude in the column corresponding to the nth mode, when shaking at the jth coordinate. The generalized mass, corresponding to the mode shape thus normalized is computed from equation (180) as:

$$m_n = \phi_{jn} \phi_{kn} / A_{jkn} = A_{jjn} / (A_{j,max,n})^2 \tag{190}$$

In order to obtain the elements of the orthonormal modes and mode shapes, the modal acceleration coefficients of all the modes for the mobilities relating the response coordinates to the shaking coordinates have to be determined. The computational scheme for determining the modal acceleration coefficients requires mobility data at discrete frequencies. The technique, herein referred to as the matrix difference method, was developed by F. D. Bartlett, Jr., of the Structures Laboratory, USARTL (AVRADCOM). The matrix difference method is well suited to processing large numbers of transducers for modal analysis using multiplexing data acquisition systems common in the helicopter industry. The natural frequencies and modal damping must be determined beforehand.

For two frequencies $\omega_i^+$ and $\omega_i^-$ in the region of the natural frequency of the ith mode, equation (124) could be written thus:

$$\Delta_i \ddot{Y}_{jk} = \ddot{Y}_{jk}(\omega_i^+) - \ddot{Y}_{jk}(\omega_i^-) = \sum_{n=1}^{N} A_{jkn} \Delta_i \ddot{F}_n \tag{191}$$

where

$$\Delta_i \ddot{F}_n = \ddot{F}_n(\omega_i^+) - \ddot{F}_n(\omega_i^-)$$

Equation (191) can be written for all the remaining modes, having selected the corresponding pairs of frequencies. The resulting system of equations is the matrix difference equation:

$$\begin{Bmatrix} \Delta_1 \ddot{Y}_{jk} \\ \Delta_2 \ddot{Y}_{jk} \\ \vdots \\ \Delta_N \ddot{Y}_{jk} \end{Bmatrix} = \begin{bmatrix} \Delta_1 \ddot{F}_1 & \Delta_1 \ddot{F}_2 & \cdots & \Delta_1 \ddot{F}_N \\ \Delta_2 \ddot{F}_1 & \Delta_2 \ddot{F}_2 & \cdots & \Delta_2 \ddot{F}_N \\ \vdots & \vdots & \cdots & \vdots \\ \Delta_N \ddot{F}_1 & \Delta_N \ddot{F}_2 & \cdots & \Delta_N \ddot{F}_N \end{bmatrix} \begin{Bmatrix} A_{jk1} \\ A_{jk2} \\ \vdots \\ A_{jkN} \end{Bmatrix} \tag{192}$$

or

$$\left\{\Delta \ddot{Y}_{jk}\right\} = [\Delta \ddot{F}] \left\{A_{jk}\right\} \tag{193}$$

From which

$$\left\{A_{jk}\right\} = [\Delta \ddot{F}]^{-1} \left\{\Delta \ddot{Y}_{jk}\right\} \tag{194}$$

An immediate observation about the matrix difference scheme is that all contributions to the mobilities near a given mode which are weakly varying with frequency, such as the effects of distant modes or rigid body modes, are subtracted out. By proper selection of $\omega_i^+$ and $\omega_i^-$, $\Delta_i \ddot{F}_n$ can be made such that $\Delta_i \ddot{F}_i$ is large and $\Delta_i \ddot{F}_j$ is small for all $j \neq i$. Experience shows that

$$\omega_i^+ = \Omega_i(1 + g_i/2) \tag{195}$$

and

$$\omega_i^- = \Omega_i(1 - g_i/2) \tag{196}$$

are the most effective choices for the upper and lower discrete frequencies. For these discrete frequencies, the matrix $[\Delta\ddot{F}]$ is well conditioned for inversion since the off diagonal terms are small compared to the diagonal terms.

Test procedure. - Figure 25 shows the schematic of the instrumentation set-up for the shake test for orthonormal modes and mode shapes. Signals from all the accelerometers and from the force gage are transmitted via telemetry to a computer where the transfer functions between the response coordinates and the force coordinate are computed and printed out. The excitation signals are sinusoidal at the discrete frequencies $\omega_i^+$ and $\omega_i^-$ for i = 1, 2, . . . N. The same force levels used for the swept sine global parameter shake test are also used for the modal shake test at the corresponding discrete frequencies.

## Derivation of Mobilities

Underlying any technique of modal analysis is the principle of linear decomposition of structural response mobility into contributions from the natural modes occurring between a chosen frequency interval. The preceding methods estimate not only the natural frequencies and damping coefficients of each mode, but also the modal acceleration coefficients of each modal contribution to the mobility between response and forcing coordinates.

Subsequent to the determination of the modal parameters and modal constants, the next logical step is to reconstruct mobilities both between a pair of forcing and response coordinates over a continuous frequency interval, and at a chosen frequency between several pairs of forcing and response coordinates. By comparing the mobility derived over a continuous frequency range with the measured mobility over the same frequency range, some assessment of the accuracy of the global parameter estimations can be made. The comparison of discrete frequency mobilities for a large number of coordinate pairs allows the assessment of the acceptability of the orthonormal mode and mode shape calculations. The results of these comparisons build the confidence in the mobilities which are derived but not actually measured.

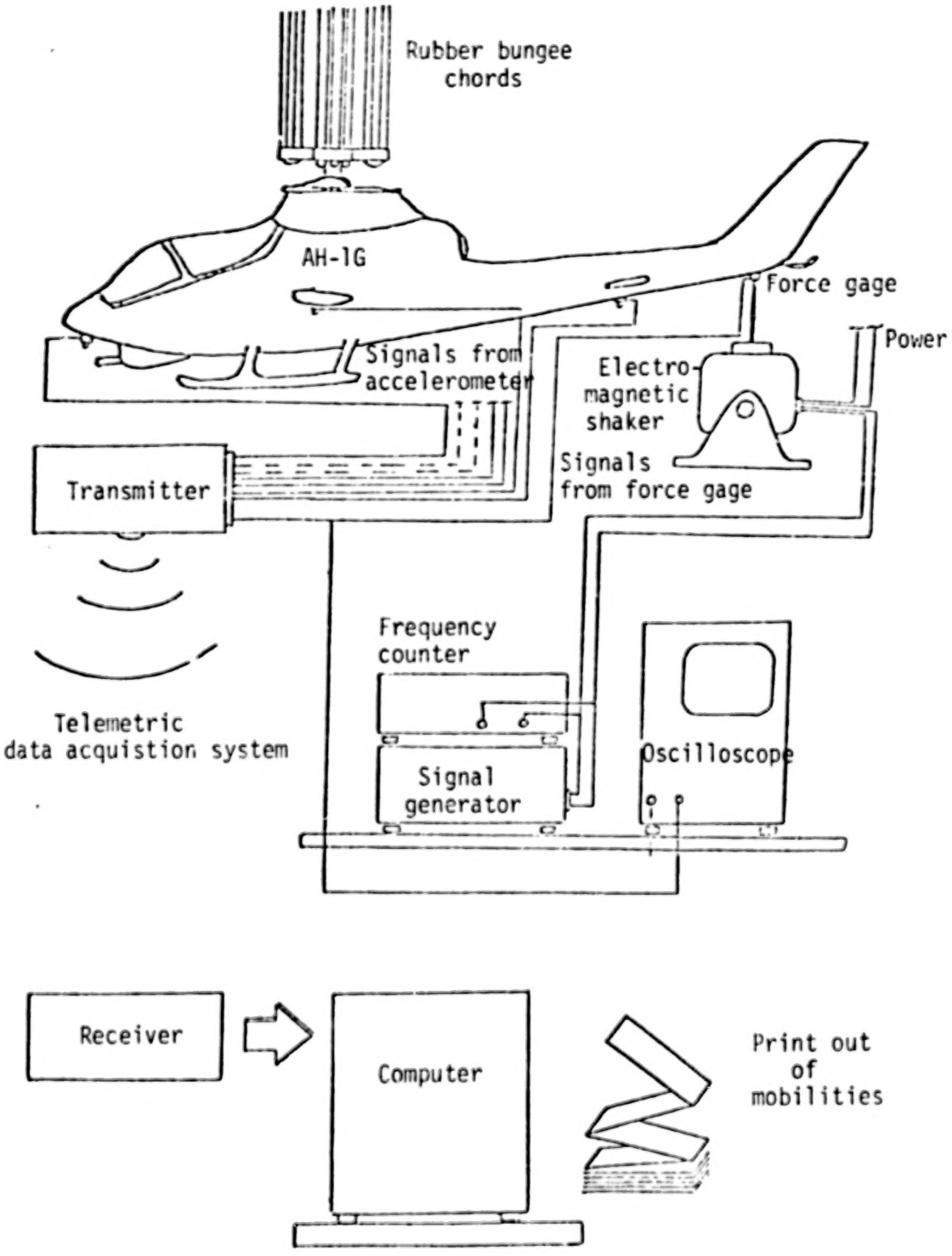


Figure 25. - Schematic of test set-up for matrix difference method of modal testing.

Comparison of measured and simulated mobilities over frequency band. - Global parameters $\Omega_n$ and $g_n$ of system modes occurring within a specified frequency range can be satisfactorily estimated using methods based on the properties of the mode functions, $F(\omega)$. The matrix difference method can then be used to calculate the modal acceleration coefficients ($A^R_{jkn}$, $A^I_{jkn}$) of the relevant elastic modes. Figure 26 shows plots of the mobility measured between 0 and 50 Hz. Table XIX summarizes the parameters estimated between 0 and 50 Hz from the tail vertical shake/nose vertical acceleration data. Using the parameters of Table XIX and equation (121), without including the rigid body coefficients, the plots of Figures 27, 28, and 29 were generated.

The computed and measured mobilities are superimposed in Figures 28 and 29. It is seen that the two plots agree to within a frequency independent complex constant, which is an estimate of the contribution of the rigid body modes.

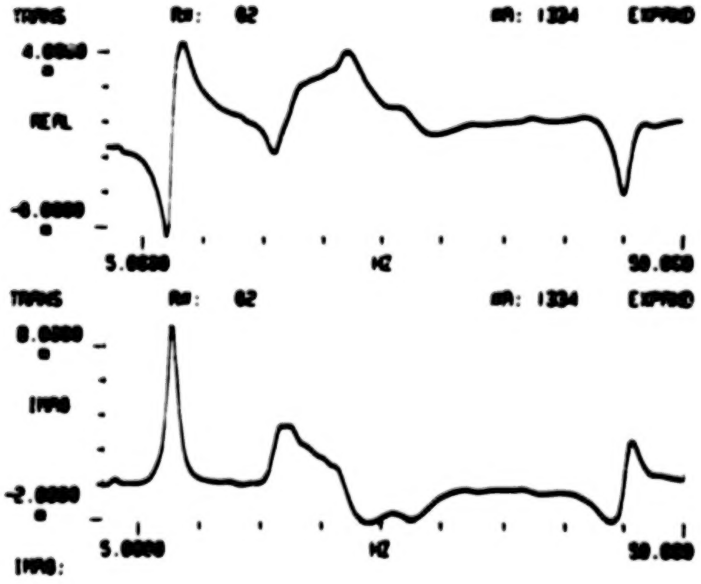


Figure 26. - Measured acceleration mobility data between 2 Hz and 50 Hz.

TABLE XIX. - ESTIMATED PARAMETERS BETWEEN 0 - 50 Hz
(TAIL VERTICAL SHAKE, NOSE VERTICAL
ACCELERATION)

| Mode No. n | Natural frequency $\Omega_n$ (Hz) | Damping coefficient $g_n$ | Nose/tail modal acceleration coefficient | |
|---|---|---|---|---|
| | | | Real $A^R_{ZN, ZT, n}$ g/1000 N | Imaginary $A^I_{ZN, ZT, n}$ g/1000 N |
| 1 | 7.33 | 0.062 | .165 | .032 |
| 2 | 8.09 | 0.12 | .102 | - .081 |
| 3 | 13.3 | 0.13 | - .004 | - .001 |
| 4 | 15.97 | 0.085 | .005 | .032 |
| 5 | 16.35 | 0.05 | .012 | 0 |
| 6 | 17.63 | 0.08 | .031 | - .013 |
| 7 | 22.1 | 0.15 | - .017 | - .092 |
| 8 | 28.4 | 0.11 | - .024 | .026 |
| 9 | 40.7 | 0.12 | .002 | - .005 |
| 10 | 45.3 | 0.026 | .009 | .032 |

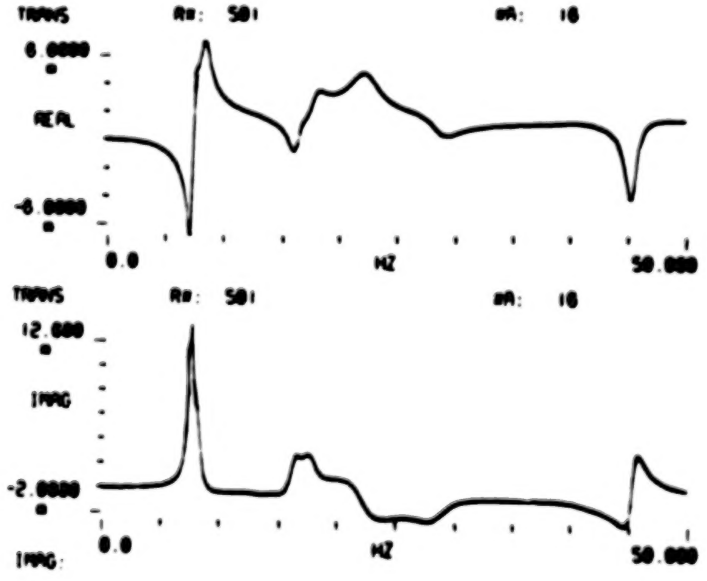


Figure 27. - Numerical simulation of the elastic component of the acceleration mobility data.

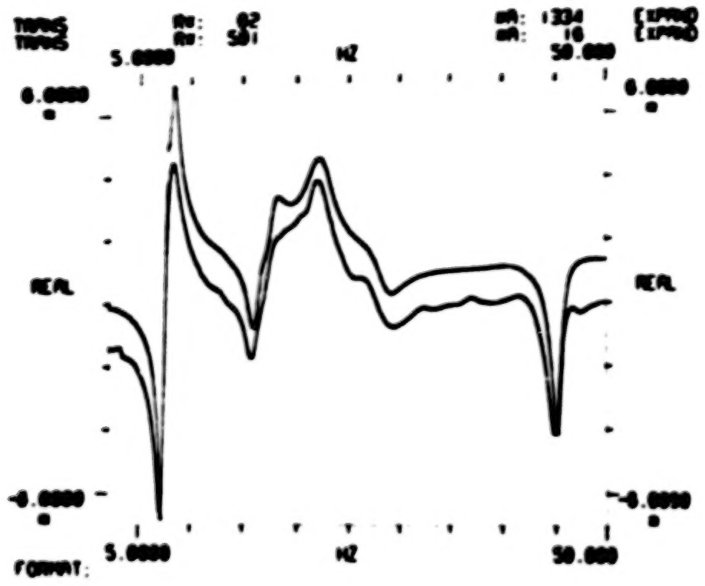


Figure 28. - Real parts superimposed.

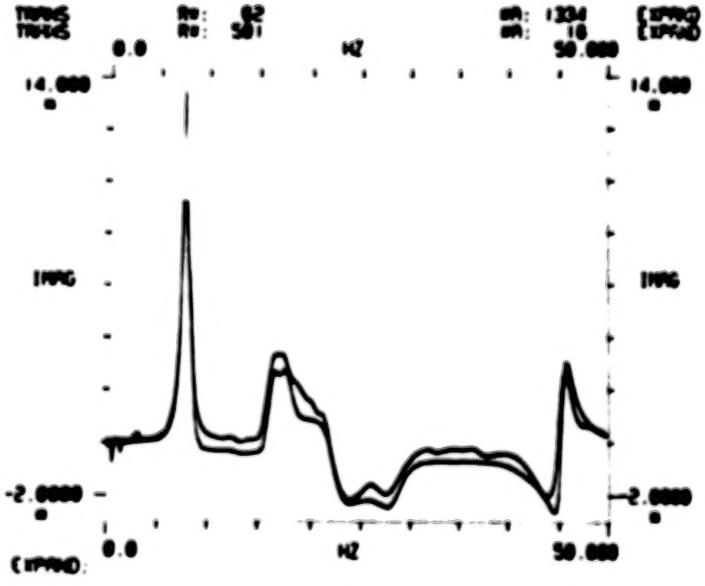


Figure 29. - Imaginary parts superimposed.

Modal Series Method. - Equation (121) can be rewritten in the following form:

$$\ddot{Y}_{jk} = E_{jk} + R^{L}_{jk}(\omega) + \sum_{n=1}^{N} A_{jkn}\, \ddot{F}_{n}(\omega) + R^{H}_{jk}(\omega) \tag{197}$$

where

$R^{L}_{jk}(\omega)$ is the low frequency mobility residual; i.e., contributions to the mobility by elastic modes which occur at frequencies below the lower test frequency limit.

$R^{H}_{jk}(\omega)$ is the high frequency mobility residual.

The rigid body acceleration coefficient, $E_{jk}$, is determined from geometry and weights data.[5]

If the lower test frequency limit is near zero, it follows that $R^{L} = 0$. The higher test frequency limit is usually selected high enough so that $R^{H}$ can be safely assumed to vanish for all but certain driving-point mobilities which may suffer either from local mode effects or from high frequency mode residuals.

When all the global modal parameters (natural frequencies and damping coefficients) and the modal acceleration coefficients have been determined (see Table XX), the acceleration mobilities between pairs of motion coordinates which do not include the shaking coordinate can be computed from:

$$\ddot{Y}_{\ell m} = E_{\ell m} + \sum_{n=1}^{N} \frac{A_{\ell kn} A_{mkn}}{A_{kkn}}\, \ddot{F}_{n}(\omega) \tag{198}$$

where k is the coordinate of the shaking station for the data which generated $A_{\ell k}$ and $A_{mk}$. It is necessary to select the shaking station k such that there is no local mode or high frequency residual effect on the estimated value of $A_{kkn}$.

If only $N_k$ of the modes are well defined by shaking at k, while the remaining $N_p$ modes are better defined by the shake at p, then

$$\ddot{Y}_{\ell m} = E_{\ell m} + \sum_{n=1}^{N_k} \frac{A_{\ell kn} A_{mkn}}{A_{kkn}}\, \ddot{F}_{n}(\omega) + \sum_{n=1}^{N_p} \frac{A_{\ell pn} A_{mpn}}{A_{ppn}}\, \ddot{F}_{n}(\omega) \tag{199}$$

TABLE XX. - SUMMARY OF ESTIMATED MODAL PARAMETERS FOR AH-1G HELICOPTER.

| High gross wt. | Low gross wt. | | Mean gross wt. | | High gross wt. aft c.g. | |
|---|---|---|---|---|---|---|
| Vert. shake | Vert. shake | Lat. shake | Vert. shake | Lat. shake | Vert. shake | Lat. shake |
| $\Omega_n$ $g_n$ | $\Omega_n$ $g_n$ | $\Omega_n$ $g_n$ | $\Omega_n$ $g_n$ | $\Omega_n$ $g_n$ | $\Omega_n$ $g_n$ | $\Omega_n$ $g_n$ |
| 7.32 .066 | 7.19 .07 | 6.29 .16 | 7.15 .08 | 6.17 .14 | 7.28 .07 | 6.28 .16 |
| 8.08 .187 | 8.01 .17 | 7.51 .05 | 8.16 .18 | 7.38 .08 | 8.35 .08 | 7.53 .05 |
| 13.23 .138 | 14.78 .1 | 8.53 .11 | 13.67 .08 | 14.39 .15 | 13.94 .06 | 8.55 .11 |
| 15.99 .103 | 16.44 .065 | 14.66 .17 | 15.04 .07 | 16.16 .09 | 15.52 .08 | 11.0 .12 |
| 17.6 .083 | 17.71 .09 | 17.36 .1 | 15.92 .05 | 29.05 .114 | 21.48 .16 | 14.35 .18 |
| 22.06 .148 | 19.14 .12 | 25.46 .1 | 16.98 .11 | | 23.71 .11 | 16.39 .068 |
| 27.91 .17 | 20.69 .2 | 27.88 .14 | 17.88 .07 | | 25.59 .31 | 18.45 .13 |
| | 24.6 .1 | 29.66 .15 | 19.83 .13 | | 29.96 .13 | 21.93 .074 |
| | 28.31 .12 | 32.42 .24 | 21.63 .16 | | 31.63 .1 | 24.12 .108 |
| | 32.88 .1 | 33.59 .36 | 24.12 .08 | | | 29.38 .112 |
| | 34.99 .06 | | 25.15 .14 | | | |
| | 37.75 .08 | | 28.44 .13 | | | |
| | | | 32.42 .06 | | | |

## SPECIAL CONSIDERATIONS IN MODAL ANALYSIS

### Shaking Locations

Nonlinearities such as gradually hardening stiffness and ankylotic stiction are alleviated by using sufficient shaking force so that the mobility is independent of the shaking force. The power input from the shaker is equal to the power dissipated by the helicopter through damping and is proportional to the product of the square of the shaking force and the imaginary velocity mobility (or real acceleration mobility divided by frequency). Maximum motion for a given shaking force occurs at shaking point locations of high mobility. These are generally at structural terminations such as high on a fin, at wing tips or the hub.

It is also important to shake in the vicinity of any possible local modes of interest. Consider the case in which, for a given mode, $\psi_j = .2$ and $\psi_k = 2.0$. For shaking at j, $A_{jj} = .04$ and $A_{kj} = .40$. The response near this natural frequency may be unnoticeable at the driving point, j, but evident in the kj transfer mobility which indicates that k, or a point near it, should be a shaking point. In this example, $A_{kk}$ is two orders of magnitude larger than $A_{jj}$.

Once modal accelerations have been obtained for and among the stations at which the aircraft is excited, one shaker at a time, all the modal accelerations can be used simultaneously for the best estimate of the orthonormal mode elements. Although the number of shaking locations depends on many factors, it appears that five or six should be sufficient for most helicopter uses. For the jth motion coordinate and N shaker locations the absolute value

$$\psi_j = \frac{|A_{j1}| + |A_{j2}| + \ldots + |A_{jN}|}{\sqrt{|A_{11}| + |A_{22}| + \ldots + 2|A_{12}| + 2|A_{13}| \ldots + 2|A_{23}| + \ldots}}$$

$$= \frac{\sum_{i=1}^{N} |A_{ji}|}{\sqrt{(|\psi_1| + |\psi_2| + |\psi_3| \ldots)^2}} \qquad (200)$$

The phase angle of the jth orthonormal mode element is given by

$$\phi_j = \frac{1}{N} \sum_{i=1}^{N} \phi_{ji} - \frac{1}{2N} \sum_{i=1}^{N} \phi_{ii} \qquad (201)$$

If the $ds/df^2$ method is used to obtain the modal accelerations at and among the shaking locations and the matrix difference method for all modal accelerations, then

$$|\psi_j| = \frac{\sum_{i=1}^{N} |A_{ji}/g|}{\sqrt{|A_{11}/g^2| + |A_{22}/g^2| + \ldots + 2|A_{12}/g^2| + 2|A_{13}/g^2| + \ldots}} \qquad (202)$$

## High Frequency Residuals

The authors discovered that high frequency (e.g., 400 Hz) local modes may cause distorted translational mobility plots, with force shaking at low frequencies (e.g., 10 Hz) at or near a driving-point on the AH-1G. Dr. Albert Klosterman and Dr. Jason Lemon of Structural Dynamics Research Corporation noted high frequency residual effects and found the means of correction in testing a 1750 HP electric motor for the United States Steel Corporation.[10] Dr. David Ewins of the Imperial College of Science and Technology, London, found the same cause and effect in rotational mobilities measured on a turbine rotor.[11] The effect does not occur at all driving-points, but it is not uncommon. It occurred in tail shaking and vertical shaking at FS Z400 on the AH-1G as shown in Figure 30. It did not occur in hub shaking or shaking at the tail rotor gear box on the AH-1G.

The effect is associated with shaking points of very small mass concentration and elastic extension as in the cantilever beam of Figure 31. In a helicopter these correspond to soft, but not weak points, as opposed to hard points usually, but not necessarily, such as skin attachment points or tail skids.

In some cases of helicopter fuselage concern, the high frequency local modes are inconsequential in engineering and should be ignored in modal

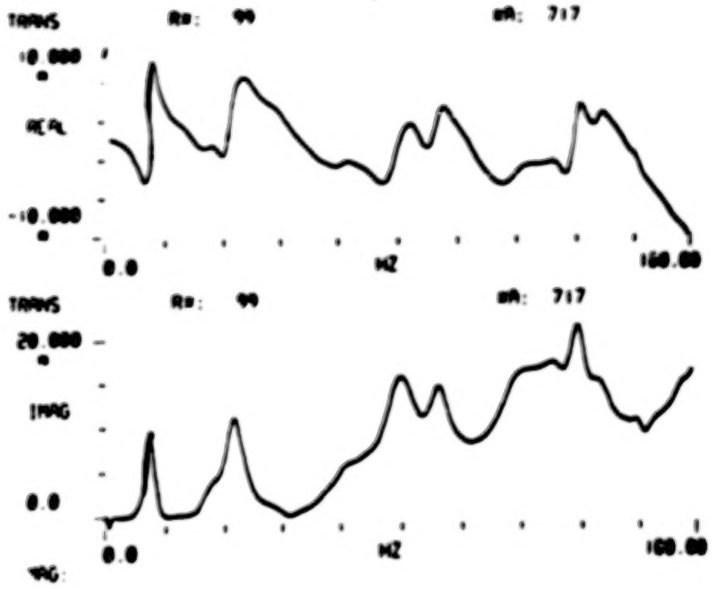


Figure 30. - Mobility curves with the high frequency residual effect measured on the AH-1G.

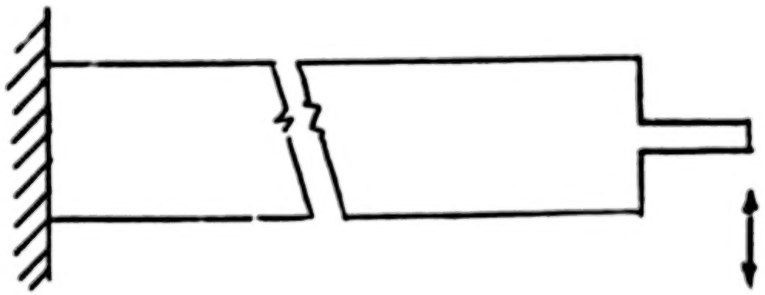

Figure 31. - Cantilever beam shaken at the tip.

superposition for mobilities. If the point in question is one at which there is a contemplated external stores change, the point would usually have to be hardened for the attachment and the effect would disappear. Only when true very local response is desired should the high frequency local modes be retained and this would be the case on panels and decks. If the high frequency residual effect occurs in direct shaking at a change point which is to be hardened and the effect not removed then there could be significant errors in the analysis of the effects of the change.

Figure 32 shows a simple chain having the residual effect. The natural frequencies are at 4.95 Hz and 123.28 Hz, the latter being a local mode of the small mass. The acceleration mobility from 1 to 10 Hz for the response at 1 due to force at 1, $\ddot{Y}(1,1)$ shown in Figure 33 shows the residual effect.

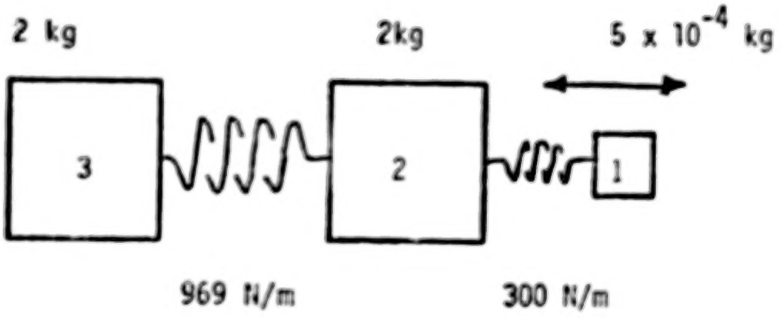


Figure 32. - Simple chain system with 5% structural damping.

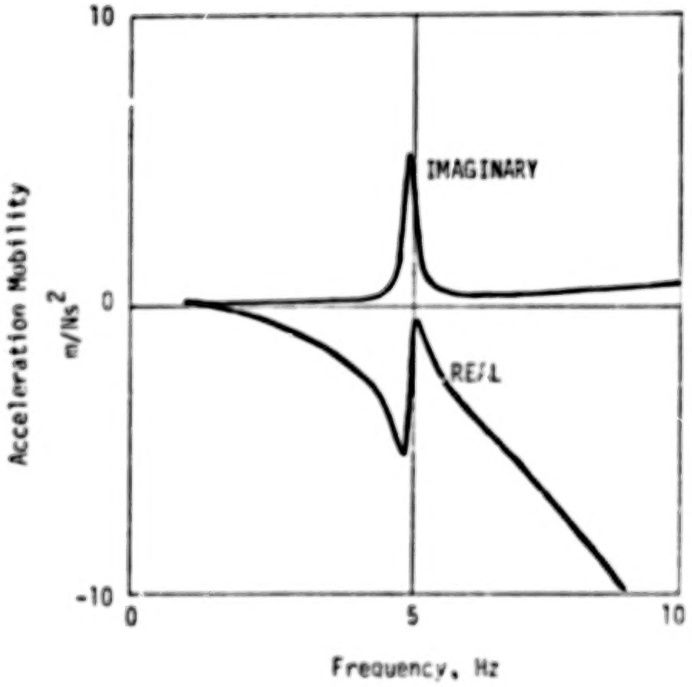


Figure 33. - Driving-point acceleration mobility at mass 1 of the chain of Figure 32.

$\ddot{Y}(1,1)$ is almost identical to $\ddot{Y}(1,2)$ and would be indistinguishable from $\ddot{Y}(2,2)$, shown in Figure 34, if the local mode were removed. The slope of the

mobility from 4.8 to 5.07 Hz is virtually the same in Figure 33 as in Figure 34 and differential mobility parameter extraction methods, such as $dS/df^2$ and the matrix difference method, on the 4.95 Hz mode would be negligibly affected by the residual effect. These methods can be used to accurately obtain modal accelerations at driving points whenever the slope ($d\ddot{Y}/d\omega$) resulting from high frequency local modes is small compared to the maximum real or imaginary mobility slope at the natural frequencies of interest. The accuracy of parameter extraction methods that are not of the differential mobility type is seriously affected at driving points exhibiting the high frequency residual effect.

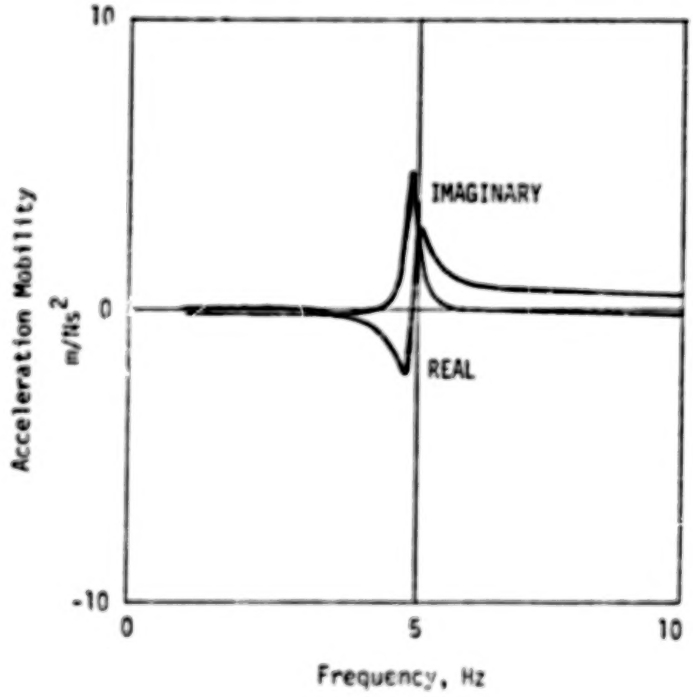


Figure 34. - Driving-point mobility of mass 2 of the chain of Figure 32.

If the high frequency residual effect is to be retained there are two ways to deal with it without shaking to very high frequencies. Because it is essentially a driving-point phenomenon, one can shake at each of the driving points having the effect and represent the effect as a flexibility term equal to the constant difference between measured displacement mobility and the displacement mobility synthesized over the frequency range of testing as shown by Klosterman

and Lemon[10], and Ewins[11]. Alternatively, one could shake at only one point with the points having the effect, and at which driving point mobilities are desired, weighted by attached masses. The effect of the attached masses could then be removed using the analytical testing equations as follows:

$$\begin{Bmatrix} \ddot{Y}_{11} \\ \ddot{Y}_{22} \\ \ddot{Y}_{33} \\ \vdots \end{Bmatrix} = \left[ [I] - [\ddot{Y}_{rr}] \left( [\ddot{Y}_{rr}] - [m_{rr}]^{-1} \right) \right] \begin{Bmatrix} \ddot{Y}_{11}(s) \\ \ddot{Y}_{22}(s) \\ \ddot{Y}_{33}(s) \\ \vdots \end{Bmatrix} \tag{203}$$

where $\ddot{Y}_{rr}$ is the matrix of measured acceleration mobilities at and among the motion coordinates with the attached masses, $m_{rr}$ is the diagonal matrix of the attached masses (in three spatial directions if necessary) and the parenthetical superscript s meaning derived from modal synthesis over the frequency range of testing.

## Effect of Damping Estimate Variations in the Matrix Difference Method

The matrix difference method involves the difference between mobilities above and below each natural frequency. Let $\omega_{x1}$ be the frequency below the xth mode and $\omega_{x2}$ be the frequency above the xth mode. For illustration purposes let

$$\omega_{x1} = \sqrt{1-s}\ \Omega_x \quad \text{and} \quad \omega_{x2} = \sqrt{1+s}\ \Omega_x \tag{204}$$

where s is much less than unity. Then

$$\Delta\omega_x \equiv \omega_{x1} - \omega_{x2} = (\sqrt{1-s} - \sqrt{1+s})\ \Omega_x \approx -s\Omega_x \text{ or } -s \approx \frac{\Delta\omega_x}{\Omega_x} \tag{205}$$

and in terms of displacement mobility:

$$Y_{jk}(\omega_{x1}) - Y_{jk}(\omega_{xz}) = \sum_{i=1}^{N} \frac{A_{jki}}{g_i \Omega_i^2} \left[ \frac{g_i}{1 - \frac{\omega_{x1}^2}{\Omega_i^2} + ig_i} - \frac{g_i}{1 - \frac{\omega_{x2}^2}{\Omega_i^2} + ig_i} \right] \tag{206}$$

let

$$g_i \, \Delta\mu_{xi} \equiv \frac{g_i}{1 - \frac{\omega_{x1}^2}{\Omega_i^2} + ig_i} - \frac{g_i}{1 - \frac{\omega_{x2}^2}{\Omega_i^2} + ig_i} \tag{207}$$

Then, in matrix form

$$\left\{ \Delta Y_{jk}(x) \right\} = \left[ g_i \, \Delta\mu_{xi} \right] \left\{ \frac{A_{jki}}{g_i \Omega_i^2} \right\} \tag{208}$$

In view of equation (205), the xm th term in the $g\Delta\mu$ matrix may be expressed as

$$g_M \, \Delta\mu_{xM} = \frac{- 2g_M \frac{\Delta\omega_x}{\Omega_x} \frac{\Omega_x^2}{\Omega_M^2}}{\left( 1 - \frac{\Omega_x^2}{\Omega_M^2} \right)^2 \left( \frac{\Omega_x^2}{\Omega_M^2} \frac{\Delta\omega_x}{\Omega_x} \right)^2 - g_M^2 + i2g_M \left( 1 - \frac{\Omega_x^2}{\Omega_M^2} \right)} \tag{209}$$

In the x row of the $g\Delta\mu$ matrix this term shows the coupling of the xth mode with the mth mode when ratioed to the diagonal term $g_x \, \Delta\mu_{xx}$. It will be shown that: (1) when the modes are widely separated (i.e., for any mode x, $\Omega_x - 1 \ll (1 - g_x) \, \Omega_x$ and $\Omega_x \gg (1 + g_{x-1}) \, \Omega_{x-1}$ and $\Omega_x \ll (1 - g_{x+1}) \, \Omega_{x+1}$ and $\Omega_{x+1} \gg (1 + g_x) \, \Omega_x$), then a frequency difference of $\Delta\omega_x/\Omega_x = g_x$ is preferred in that it is least sensitive to errors in g; (2) for close modes, $\Delta\omega_x/\Omega_x$ should be less than $g_x$; and (3) for $\Delta\omega_x/\Omega_x$ much less than $g_x$, the maximum error in the diagonal term will be proportional to the error in $g_x$.

Figure 35 shows a plot of the x row real part of the $g\Delta\mu$ matrix for hysteretic damping of 10% for various values of $\Delta\omega_x/\Omega_x$ equal to or less than

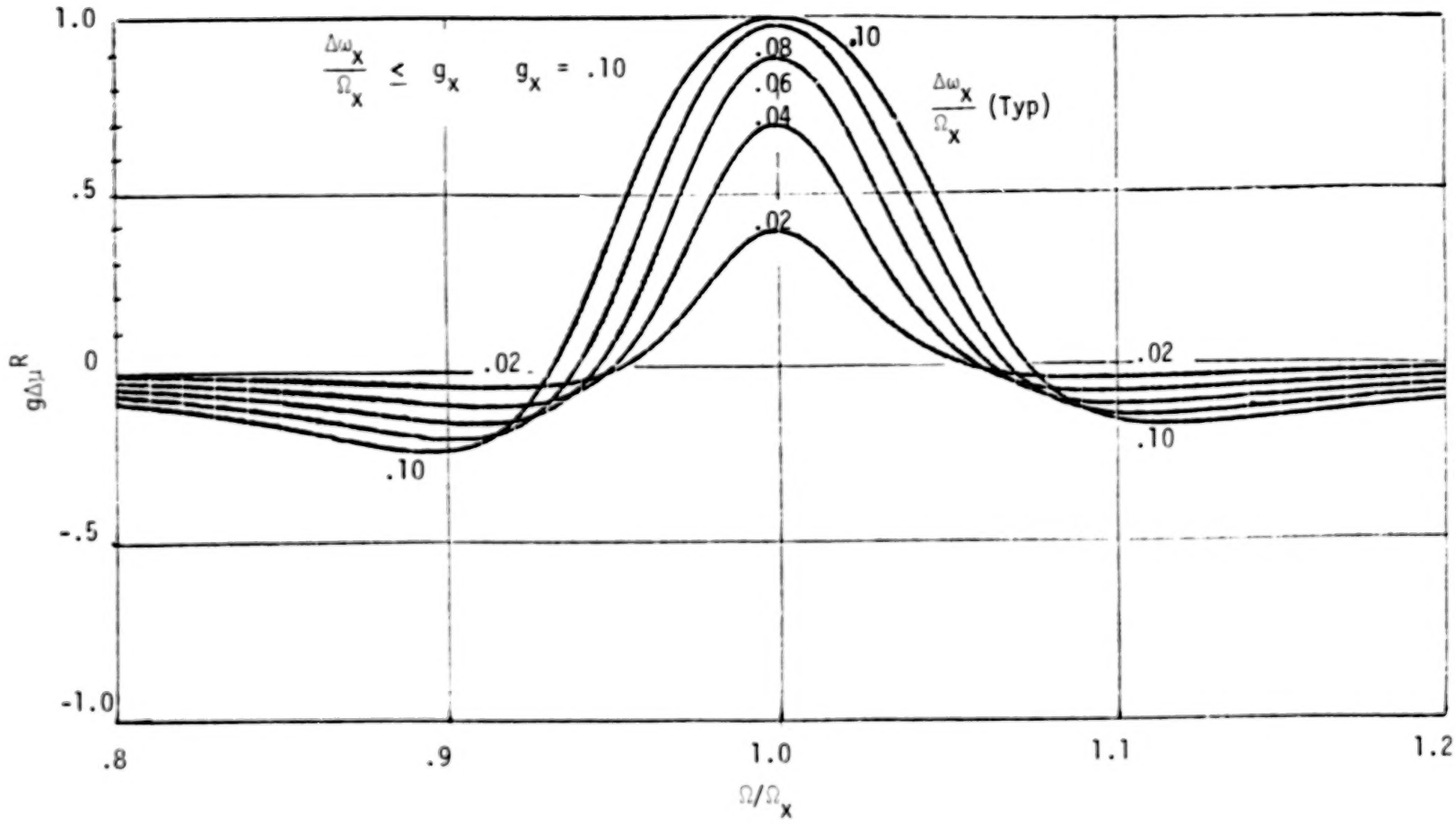


Figure 35. - The real part of the row for the $\Omega_x$ natural frequency in the $g\Delta\mu$ matrix when $\Delta\omega_x/\Omega_x < g_x$.

$g_x$ = .1. As seen from Figure 36, the imaginary part of the coupling of the x mode with all other modes also drops off with decreasing $\Delta\omega_x/\Omega_x$. This also occurs in Figure 35. Figures 37 and 38 illustrate the severe coupling effects when $\Delta\omega_x/\Omega_x$ is greater than g by a large amount. Note the development of two peaks when $\Delta\omega_x/\Omega_x$ is .4 for g = .1 in Figure 37.

The matrix difference method remains exact for values of $\Delta\omega_x/\Omega_x$ much larger than g but the increased coupling with nearby modes tends to make the $g\Delta\mu$ matrix less well conditioned both physically and numerically.

As an illustration of the variation in coupling of two modes in the g matrix with variation in $\Delta\omega_x/\Omega_x$, consider a case of g = .1 and $\Omega_x^2 = (1 - g_M)\Omega_M^2$. The following calculations are made for $\Omega_M$ = 1.05409 and g = .1.

| $\frac{\Delta\omega_x/\Omega_x}{g}$ | $\frac{\Delta\omega_x}{\Omega_x}$ | $g\Delta\mu$ | | | |
|---|---|---|---|---|---|
| | | @ $\Omega_M$ | | @ $\Omega_x$ | |
| 2 | .2 | .946 | 68° | .800 | 0° |
| 1 | .1 | .834 | 32° | 1.000 | 0° |
| .8 | .08 | .697 | 75° | .976 | 0° |
| .5 | .05 | .447 | 84° | .800 | 0° |
| .2 | .02 | .180 | 89° | .385 | 0° |
| .1 | .01 | .090 | 90° | .198 | 0° |

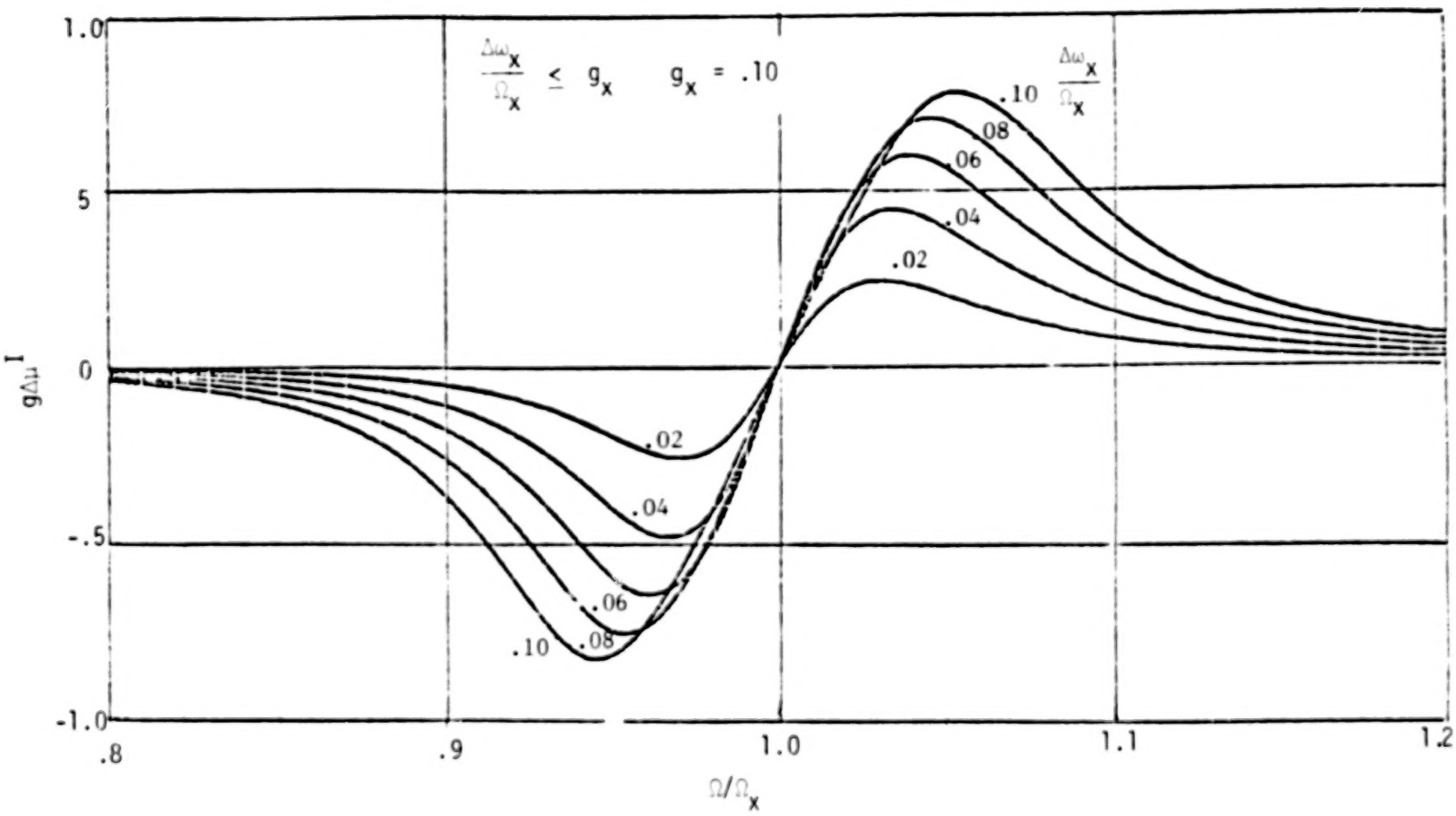


Figure 36. - The imaginary part of the row for the $\Omega_x$ natural frequency in the $g\Delta\mu$ matrix when $\Delta\omega_x/\Omega_x < g_x$.

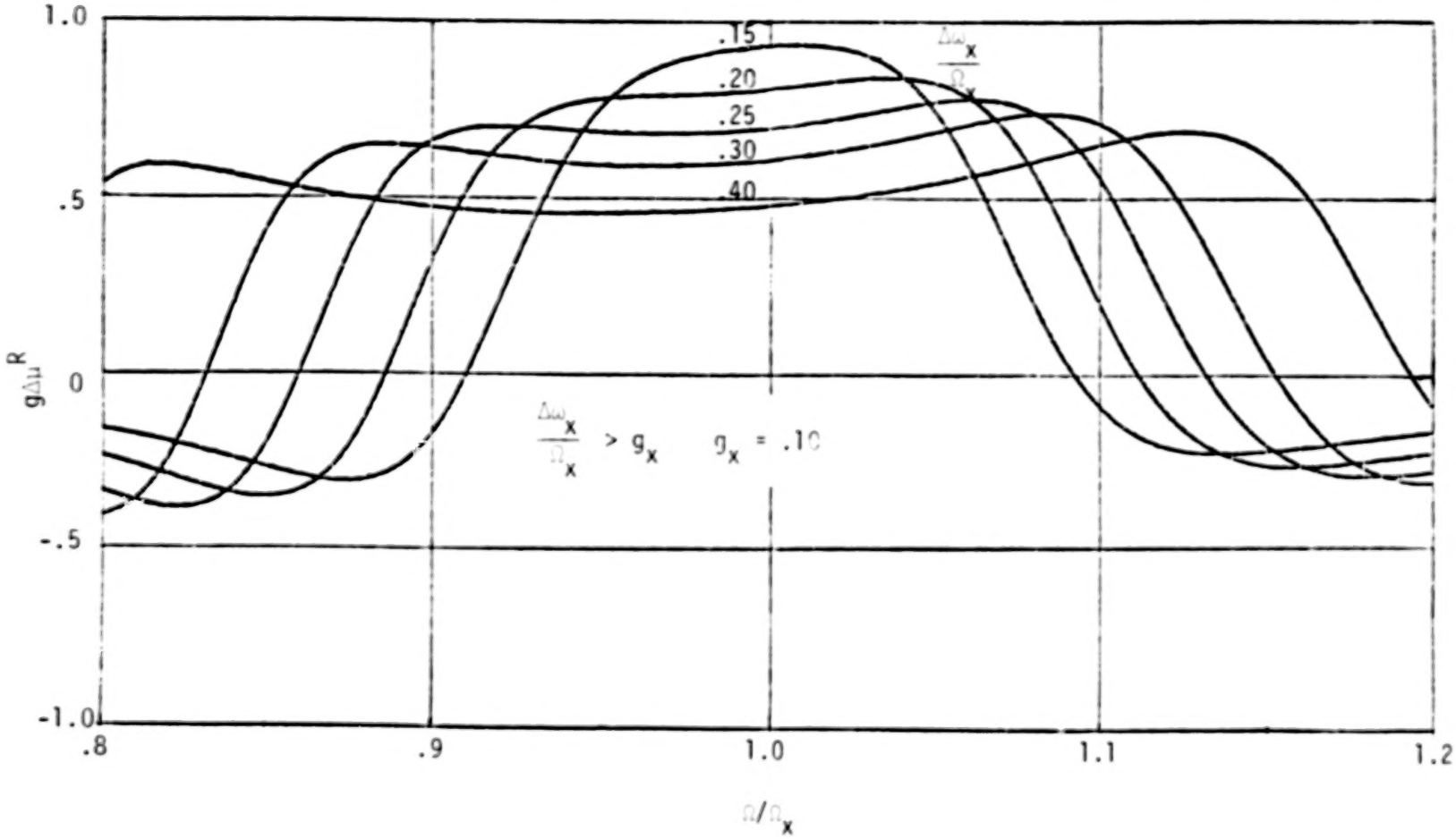


Figure 37. - The real part of the row for the $\Omega_x$ natural frequency in the $g\Delta\mu$ matrix when $\Delta\omega_x/\Omega_x > g_x$.

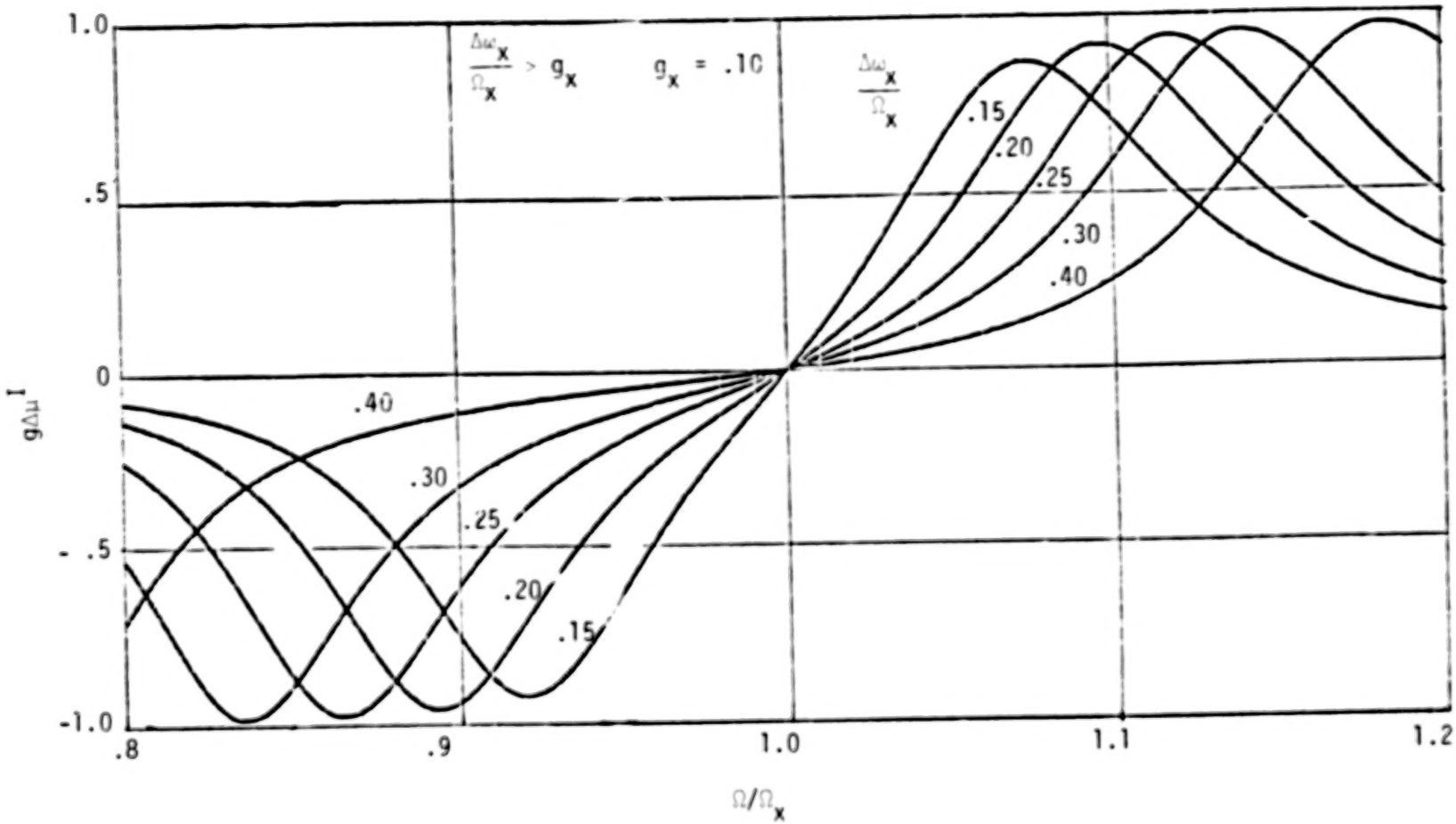


Figure 38. - The imaginary part of the row for the $\Omega_x$ natural frequency in the $g\Delta\mu$ matrix when $\Delta\omega_x/\Omega_x > g_x$.

If g were .01 the same case of close modes has the following coupling terms.

| $\frac{\Delta\omega_x/\Omega_x}{g}$ | $\frac{\Delta\omega_x}{\Omega_x}$ | $g\Delta\mu$ | | | |
|---|---|---|---|---|---|
| | | @ $\Omega_M$ | | @ $\Omega_x$ | |
| 20 | .2 | .159 | 5° | .100 | 0° |
| 10 | .1 | .670 | 137° | .198 | 0° |
| 8 | .08 | .281 | 157° | .246 | 0° |
| 5 | .05 | .111 | 166° | .385 | 0° |
| 2 | .02 | .037 | 168° | .800 | 0° |
| 1 | .01 | .018 | 168° | 1.000 | 0° |
| .5 | .005 | .009 | 169° | .800 | 0° |

Sensitivity to g

When $\Omega_x = \Omega_M$ the diagonal term from equation (209) reduces to

$$g_x \Delta\mu_{xx} = \frac{2g_x \frac{\Delta\omega_x/\Omega_x}{}}{\left(\frac{\Delta\omega x}{\Omega_x}\right)^2 + g_x^2} \qquad (210)$$

As seen in Figure 39, the diagonal term in $g\Delta\mu$ is least sensitive to the value of g when $\Delta\omega_x/\Omega_x = g$. In that vicinity a 4:1 variation in g produces only a $\pm$ 10% change in the value of the diagonal term.

If $\Delta\omega_x/\Omega_x$ is very small in equation (210) compared to g then

$$g_x \Delta\mu_{xx} \approx +2 \frac{\Delta\omega_x/\Omega_x}{g_x} \qquad (211)$$

and percentage errors in the diagonal term become proportional to percentage errors in g.

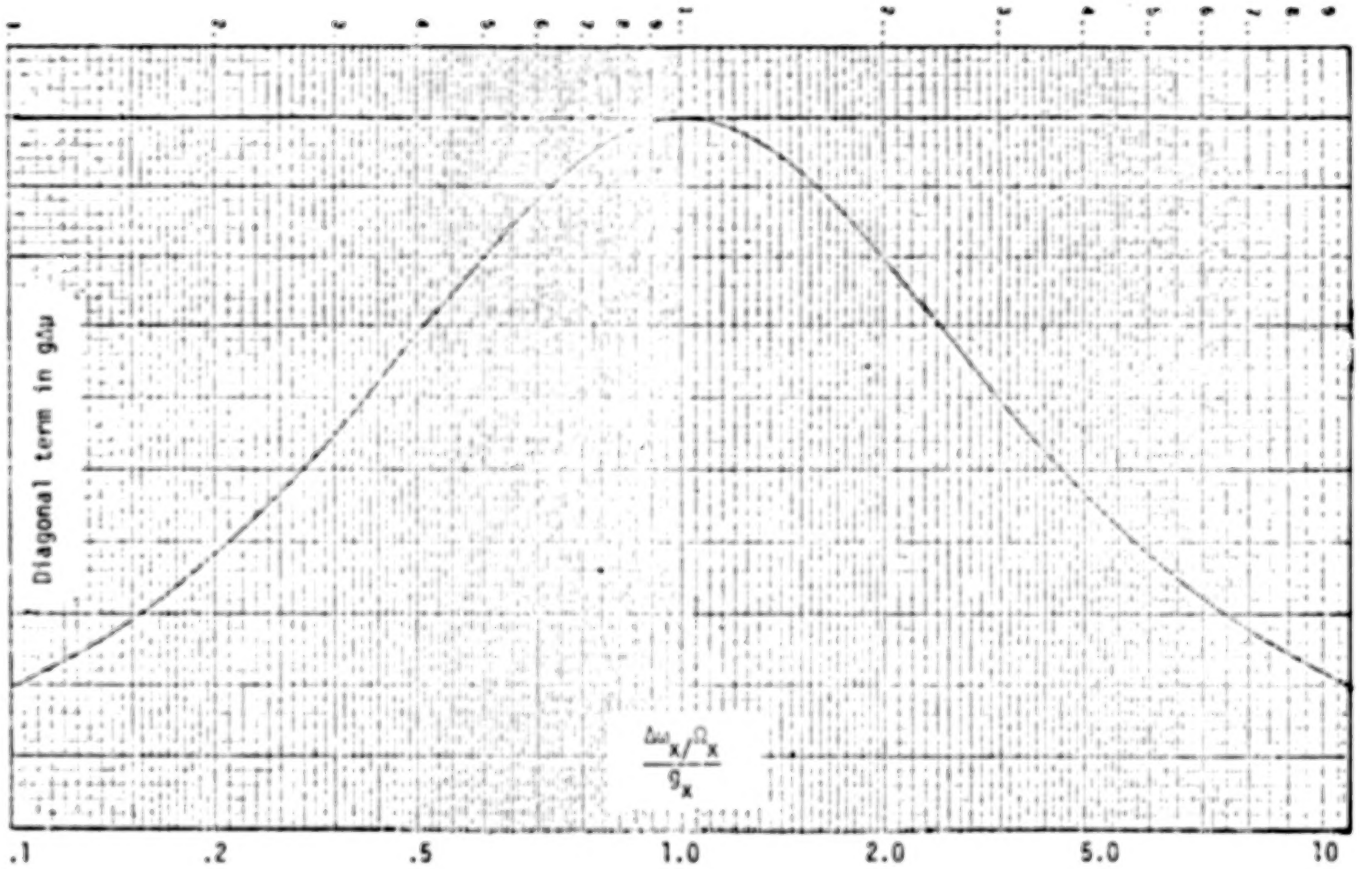


Figure 39. - The diagonal term in gΔμ vs frequency spread.

If g is so small that there is negligible damping coupling with other modes then one can assume any small value for g.

Let $\frac{\Delta\omega_x}{\Omega_x} = .05$ as an illustration of a case with small g. Then,

| g | $\Delta\mu_{xx}$ | $\Delta\mu_{xM}$ for $\Omega_M = 1.1\ \Omega_x$ | |
|---|---|---|---|
| 0 | 40 | 2.91 | 0° |
| .001 | 39.98 | 2.91 | 0.7° |
| .005 | 39.6 | 2.91 | 3.5 |
| .01 | 38.46 | 2.9 | 7.0 |
| .02 | 34.48 | 2.86 | 14.0 |

Effects of Close Modes

Modes i and i+1 are considered to be close when

$$\Omega_{i+1} < (1 + g_i)\ \Omega_i \quad \text{or} \quad \Omega_i > (1 - g_{i+1})\ \Omega_{i+1} \tag{212}$$

where g is structural damping and the natural frequency $\Omega_{i+1} > \Omega_i$.

It should first be noted that $\Omega_i$ and $g_i$ are global properties. Therefore, one might find $\Omega_i$ and $g_i$ from one mobility plot and $\Omega_{i+1}$ and $g_{i+1}$ from a different mobility. One must be very cautious in dealing with what are presumably close modes and make certain that they are, indeed, different modes if the modal information is used to synthesize mobilities at which the structure was not shaken. The method for doing that is beyond the scope of this report. Structures are not purely linear systems and slight differences in measured natural frequencies from mobility to mobility do not necessarily indicate different modes.

The jkth displacement mobility of a free system at frequency $\omega$ is given by

$$Y_{jk}(\omega) = -\frac{E_{jk}}{\omega^2} + \sum_{i=1}^{N} \frac{A_{jki}}{\Omega_i^2} \frac{1}{1 - \frac{\omega^2}{\Omega_i^2} + ig} \tag{213}$$

$$\frac{dY_{jk}(\omega)}{d\omega^2} = \frac{E_{jk}}{\omega^4} + \frac{d}{d\omega^2} \sum_{i=1}^{N} \frac{A_{jki}}{\Omega_i^2} \frac{1}{1 - \frac{\omega^2}{\Omega_i^2} + ig} \tag{214}$$

where $E_{jk}$ is the jkth rigid body acceleration coefficient. At 1 Hertz, $E_{jk}/\omega 4 = E_{jk}/1559$, so for practical purposes in such structures as helicopters and airplanes

$$\frac{dY_{jk}(\omega)}{d\omega^2} \simeq \frac{d}{d\omega^2} \sum_{i=1}^{N} \frac{A_{jki}}{\Omega_i^2} \frac{1}{1 - \frac{\omega^2}{\Omega_i^2} + ig} \tag{215}$$

As shown by Kennedy and Pancu[9]

$$\frac{d}{d(\omega^2/\Omega_i^2)} \left[\frac{1}{1 - \omega^2/\Omega_i^2 + ig}\right] = \frac{1}{(1 - \omega^2/\Omega_i^2 + ig)^2} \tag{216}$$

or

$$\frac{d}{d\beta^2} \mu = \mu^2 \tag{217}$$

and furthermore

$$\frac{dY_{jk}}{d\beta_i^2} \equiv \frac{dS_{jk}}{d\beta_i^2} = N_i^2 \frac{dS_{jk}}{df^2} = \sum_{i=1}^{N} \frac{A_{jki}}{\Omega_i^2} \mu_i^2 = \sum_{i=1}^{N} \frac{A_{jki}}{g_i^2 \Omega_i^2} g_i^2 \mu_i^2 \tag{218}$$

Let $\left(\frac{dS_{jk}}{df^2}\right)_i$ be the value of $\frac{dS_{jk}}{df^2}$ at the ith natural frequency. Then

$$N_i^2 \left(\frac{dS_{jk}}{df^2}\right)_i = - \left(\frac{d\ddot{S}_{jk}}{df^2}\right)_i \tag{219}$$

and equation (218) can be written as

$$\left\{ - \left(\frac{d\ddot{S}_{jk}}{df^2}\right)_i \right\} = \left[ g_i^2 \mu_i^2 \right] \left\{ \frac{A_{jki}}{g_i^2 \Omega_i^2} \right\} \tag{220}$$

or

$$\left\{ \frac{A_{jki}}{g_i^2 \Omega_i^2} \right\} = \left[ g_i^2 \mu_i^2 \right]^{-1} \left\{ - \left(\frac{d\ddot{S}_{jk}}{df^2}\right)_i \right\}, \tag{221}$$

a limiting case of the matrix difference method. It is not necessary for any i that $\frac{d\ddot{S}_{jk}}{df^2}$ be a peak. If the modes are not very close, as defined by equation (212), then the $g^2\mu^2$ matrix approaches the unit matrix. In any case, the diagonal terms of the real $g^2\mu^2$ matrix will always be -1.00 and all other terms will have an absolute value less than unity.

Defining

$$\psi_{ki} = \sqrt{A_{kki} / g_i^2 \Omega_i^2} \tag{222}$$

The orthonormal modal elements are obtained in the usual manner and any mobility

$$Y_{\ell m}(\omega) = - \frac{E_{\ell m}}{\omega^2} + \sum_{i=1}^{N} \psi_{\ell i} \psi_{mi} \, g_i^2 \mu_i \tag{223}$$

or, in terms of acceleration mobility

$$\ddot{Y}_{\ell m}(\omega) = E_{\ell m} - \omega^2 \sum_{i=1}^{N} \psi_{\ell i} \psi_{mi} \, g_i^2 \mu_i$$

The advantage in using $g^{2}{}_{\mu}{}^{2}$ matrix for a system with the following natural frequencies and modal structural damping coefficients is shown below.

| Damping g | .1 | .2 | .1 | .15 | .1 | |
|---|---|---|---|---|---|---|
| Natural frequency (Hz) | 5 | 9 | 10 | 11 | 15 | |
| Forcing frequency (Hz) | | | | | | |
| 5 | -1.000 | .065 | .017 | .032 | .012 | |
| 9 | .002 | -1.000 | .123 | .112 | .023 | |
| 10 | .001 | .067 | -1.000 | .062 | .029 | REAL $g^{2}{}_{\mu}{}^{2}$ |
| 11 | 0 | .100 | .117 | -1.000 | .041 | |
| 15 | 0 | .012 | .006 | .028 | -1.000 | |
| 5 | 0 | - .041 | - .005 | - .013 | - .003 | |
| 9 | 0 | 0 | - .179 | - .128 | - .007 | |
| 10 | 0 | .416 | 0 | - .423 | - .011 | IMAGINARY $g^{2}{}_{\mu}{}^{2}$ |
| 11 | 0 | .098 | .144 | 0 | - .018 | |
| 15 | 0 | .003 | .001 | .010 | 0 | |
| 5 | 1.000 | .077 | .017 | .035 | .013 | |
| 9 | .002 | 1.000 | .217 | .170 | .024 | |
| 10 | .001 | .421 | 1.000 | .428 | .031 | MAGNITUDE $g^{2}{}_{\mu}{}^{2}$ |
| 11 | 0 | .141 | .186 | 1.000 | .045 | |
| 15 | 0 | .013 | .006 | .030 | 1.000 | |

The 5 Hz mode is seen to be essentially decoupled from the other modes in $g^{2}{}_{\mu}{}^{2}$. That is, it is decoupled insofar as $dS/df^{2}$ is concerned. The 9 Hz mode is influential at 10 Hz since 9 Hz x (1 + .2) = 10.8. In the magnitude table of $g^{2}{}_{\mu}{}^{2}$ the 9 Hz mode has a value of .421 at 10 Hz. The coupling, it is seen, occurs in the imaginary $g^{2}{}_{\mu}{}^{2}$. Note that the 10 Hz mode is only half as influential at 9 Hz as the 9 Hz mode is at 10 Hz. Similarly, the 11 Hz mode is 2.3 times as influential at 10 Hz than the 10 Hz mode at 11 Hz as equation (212) indicates. In other words, 11 x (1 - .15) = 9.35, less than 10, but 10 x (1 + .1) = 11, just equal to the next higher mode.

The $g^2{}_\mu{}^2$ matrix is clearly well conditioned. If the 9 Hz mode were, instead, 9.9 Hz the .421 value in the magnitude table would become .999 at 10 Hz and the value at 9.9 Hz from the 10 Hz mode would be .962 and the coupling would appear mainly in the real matrix. The conditioning is worsened but not necessarily unacceptable.

## CONCLUDING REMARKS

Analytical testing provides a practical methodology for combining structural dynamic analyses with flight vibration performance. This report has presented analytical methods for evaluating the flight vibration and strain effects of structural changes. The changed flight responses are characterized by the dynamics of the change, original flight test data, and shake test data. Basic analytical testing equations were derived to accommodate a category of changes which included mass, stiffness, absorbers, and active vibration suppressors.

Illustrations of the analytical testing methodology were presented using flight test and shake test data measured on an AH-1G helicopter. The applications were directed to the practical acquisition of helicopter vibration data and the utilization of the method. Results of this investigation indicate the possibility of combining flight data and shake test data with structural changes in the helicopter airframe to predict the effects on flight vibrations and strains. The results do not represent experimental verification of analytical testing in any particular application.

Modal analysis based upon the measurement and past test processing of transfer functions constituted a major part of the research associated with analytical testing. The vibration testing procedures and modal analysis techniques of the AH-1G were described. In addition, special considerations were discussed to establish consistent data acquistion and to minimize problems associated with modal analysis of complex structures.

## APPENDIX A

## DERIVATION OF THE BASIC ANALYTICAL TESTING EQUATION

Consider two structures with degrees of freedom F and C connected at I interface coordinates.

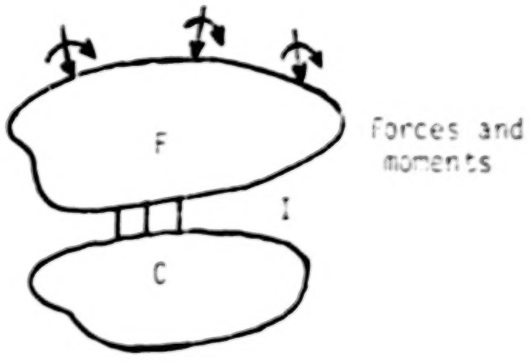


The structure F is excited by several external forces and moments, referred to as forces for brevity. Let $\{q\}$ define the response of structure F alone such that

$$\begin{bmatrix} Z_{FF} & Z_{FI} \\ Z_{IF} & Z_{II} \end{bmatrix} \begin{Bmatrix} q_F \\ q_I \end{Bmatrix} = \begin{Bmatrix} f_F \\ 0 \end{Bmatrix} \tag{A1}$$

The structure C represents a dynamic change and the coupled equations of motion are, assuming the external forces do not change

$$\begin{bmatrix} Z_{FF} & Z_{FI} & 0 \\ Z_{IF} & (Z_{II} + Z^C_{II}) & Z^C_{IC} \\ 0 & Z^C_{CI} & Z^C_{CC} \end{bmatrix} \begin{Bmatrix} q'_F \\ q'_I \\ q'_C \end{Bmatrix} = \begin{Bmatrix} f_F \\ 0 \\ 0 \end{Bmatrix} \tag{A2}$$

where the superscript C defines the free body impedances for structure C and $\{q'\}$ defines the response of the coupled system. From the definition of the matrix inverse it follows that

$$\begin{bmatrix} Z_{FF} & Z_{FI} & 0 \\ Z_{IF} & Z_{II} + Z_{II}^{C} & Z_{IC}^{C} \\ 0 & Z_{CI}^{C} & Z_{CC}^{C} \end{bmatrix} \begin{bmatrix} Y'_{FF} & Y'_{FI} & Y'_{FC} \\ Y'_{IF} & Y'_{II} & Y'_{IC} \\ Y'_{CF} & Y'_{CI} & Y'_{CC} \end{bmatrix} = \begin{bmatrix} I \end{bmatrix} \tag{A3}$$

Equation A3 gives the following relationships.

$$Z_{FF}\ Y'_{FF} + Z_{FI}\ Y'_{IF} = \begin{bmatrix} I \end{bmatrix} \tag{A4}$$

$$Z_{IF}\ Y'_{FF} + (Z_{II} + Z_{II}^{C})\ Y'_{IF} + Z_{IC}^{C}\ Y'_{CF} = 0 \tag{A5}$$

$$Z_{CI}^{C}\ Y'_{IF} + Z_{CC}^{C}\ Y'_{CF} = 0 \tag{A6}$$

Substituting for $Y'_{CF}$ from equation (A6) into equation (A5) and simplifying leads to the result

$$Z_{IF}\ Y'_{FF} + (Z_{II} + Y_{II}^{C-1})\ Y'_{IF} = 0 \tag{A7}$$

where

$$Y_{II}^{C-1} = Z_{II}^{C} - Z_{IC}^{C}\ Z_{CC}^{C-1}\ Z_{CI}^{C} \tag{A8}$$

Equation (A8) is obtained by considering the matrix inverse definition for structure C alone such that

$$\begin{bmatrix} Z_{II}^{C} & Z_{IC}^{C} \\ Z_{CI}^{C} & Z_{CC}^{C} \end{bmatrix} \begin{bmatrix} Y_{II}^{C} & Y_{IC}^{C} \\ Y_{CI}^{C} & Y_{CC}^{C} \end{bmatrix} = \begin{bmatrix} I \end{bmatrix} \tag{A9}$$

Solving for $Y_{II}^{C}$ from equation (A9) gives equation (A8). Considering equation (A3), it also follows that

$$Z_{FF}\ Y'_{FI} + Z_{FI}\ Y'_{II} = 0 \tag{A10}$$

$$Z_{IF}\ Y'_{FI} + (Z_{II} + Z^{C}_{II})\ Y'_{II} + Z^{C}_{IC}\ Y'_{CI} = \begin{bmatrix} I \\ \\ \end{bmatrix} \tag{A11}$$

$$Z^{C}_{CI}\ Y'_{II} + Z^{C}_{CC}\ Y'_{CI} = 0 \tag{A12}$$

Substituting for $Y'_{CI}$ from equation (A12) into equation (A11) and simplifying leads to the result

$$Z_{IF}\ Y'_{FI} + (Z_{II} + Y^{C-1}_{II})\ Y'_{II} = \begin{bmatrix} I \\ \\ \end{bmatrix} \tag{A13}$$

Combining equations (A4), (A7), (A10), and (A13) gives

$$\begin{bmatrix} Z_{FF} & Z_{FI} \\ Z_{IF} & Z_{II} + Y^{C-1}_{II} \end{bmatrix} \begin{bmatrix} Y'_{FF} & Y'_{FI} \\ Y'_{IF} & Y'_{II} \end{bmatrix} = \begin{bmatrix} I \\ \\ \end{bmatrix} \tag{A14}$$

or, after rearranging equation (A14)

$$\begin{bmatrix} Y'_{FF} & Y'_{FI} \\ Y'_{IF} & Y'_{II} \end{bmatrix} = \begin{bmatrix} Y_{FF} & Y_{FI} \\ Y_{IF} & Y_{II} \end{bmatrix} \begin{bmatrix} I & 0 \\ Y^{C-1}_{II}\ Y_{IF} & I + Y^{C-1}_{II}\ Y_{II} \end{bmatrix}^{-1} \tag{A15}$$

Making use of the matrix inverse definition, matrix algebra reduces equation (A15) to

$$\begin{bmatrix} Y'_{FF} & Y'_{FI} \\ Y'_{IF} & Y'_{II} \end{bmatrix} = \begin{bmatrix} Y_{FF} & Y_{FI} \\ Y_{IF} & Y_{II} \end{bmatrix} \begin{bmatrix} I & 0 \\ -(Y^{C}_{II} + Y_{II})^{-1}\ Y_{IF} & (I + Y^{C-1}_{II}\ Y_{II})^{-1} \end{bmatrix} \tag{A16}$$

or,

$$Y'_{FF} = Y_{FF} - Y_{FI} \left(Y^{C}_{II} + Y_{II}\right)^{-1} Y_{IF} \tag{A17}$$

$$Y'_{IF} = Y_{IF} - Y_{II} \left(Y^{C}_{II} + Y_{II}\right)^{-1} Y_{IF} \tag{A18}$$

Since the external forces are on structure F, postmultiplying equations (A17) and (A18) by the force vector yields

$$\left\{q'\right\} = \left\{q\right\} - \left[Y_{qI}\right] \left[Y^{C}_{II} + Y_{II}\right]^{-1} \left\{q_I\right\} \tag{A19}$$

or, in a slightly different form

$$\left\{q'\right\} = \left\{q\right\} - \left[Y_{qI}\right] \left[I + Y^{C-1}_{II} Y_{II}\right]^{-1} \left[Y^{C}_{II}\right]^{-1} \left\{q_I\right\} \tag{A20}$$

Equations (A19) and (A20) are independent of the number of degrees of freedom of structures F and C. In other words, the change in response at any point on structure F only requires information at that point and at the interface points.

## APPENDIX B

## COUPLED ROTOR/FUSELAGE VIBRATIONS AND LOADS

Consider the helicopter dynamics representation shown below.

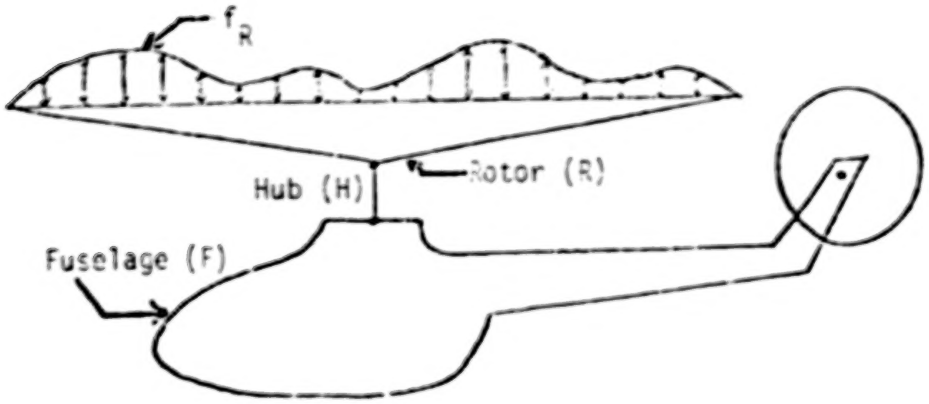


Let z', z", and z define the equations of motion (impedances) of the rotor alone, fuselage alone, and coupled rotor/fuselage, respectively. Similarly, let y', y", and y define the corresponding rotor alone, fuselage alone, and coupled rotor/fuselage responses. The matrix equations of motion can be expressed in terms of impedances as:

Rotor alone

$$\begin{bmatrix} z'_{RR} & z'_{RH} \\ z'_{HR} & z'_{HH} \end{bmatrix} \begin{Bmatrix} y'_R \\ y'_H \end{Bmatrix} = \begin{Bmatrix} f_R \\ 0 \end{Bmatrix} \tag{B1}$$

Fuselage alone

$$\begin{bmatrix} z''_{HH} & z''_{HF} \\ z''_{FH} & z''_{FF} \end{bmatrix} \begin{Bmatrix} y''_H \\ y''_F \end{Bmatrix} = \begin{Bmatrix} 0 \\ 0 \end{Bmatrix} \tag{B2}$$

Coupled rotor/fuselage

$$\begin{bmatrix} z_{RR} & z_{RH} & 0 \\ z_{HR} & z_{HH} & z_{HF} \\ 0 & z_{FH} & z_{FF} \end{bmatrix} \begin{Bmatrix} y_R \\ y_H \\ y_F \end{Bmatrix} = \begin{Bmatrix} f_R \\ 0 \\ 0 \end{Bmatrix} \tag{B3a}$$

or

$$\begin{bmatrix} z'_{RR} & z'_{RH} & 0 \\ z'_{HR} & (z'_{HH}+z''_{HH}) & z''_{HF} \\ 0 & z''_{FH} & z''_{FF} \end{bmatrix} \begin{Bmatrix} y_R \\ y_H \\ y_F \end{Bmatrix} = \begin{Bmatrix} f_R \\ 0 \\ 0 \end{Bmatrix} \tag{B3b}$$

Equation (B3a) can be rearranged in the form

$$z_{RR}\ y_R + z_{RH}\ y_H = f_R \tag{B4a}$$

$$\begin{bmatrix} z_{HH} & z_{HF} \\ z_{FH} & z_{FF} \end{bmatrix} \begin{Bmatrix} y_H \\ y_F \end{Bmatrix} = \begin{Bmatrix} -z_{HR} & y_R \\ 0 & 0 \end{Bmatrix} \tag{B4b}$$

Define

$$f_H = -z_{HR}\ y_R \tag{B5}$$

where $f_H$ are the rotor hub loads applied to the coupled rotor/fuselage to give the coupled hub and fuselage responses as shown below.

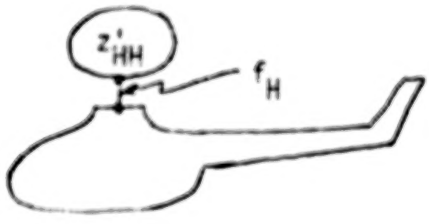

By definition from equation (B4b)

$$f_H = Y_{HH}^{-1} y_H \tag{B6}$$

From the definition of mobility

$$\begin{bmatrix} z_{HH} & z_{HF} \\ z_{FH} & z_{FF} \end{bmatrix} \begin{bmatrix} Y_{HH} & Y_{HF} \\ Y_{FH} & Y_{FF} \end{bmatrix} = \begin{bmatrix} I & 0 \\ 0 & I \end{bmatrix} \tag{B7}$$

Solving equation (B7) shows that

$$Y_{HH} = (z_{HH} - z_{HF}\, z_{FF}^{-1}\, z_{FH})^{-1} \tag{B8}$$

Thus, equation (B6) becomes

$$f_H = (z_{HH} - z_{HF}\, z_{FF}^{-1}\, z_{FH})\, y_H \tag{B9}$$

Since $z_{HH} = z'_{HH} + z''_{HH}$, equation (B9) can be written as

$$f_H = (z'_{HH} + z''_{HH} - z''_{HF}\, z''^{-1}_{FF}\, z''_{FH})\, y_H \tag{B10}$$

From the definition of mobility for the fuselage alone

$$\begin{bmatrix} z''_{HH} & z''_{HF} \\ z''_{FH} & z''_{FF} \end{bmatrix} \begin{bmatrix} Y''_{HH} & \\ Y''_{FH} & Y''_{FF} \end{bmatrix} = \begin{bmatrix} I & 0 \\ 0 & I \end{bmatrix} \tag{B11}$$

Solving equation (B11) shows that

$$Y''_{HH} = (z''_{HH} - z''_{HF}\, z''^{-1}_{FF}\, z''_{FH})^{-1} \tag{B12}$$

and equation (B10) reduces to

$$f_H = (z'_{HH} + Y''^{-1}_{HH})\, y_H \tag{B13}$$

Substituting for $y_R$ from equation (B4a) into equation (B5) also gives

$$f_H = - z_{HR}\, z_{RR}^{-1}\, f_R + z_{HR}\, z_{RR}^{-1}\, z_{RH}\, y_H \tag{B14}$$

Equation (B14) can be simplified by considering a rotor to a fixed hub so that equation (B1) becomes

Rotor to fixed hub

$$\begin{bmatrix} z'_{RR} & z'_{RH} \\ z'_{HR} & z'_{HH} \end{bmatrix} \begin{Bmatrix} y'_R \\ 0 \end{Bmatrix} = \begin{Bmatrix} f_R \\ f'_H \end{Bmatrix} \tag{B15}$$

Solving for $f'_H$ from equation (B15) gives

$$f'_H = z'_{HR}\, y'_R = z'_{HR}\, z'^{-1}_{RR}\, f_R \tag{B16}$$

The forces transmitted to a fixed hub are

$$f_0 = - f'_H = - z'_{HR}\, z'^{-1}_{RR}\, f_R \tag{B17}$$

Since $z'_{HR} = z_{HR}$ and $z'_{RR} = z_{RR}$, equation (B14) becomes

$$f_H = f_0 + z'_{HR}\, z'^{-1}_{RR}\, z'_{RH}\, y_H \tag{B18}$$

Some additional observations concerning $f_0$ can be made by considering equation (B3b) rearranged as follows:

$$\begin{bmatrix} z'_{RR} & z'_{RH} \\ z'_{HR} & (z'_{HH}+z''_{HH}) \end{bmatrix} \begin{Bmatrix} y_R \\ y_H \end{Bmatrix} + \begin{bmatrix} 0 \\ z''_{HF} \end{bmatrix} y_F = \begin{Bmatrix} f_R \\ 0 \end{Bmatrix} \tag{B19a}$$

$$\begin{bmatrix} 0 & z''_{FH} \end{bmatrix} \begin{Bmatrix} y_R \\ y_H \end{Bmatrix} + (z''_{FF})\, y_F = 0 \tag{B19b}$$

Substituting for $y_F$ from equation (B19b) into equation (B19a) gives

$$\begin{bmatrix} z'_{RR} & z'_{RH} \\ z'_{HR} & (z'_{HH} + z''_{HH} - z''_{HF}\, z''^{-1}_{FF}\, z''_{FH}) \end{bmatrix} \begin{Bmatrix} y_R \\ y_H \end{Bmatrix} = \begin{Bmatrix} f_R \\ 0 \end{Bmatrix} \tag{B20}$$

Further simplification of equation (B20) results in

$$[(z'_{HH} - z'_{HR}\, z'^{-1}_{RR}\, z'_{RH}) + (z''_{HH} - z''_{HH}\, z''^{-1}_{FF}\, z''_{FH})]\, y_H = - z'_{HR}\, z'^{-1}_{RR}\, f_R \tag{B21}$$

Equation (B21) can be reduced still further by taking advantage of the mobility definition for the rotor alone.

$$\begin{bmatrix} z'_{RR} & z'_{RH} \\ z'_{HR} & z'_{HH} \end{bmatrix} \begin{bmatrix} Y'_{RR} & Y'_{RH} \\ Y'_{HR} & Y'_{HH} \end{bmatrix} = \begin{bmatrix} I & 0 \\ 0 & I \end{bmatrix} \tag{B22}$$

Solving equation (B22) shows that

$$Y'_{HH} = (z'_{HH} - z'_{HR}\, z'^{-1}_{RR}\, z'_{RH})^{-1} \tag{B23}$$

Substituting equations (B12) and (B23) into equation (B21) gives

$$(Y'^{-1}_{HH} + Y''^{-1}_{HH})\, y_H = - z'_{HR}\, z'^{-1}_{RR}\, f_R \tag{B24}$$

and equation (B17) can also be written as

$$f_0 = (Y'^{-1}_{HH} + Y''^{-1}_{HH})\, y_H \tag{B25}$$

Substituting equation (B25) into equation (B18) and making use of equation (B23) results in

$$f_H = (z'_{HH} + Y''^{-1}_{HH})\, y_H \tag{B26}$$

which is identical to the result derived in equation (B13). Eliminating $y'_R$ from equation (B1) gives

$$Y'^{-1}_{HH}\, y'_H = -\, z'_{HR}\, z'^{-1}_{RR}\, f_R \tag{B27}$$

so that

$$f_0 = Y'^{-1}_{HH}\, y'_H \tag{B28}$$

Combining equations (B25) and (B28) shows that

$$(Y'^{-1}_{HH} + Y''^{-1}_{HH})\, y_H = Y'^{-1}_{HH}\, y'_H \tag{B29a}$$

or,

$$Y''^{-1}_{HH}\, y_H = Y'^{-1}_{HH}\, (y'_H - y_H) \tag{B29b}$$

Therefore, $f_H$ can be expressed as

$$f_H = f_0 + z'_{HR}\, z'^{-1}_{RR}\, z'_{RH}\, y_H \tag{B30a}$$

$$f_H = f_0 + (z'_{HH} - Y'^{-1}_{HH})\, y_H \tag{B30b}$$

$$f_H = (z'_{HH} + Y''^{-1}_{HH})\, y_H \tag{B30c}$$

$$f_H = z'_{HH}\, y_H + Y'^{-1}_{HH}\, (y'_H - y_H) \tag{B30d}$$

$$f_H = Y^{-1}_{HH}\, y_H \tag{B30e}$$

where

$$Y_{HH} = (z'_{HH} + Y''^{-1}_{HH})^{-1} \tag{B31}$$

In summary, the rotor hub loads, $f_H$, can be expressed in terms of loads transmitted to a fixed hub and modified by the rotor hub impedances alone, as well as the coupled rotor/fuselage hub responses.

From another point of view equation (B3b) can be written as

$$z'_{RR}\, y_R + z'_{RH}\, y_H = f_R \tag{B32a}$$

$$\begin{bmatrix} z''_{HH} & z''_{HF} \\ z''_{FH} & z''_{FF} \end{bmatrix} \begin{Bmatrix} y_H \\ y_F \end{Bmatrix} = \begin{Bmatrix} -\, z'_{HR}\, y_R - Z'_{HH}\, y_H \\ 0 \end{Bmatrix} \tag{B32b}$$

Define $$\hat{f}_H = -\, z'_{HR}\, y_R - z'_{HH}\, y_H \tag{B33}$$

where $\hat{f}_H$ are the rotor hub loads applied to the fuselage alone to give the coupled hub and fuselage responses.

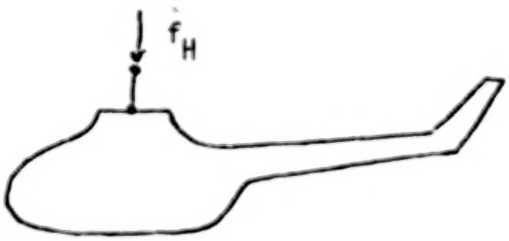


Comparing equations (B5) and (B33) shows that

$$\hat{f}_H = f_H - z'_{HH}\, y_H \tag{B34}$$

Applying equations (B30), $\hat{f}_H$ can be expressed as

$$\hat{f}_H = f_0 - Y'^{-1}_{HH}\, y_H \tag{B35a}$$

$$\hat{f}_H = Y''^{-1}_{HH}\, y_H \tag{B35b}$$

$$\hat{f}_H = Y'^{-1}_{HH}\, (y'_H - y_H) \tag{B35c}$$

Also from equation (B32b)

$$\begin{Bmatrix} y_H \\ y_F \end{Bmatrix} = \begin{bmatrix} Y''_{HH} \\ Y''_{FH} \end{bmatrix} \hat{f}_H \tag{B36}$$

Equations (B35) and (B36) serve to explain the nature of coupled rotor/fuselage vibrations with respect to rotor/fuselage dynamic interactions. In particular, the impact of fuselage dynamics on $f_H$ and consequently on fuselage vibrations. Helicopter rotor excitations are very large and one might suspect that hub responses of a rotor with no fuselage ($y'_H$) may be very large when compared with hub responses of the coupled rotor/fuselage ($y_H$). In other words,

$$y'_H >> y_H \tag{B37}$$

As a consequence of equations (B37) and (B28), equation (B35c) becomes

$$f_H = Y'^{-1}_{HH}\, y'_H = f_0 \tag{B38}$$

Therefore, the rotor hub loads acting on a fuselage without the rotor are nearly independent of the fuselage dynamics. Under this restriction the rotor hub loads are equal to the forces transmitted to a rigid support. Consider the extreme case of a fuselage with zero damping which has a natural frequency precisely at a harmonic of the blade passage frequency. Then $y'_H = y_H$ since the fuselage has zero hub impedance (or infinite hub mobility) in this extreme case. If the undamped fuselage has a natural frequency only slightly removed from the excitation frequency, then $y'_H >> y_H$ appears plausible and the conclusion of equation (B38) follows. Also, if with fuselage dynamic changes $y_H$ remains small compared to $y'_H$, then there is little change in the transmitted forces as concluded in equation (B38).

However, the condition that $y_H$ is small compared to $y'_H$ is a sufficient but not necessary condition for small changes in $f_H$. From equation (B20)

$$\begin{Bmatrix} y_R \\ y_H \end{Bmatrix} = \begin{bmatrix} z'_{RR} & z'_{RH} \\ z'_{HR} & (z'_{HH} + Y''^{-1}_{HH}) \end{bmatrix}^{-1} \begin{Bmatrix} f_R \\ 0 \end{Bmatrix} \tag{B39}$$

Consider the case of a fuselage with a natural frequency at the blade passage frequency for a system without the rotor. In this example $Y''_{HH}$ is very large or $Y''^{-1}_{HH}$ is very small and equation (B39) indicates that

$$y_H \approx y'_H \tag{B40}$$

and from equation (B35b)

$$\dot{f}_H = Y''^{-1}_{HH}\, y_H \tag{B41}$$

If $Y''^{-1}_{HH}$ does not change appreciably due to fuselage dynamic changes and remains small, then there is negligible change in $y_H$ as equation (B39) shows. As a result there is negligible change in the transmitted rotor loads, $\dot{f}_H$, given by equation (B41). To illustrate this case, consider an isolated hub-transmission where

$$Y''_{HH} >> Y''_{HF} \tag{B42}$$

and $Y''^{-1}_{HH}$ is very small. For a change in the Fth degree of freedom of the fuselage due to an impedance change $\Delta z_{FF}$, the changed driving-point hub mobility is given by

$$\Delta Y''_{HH} = Y''_{HH} - \frac{Y''_{HF}\, Y''_{FH}}{\frac{1}{\Delta z_{FF}} + Y''_{FF}} \tag{B43}$$

Since $Y''_{HH} >> Y''_{HF}$, it follows that

$$\Delta Y''_{HH} \approx Y''_{HH} \tag{B44}$$

and $\Delta Y''^{-1}_{HH}$ remains very small.

Now consider the opposite situation where $Y''^{-1}_{HH}$ is very large or $Y''_{HH}$ is very small compared to the z' matrix in equation (B39). This makes $y_H$ very small compared to $y'_H$ and the conclusion in equation (B38) follows.

If at blade passage harmonics, equation (B42) does not hold for various fuselage degrees of freedom, then the fuselage has a major as opposed to local resonance and the transmitted forces may change considerably due to fuselage dynamic changes. However, if the fuselage were separated from the rotor, then

such a condition could not be tolerated in practice. A major resonance has modal accelerations relative to points other than the hub which are larger relative to modal accelerations of other modes. A large modal acceleration can be looked upon as a small effective mass since

$$A_{jkn} \quad \frac{\phi_{jn}\,\phi_{kn}}{m_n} \tag{B45}$$

Physically, a small effective mass contributes to the response more significantly than a large effective mass for the same loading conditions.

## REFERENCES


1. Schrage, D. P.; and Peskar, R. E.: Helicopter Vibration Requirements. Preprint No. 77.33-33, American Helicopter Society, 33rd Annual National Forum, May 1977.

2. Veca, Angelo C.: Vibration Effects on Helicopter Reliability and Maintainability. USAAMRDL TR73-11, April 1973.

3. Berman, A.: A Generalized Coupling Technique for the Dynamic Analysis of Structural Systems. AIAA/ASME/ASCE/AHS 20th Structures and Materials Conference, St. Louis, Missouri, April 1979.

4. Ormiston, R. A.: Comparisons of Several Methods for Predicting Loads on a Hypothetical Helicopter Rotor. Proceedings of the Meeting of Specialists on Rotorcraft Dynamics, American Helicopter Society and Ames Research Center, February 1974.

5. Flannelly, W. G.; Bartlett, F. D., Jr.; and Forsberg, T. D.: Laboratory Verification of Force Determination, A Potential Tool for Reliability Testing. USAAMRDL TR76-38, January 1977.

6. Berman, A.; and Flannelly, W. G.: Theory of Incomplete Models. AIAA Journal, vol. 9, August 1971, pp. 1481-1487.

7. Berman, A.: System Identification of a Complex Structure. AIAA Paper 75-809, Denver, Colorado, May 1975.

8. Chen, J. C.; and Garba, J. A.: Matrix Perturbation for Analytical Model Improvement. AIAA Paper 79-0831, St. Louis, Missouri, April 1979.

9. Kennedy, C. C.; and Pancu, C. D. P.: Use of Vectors in Vibration Measurement and Analysis. Journal Aeronautical Sciences, vol. 14, no. 11, November 1947.

10. Klosterman, A. L.; and Lemon, J. R.: Dynamic Analysis via the Building Block Approach. Shock and Vibration Bulletin, 42 (4), 97-104, January 1972.

11. Ewins, D. J.: Whys and Wherefores of Modal Testing. SEE Journal, September 1979.

| 1 Report No | 2 Government Accession No | 3 Recipient's Catalog No |
|---|---|---|
| NASA CR-3429 | | |

| 4 Title and Subtitle | 5 Report Date |
|---|---|
| ANALYTICAL TESTING | May 1981 |
| | 6 Performing Organization Code |

| 7 Author(s) | 8 Performing Organization Report No |
|---|---|
| W. G. Flannelly, J. A. Fabunmi, and E. J. Nagy | R-1614 |
| | 10 Work Unit No |

| 9 Performing Organization Name and Address | 11 Contract or Grant No |
|---|---|
| Kaman Aerospace Corporation<br>Old Windsor Road<br>Bloomfield, Connecticut 06002 | NAS1-15414 |
| | 13 Type of Report and Period Covered<br>Contractor Report<br>6/27/78 - 9/15/80 |

| 12 Sponsoring Agency Name and Address | 14 Sponsoring Agency Code |
|---|---|
| National Aeronautics and Space Administration<br>Washington, DC 20546 | |

15 Supplementary Notes Langley Technical Monitor: F. D. Bartlett, Jr.
The Contract research effort which has led to the results in this report was financially supported by the Structures Laboratory, AVRADCOM Research and Technology Laboratories. Final Report

16 Abstract
Analytical methods for combining flight acceleration and strain data with shake test mobility data to predict the effects of structural changes on flight vibrations and strains are presented. This integration of structural dynamic analysis with flight performance is referred to as analytical testing. The objective of this methodology is to analytically estimate the results of flight testing contemplated structural changes with minimum flying and change trials. The category of changes to the aircraft includes mass, stiffness, absorbers, isolators, and active suppressors. Examples of applying the analytical testing methodology using flight test and shake test data measured on an AH-1G helicopter are included. The techniques and procedures for vibration testing and modal analysis are also described.

17 Key Words (Suggested by Author(s))
Structural dynamics
Flight testing
Shake testing
Vibrations
Absorbers
Modal analysis
Stress analysis
Helicopters
Suppressors
Isolators

18 Distribution Statement
Unclassified - Unlimited
Subject Category 39

| 19 Security Classif (of this report) | 20 Security Classif (of this page) | 21 No of Pages | 22 Price |
|---|---|---|---|
| Unclassified | Unclassified | 152 | A08 |

For sale by the National Technical Information Service, Springfield, Virginia 22161

NASA-Langley, 1981

# END

July 29, 1981